The Thesis Committee for Anmar Carolina Davila-Chacon
Certifies that this is the approved version of the following thesis:

Sand Distribution along Shelf-edge Deltaic Systems: A case study from Eastern Offshore Trinidad

APPROVED BY
SUPERVISING COMMITTEE:

Lesli Wood, Supervisor

Lorena Moscardelli, Co-Supervisor

William Fisher

Ronald Steel

Sand Distribution along Shelf-edge Deltaic Systems: A case study from Eastern Offshore Trinidad

by

Anmar Carolina Davila-Chacon, BE

Thesis

Presented to the Faculty of the Graduate School of

The University of Texas at Austin

in Partial Fulfillment

of the Requirements

for the Degree of

Master of Science in Geological Sciences

The University of Texas at Austin

December 2010

Dedication

A mi Abuelo Mauricio, quien extraño todos los días.

Acknowledgements

First of all I would like to thank my supervisors Dr. Lorena Moscardelli and Dr. Lesli Wood for their time, patience and support during my master research. Special thanks to Lorena who dedicated long hours of discussion on my results and polished my manuscript. I also would like to thank both for encouraging me to give the best of myself.

I am truly grateful to the Jackson School of Geosciences and the Quantitative Clastic Industrial Associate Lab at the Bureau of Economic Geology in The University of Texas at Austin, who provided me fully financial support during my two years of study.

I am very thankful to my parents who always give me support and love and even though they were not physically in Austin, it felt always as they were walking by my side. Mema y Tony: los quiero con todo mi corazón.

To my sister Tere, who always shows me the importance of living without limits.

To Abuela Sara who always supported me and called me by phone every week to remind me that everything is possible if you work hard. Abuela tú eres mi inspiración.

To my cousins Luisito and Antonio for your support and love since the very moment I arrived to the U.S.

To my cousins, aunts, uncles and all the family that remains in Venezuela and that I have missed every day since I moved away.

To my friends Carla y Ryan, who adopted me as their daughter and helped me since the very beginning and with whom I have shared many fun moments during these two years in Austin.

To my friends Mary, Pedro, Deivid, Eve, Gordis for their faithful friendship, long hours of conversation (even though some live in other time zones), encouragement, and love. You really make my life happy.

To my friends in Austin: Lin, Henry, Jah, Diego, Saya and Renas with whom I spent many long hours of study but also fun moments. Special thanks to Paola and Daniel that always cheered me up and listened to all my complaints and still care about me.

I am very thankful to have met a very smart and funny guy that loves me even when I am grumpy. I feel very lucky to have met you. Thanks Jud.

To all my friends in Venezuela and the rest of the world that will complain because I did not named them individually. I am very thankful to have many good and amazing friends.

To the Universe, because it always shows me its magic power.

December 2010

Abstract

Sand Distribution along Shelf-edge Deltaic Systems: A case study from Eastern Offshore Trinidad

Anmar Carolina Davila-Chacon, M.S.Geo.Sci

Co-Supervisors: Lesli Wood and Lorena Moscardelli

The study area is situated along the obliquely converging boundary of the Caribbean and South American plates offshore eastern offshore Trinidad. Major structural elements in the shelf break and deep-water slope regions include normal and counter-normal faults to the south and large transpressional fault zones to the north.

Well logs and biostratigraphic information were analyzed for twenty-four wells in the study area to refine previous depositional environment interpretations.

For purposes of this net sand distribution analysis it was decided to consider the deltaic portion of the shelf transit cycle, against the marine portion of the shelf transit cycle and were named T and R cycles, respectively.

T and R cycles were interpreted based on well log patterns and depositional facies shifts. Six T/R cycles were interpreted within the Pliocene to recent stratigraphic succession and shelf edge trajectories were also mapped for each of these cycles based on earlier stratigraphic correlations. Net-to-gross (NTG) ratios were calculated for each

component of the T/R cycles and plotted against total thicknesses and net sand values. In addition, NTG trends were mapped for each interval and analyzed based on their proximity to the corresponding shelf edge.

Mapping of the shelf edge trajectories (SET) revealed that (1) SET migrate northeasterly across the Columbus Basin through time and (2) shelf edge orientations are parallel to the strike of growth faults in the south but deflect to the northeast near the Darien Ridge indicating a strong underlying structural control. The NTG plots and maps also revealed that (1) For T cycles, NTG values never exceed 60% and are inversely proportional to total thickness, (2) For R cycles, NTG values are highly variably ranging from 35% to 90%, (3) NTG values increase as the shelf break is approached and (4) The distribution of NTG ratios is also controlled by accommodation space created by local structures.

The Guiana current is believed to play an important role in the redistribution and reworking of sand in the Columbus Basin.

Aggradation and progradation distances were computed for each interval and the results suggest that the younger Sequences C2 (T-R cycle E) and C3 (T-R cycle F) show a stronger progradational trend than the older C4, C5 and C6. This strong progradational trend might indicate delivery of sand basinwards, while for the older intervals; the aggradational trend suggests an increase in sediment storage.

In long-term scale (1-2 m.y.) the Orinoco Delta seems to behave as an aggradational delta that increases sediment storage due to growth fault and high subsidence rates. However, in the short-term scale, the Orinoco delta seems to behave as a rapid progradational delta, for the younger sequences C2 and C3, where sediment bypass is more likely to occur; and as a rapid aggradational (slow prograding) margin for the older intervals C4, C5 and C6.

Table of Contents

List of Tables

List of Figures

Chapter 1: Introduction

1.1 INTRODUCTION

Trinidad and Tobago, the world's 18th largest supplier of oil and gas to the United States, provides approximately 0.7% of the oil to the United States (Garciacaro et al., 2009; U.S. Energy Information Administration, 2010). Most of this production comes from the Columbus Basin located in eastern offshore Trinidad, where hydrocarbon exploration began in the late 1960s and production now totals 2.6 billion bbl of oil. Most of the production comes from fluvial-deltaic, shallow marine, and deep marine turbidite deposits of Miocene to Pliocene age. Reserves are estimated to be more than 3.27 billion bbl of oil and 20 tcf of gas in place (Wood, 2000).

Within the Columbus Basin, over 60 pay zones have been identified as part of shelf-edge reservoirs that are located in the Trinidad outer-shelf (Sydow and Bowman, 2003). The shelf-edge is often a structurally complex region where high accommodation zones interact with a variety of depositional processes to generate some of the most opportunistic petroleum reservoirs in a basin (e.g.: Trinidad Columbus Basin, offshore Niger Delta, etc.). These reservoirs represent the link between the shelf and deep-water deposits and form the most laterally continuous and thickest reservoir units in a variety of petroleum basins around the world (Pocknall et al, 2001). Understanding of shelf-edge deltas, trajectories and architectures is also key to identify sediment bypass zones to deepwater regions, as well as to define areas of potential sediment accumulation on the outer shelf. The accurate description of depositional facies, vertical stacking patterns and lateral architectural changes within shelf-edge deltaic successions through time is crucial

to improve our capacity to evaluate hydrocarbon reservoirs within these important deposits.

1.1.1 Study Area

The study area is located in the Columbus Basin, eastern offshore Trinidad (Fig. 1.1). The Columbus Basin was defined by Leonard (1983) as the easternmost continuation of the Eastern Venezuela Basin (EVB). The Columbus Basin is limited to the north by the Darien Ridge, to the east by the modern continental shelf-break, to the south by the Delta Amacuro Platform, and to the west by the Island of Trinidad (Leonard, 1983; Wood, 2000).

The Columbus Basin lies on the Caribbean-South America Plate Boundary Zone (CSAPBZ), this tectonic zone has been defined as a roughly east-west, right-lateral strike-slip shearing region between the Caribbean and South American plates (Soto, 2007). Most of the interplate deformation to the west of the study area is accommodated by El Pilar fault system, which defines an active east-west striking fault zone where 80% of the plate motion occurs (Perez et al., 2001; Soto, 2007). The plate boundary zone to the north of the study area is more difficult to define since several widely spaced, east-west to northeast oriented strike-slip faults have been identified in the Trinidad area (faults have been mapped in a 90 km wide area), from north to south: (1) the North Coast fault system, (2) the eastern continuation of the El Pilar strike-slip fault, (3) the Warm Springs-Central range fault zone and (4) the Los Bajos fault zone (Soto, 2007). However, the behavior of the CSAPBZ in the Trinidad area differs from what have been reported in northeastern Venezuela because most of the interplate movement occurs along the Central Range fault zone and not along the eastern continuation of the El Pilar

fault as would be expected (Saleh et al., 2004). The Central Range fault zone has also been interpreted as having a highly transpressional component due to its northeasterly strike orientation, the topographic elevation of the Central Range of Trinidad and the exposure of some Cretaceous and Paleogene rocks (Kugler, 1959 in Weber, 2001). Recent Global Positioning System (GPS) measurements indicate that the Caribbean plate moves 20 mm/yr eastward along northern South America (Weber, 2001). Figure 1.1 shows the boundary location, as well as the movement direction of both plates, and the study area.

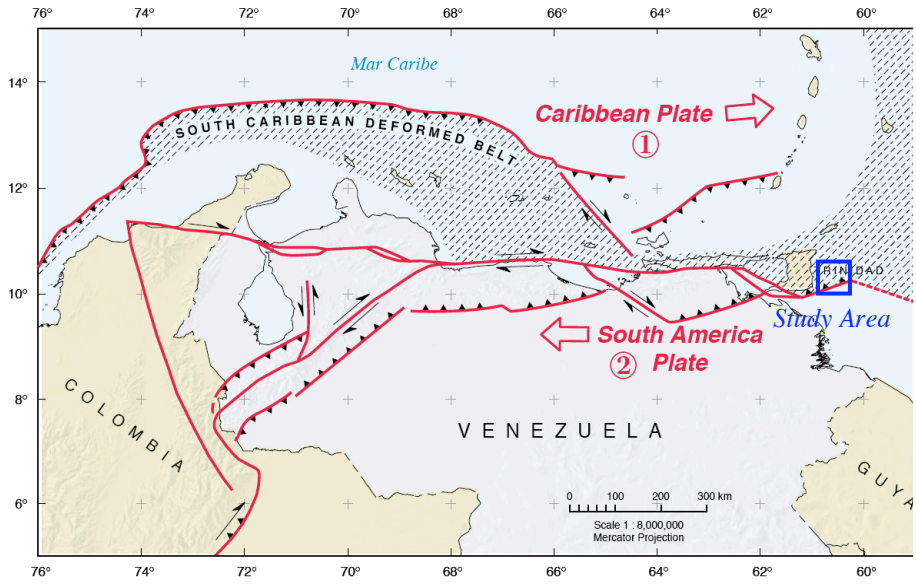

Figure 1.1 Location of Study Area and its relationship to the Caribbean – South American Plate Boundary (Audemard, 2000)

The Columbus Basin is located in a highly complex and active structural setting but it has also been subjected to high sedimentation rates associated with the evolution of

the Orinoco Delta system (Wood, 2000; Sydow et al., 2003?). The Orinoco Delta started to develop during the Miocene in the study area (Diaz de Gamero, 1996) and some of the aspects that controlled the stratigraphy of the Columbus Basin will be summarized in the next chapters.

1.2 RESEARCH OBJECTIVES

This research seeks to answer the following questions:

- How has the continental margin of eastern offshore Trinidad evolved through time from the Pliocene to Recent time?
- How does sand distribution within Pliocene to Recent shelf-edge deltas vary from the outer shelf to the upper slope region along the structurally complex margin of eastern offshore Trinidad?
- How do we translate data from log penetrations in Pliocene to Recent edge deltas in the basin to the seismic character and architectures being interpreted in younger deposits (last glacial maximum lowstand)?

This thesis is divided into five chapters. Chapter 1 presents an introduction to the most relevant aspects associated with the regional geology of the study area, the importance and motivation behind this research project, and a brief bibliographic review showcasing the most relevant and recent research in this area. Chapter 2 introduces the regional tectonic setting and defines the structural domains that are observed within the study area by using regional 2D seismic data. Chapter 3 explains the methodology that was followed in this research and the data that was used. Chapter 4 presents the research

results and their interpretation within the regional context. Finally, Chapter 5 contains some conclusions and recommendations for future work.

1.3 PREVIOUS WORK

Several authors have tried to tackle issues associated with the evolution of the eastern offshore continental margin before and this topic continues to be of high interest for companies that are actively exploring for hydrocarbons in this region. Most of these studies have tried to establish the relationship that exists between the tectonic regime and the evolution of the Orinoco Delta system through time with the intend of (1) increase the understanding of shelf edge architectures, (2) to identify areas of sediment accumulation along the margin, (3) to locate areas of sediment bypass toward deepwater depocenters and (4) to predict sediment composition and reservoir qualities. The following section provides a brief summary of the most influential work on this research from the literature review.

1.3.1 Chronostratigraphy and tectonostratigraphy of the Columbus Basin, eastern offshore Trinidad (Wood, 2000)

Wood (2000) analyzed biostratigraphic data from 41 wells and integrated the age and paleoenvironmental results with the well log signatures. The resulting chronostratigraphic framework was then transferred to the seismic interpretation that was generated using two-dimensional and three-dimensional seismic data. The author integrated a variety of information derived from the wells including biostratigraphic data (planktonic microfossils and palynomorphs), casing points, sampling intervals, well log motifs, seismic facies, and location of the wells with respect to the shelf break to

recognize erosional and flooding surfaces that were used as key stratigraphic horizons. The integration of data derived from the wells to the seismic data facilitated the mapping of key stratigraphic surfaces across fault boundaries within the study area allowing for a better understanding of the Plio-Pleistocene basin geometry. The key stratigraphic surfaces defined by Wood (2000) are also used in this thesis and the original nomenclature is preserved, from oldest to youngest: (1) "the "N" LS (R Cycle N; 2.0 m.y.), (2) the "J" LS (R Cycle J or base Alnus lowstand; 1.78 m.y.), (3) the "H" LS (R Cycle H; 1.5 m.y.), (4) the "F" LS (R Cycle F; 1.3 m.y.), (5) the "F" transgressive surface (T Cycle F; 1.2 m.y.), (6) the "E" LS (R Cycle E; 1.0 m.y.) and (7) the "D" LS (R Cycle D; 0.8 m.y.)" (Wood, 2000). These surfaces were also used to define the base and top of megasequences; these units tend to show a rapid thickening in their stratigraphic section as growth faults are crossed in the downdip direction (Wood, 2000). Megasequences, limited at the base and top by shelfal regional unconformities and their correlative basinal conformities, become younger to the east. According to this work, by the time all the defined megasequences were deposited, the Orinoco Delta was wave-dominated and had prograded onto a storm and current-influenced outer shelf closer to the shelf break. The inferred paleoenvironmental conditions at the time the last megasequence was deposited suggested to Wood (2000) that the resultant shelf-edge delta was a cuspate and strike-continuous architectural element that was exposed to high waves and current energy (sand rich system).

1.3.2 Stacked Shelf-edge Delta Reservoirs of the Columbus Basin, Trinidad, West Indies (Sydow and Bowman, 2003)

Sydow and Bowman (2003) studied shelf-edge delta reservoirs associated with the northeastern migration of the paleo-Orinoco delta system in the Columbus Basin. These authors noticed that good reservoir intervals associated with shelf edge deltas mostly developed in the downthrown side of growth faults where high accommodation space allowed for the thickening of the deltaic stratigraphic succession. Over 60 pay zones on the Trinidad shelf occur in these shelf-edge intervals, which are located within 10 Km (6 mi) of their respective paleo shelf-edges. These reservoirs are generally very thick (300 to 500 ft, up to 1,000 ft), they have a high net-to-gross ratio (>85%) and they are laterally extensive and continuous. Proven gas reserves within these units have been reported around 20 TCF and it is estimated that these intervals might also contain more than one billion barrels of oil (Sydow and Bowman, 2003).

These authors also identify the challenges associated with the mapping of shelf-edge trajectories (SET) within the basin by reporting that the correlation task was difficult due to fault density and the presence of fault roll-overs. The structural configuration within the Columbus Basin certainly can mask the shelf-break and this particular complication represents a major problem for seismic interpreters when they are trying to predict the location of the shelf break for a given stratigraphic interval. Previous experiences have shown that the best way to track shelf-edge trajectories in the study area involves the performance of four basic steps (1) identify key stratigraphic picks on the wells, (2) transfer the well interpretation to the seismic, (3) perform extensive and detailed mapping of the key stratigraphic picks using the available three dimensional data and (4) perform surface manipulation (attribute extraction maps, strata slicing, etc) to

identify geomorphological characteristics in plan view that can reveal the location of the paleo shelf edge.

The authors also suggested in this work that sequence architecture within the basin is driven by glacio-eustatic cycles in the 20 to 100 Ka Milankovitch orbital periodicity range. However, this thesis postulates that sequence architecture within the Columbus Basin is driven by a variety of factors that are not exclusively related to glacio-eustasy and the arguments for this hypothesis will be postulated in chapters 4 and 5.

1.3.3 Mass-transport complexes (MTC) and associated processes in the offshore area of Trinidad and Venezuela (Moscardelli et al., 2006)

Mass-transport complexes (MTCs) (slides, slumps, and debris flows) constitute an important part of the stratigraphic record in the easterly termination of the Columbus Basin (shelf-break region). The low porosity and permeability values associated with sediments that are contained within MTCs make these units an efficient stratigraphic seal and their erosive nature has the capacity to shape stratigraphic traps even though these deposits are not commonly associated with good reservoir units. Predicting the occurrence of MTCs in these settings is important to appropriately evaluate some elements of the petroleum system in the outer shelf and upper slope region. The occurrence of MTCs is closely link to the evolution of shelf edge deltaic systems since the later define areas of sediment bypass through which MTCs and other gravity induced deposits can generate.

An extensive MTC (MTC_1) (Moscardelli et al., 2006) has been recognized in the deep-water blocks located to the east of the Columbus Basin. This unit (MTC_1) is bounded at its base by an extensive and irregular erosional surface and at its top by the base of an overlying levee-channel system (Wood and Mize, 2009). A paleocanyon

located in the northwestern portion of the study area (blocks 4ab) is believed to be one of the main feeders of MTC_1. More recently, it has been suggested that a shelf edge deltaic lobe was feeding sediments directly into the paleocanyon area (Moscardelli personal communication) illustrating how the understanding of shelf margin architectures can also help identify areas of sediment bypass where MTCs and other gravity induced deposits can develop.

The authors point out that due to the complex geology of the area, others factors besides sea level fluctuations alone should be considered to explain the origin of MTC_1. Two causal mechanisms have been proposed: (1) initial instabilities might have been generated by rapid relative sea-level fluctuations and high sedimentation rates and (2) catastrophic failures of upper-slope sediments caused by gas-hydrate disruption and/or earthquakes. Based on biostratigraphic data, Sydow et al (2003) established that the base of the overlying levee channel system was equivalent to the Last Glacial Maximum Lowstand surface (LGML) therefore the base of MTC_1 was assumed to be slightly older than 18,000-yr (Moscardelli et al., 2006).

1.3.4 Tectonic Geomorphology of the Eastern Trinidad Shelf, Implications for Influence of Structure on Reservoir Distribution and Nature in Older Basin Fill (Alvarez, 2008)

This master project used a 3D mega-merged seismic survey and integrated some of the available well information to examine the modern shelf and the near-modern basin fill. The objective of the thesis was to examine the influence of the regional structures on the morphology and architecture of the young stratigraphic succession. As a result, the author mapped three key seismic horizons (D, E and F) across the study area using the final surfaces to perform attribute amplitude extractions that help with the reconstruction

of the shelf evolution through time. The author recognized several features that are important for reservoir characterization, such as: “channels and channel belts, tidally inundated interfluves, shelf delta topsets, interdistributary areas, and ridge and swale topography.” The channels range “from 1-4 km wide to smaller channels of less than 100 meters in width”, and can be recognized everywhere across the shelf during lowstand periods. Avulsion and lateral migration of the channels were often observed. The author concluded that depositional systems were controlled by active listric faults and landward and basinwards shoreline migration during times of sea level change. This research also pointed out that the detailed analysis and interpretation of the architecture of the previously described depositional elements, as well as the understanding of their spatial orientation and distribution is necessary to improve 3D modeling of these reservoirs. Also, a better understanding of the spatial distribution of the different depositional elements that are present in the shelf edge area was identified as a key factor to improve our capacity to predict sand distribution in these settings.

Chapter 2: Regional Tectono-Stratigraphic Framework

2.1 CARIBBEAN TECTONICS

There are a variety of tectonic models that try to explain the tectonostratigraphic evolution of the southeastern Caribbean region (Speed, 1985; Robertson and Burke, 1989; Russo and Speed, 1992; Baab and Mann, 1999; Flinch et al., 1999; Pindell and Keenan, 2001; Garciacaro, 2009). Despite the abundance of different theories, the details associated with the tectonic evolution of this region are still not completely understood. Most of the existing models include a combination of interpretations that fall in one of the following categories (Baab and Mann, 1999; Garciacaro et al., 2009): (1) oblique collision and thrusting (Speed, 1985; Russo and Speed, 1992) (2) strike-slip faulting motion as dominant mechanism (Robertson and Burke, 1989; Babb and Mann, 1999; Flinch et al., 1999), (3) tectonically-controlled normal faulting related to strike-slip faulting (pull-apart basins) as the dominant process (Pindell and Keenan, 2001).

The evolution of the Orinoco Delta has been associated to the Caribbean Plate migration through time. Figure 2.1 illustrates the evolution of the Caribbean Plate (curved yellow lines) from west to east through time (Lugo and Mann, 1995; Garciacaro et al., 2009).

The tectonic evolution of the Columbus Basin can be summarized as follows:

Middle to Late Jurassic:

As a result of the break-up of Pangea, the American continental margin was formed (Pindell et al., 2005). This period was characterized by rifting and seafloor spreading associated with the separation of North and South America.

Late Jurassic to Late Cretaceous:

Passive margin conditions were dominant along the northern margin of the South American Plate. During the Cretaceous the principal hydrocarbon source rocks were deposited both in western and eastern Venezuela (including the Columbus Basin region) (Bowman, 2003). Dominant depositional systems included the development of a carbonate megaplatform with overlying carbonate bank buildups (Baab and Mann, 1999). The Caribbean oceanic plate was created "about 88 Ma ago" (Baab and Mann, 1999). By the Late Cretaceous western Venezuela was starting to be affected by structural deformation associated with the easterly migration of the Caribbean Plate (Parra et al., 2003) while eastern Venezuela (including the Columbus Basin region) remained under as a passive margin configuration.

Oligocene:

During the Oligocene, the effects of the dextral oblique collision between the Caribbean and South American plates were already affecting western Venezuela generating a foreland basin. Eastern Venezuela and the Columbus Basin were still dominated by passive margin conditions (Baab and Mann, 1999)..

Paleocene to Middle Miocene:

The dextral oblique collision between the Caribbean and South American plates started to affect western Venezuela during the Late Cretaceous (See figure 3.1, curved feature 2, 3 and 4) (i.e.: Colombia). This collision progressively migrated eastwards affecting the eastern Venezuela and Trinidad region during the Paleocene and Middle Miocene (Pindell et al., 2005). Consequences of the collision are: cessation of arc magmatism, formation of strike-slip structures and associated basins, arc fragmentation, metamorphic terrain accretion and exhumation, and folded belt/foreland basin formation

(Levander, 2003). The Columbus Basin and associated structural configuration started to form at this time.

Middle Miocene:

Dextral oblique collision ceases by the end of the Middle Miocene (see Caribbean plate position in figure 2.1, curved feature 5). The northern portion of the Columbus Basin and the Trinidad region were affected by oblique thrusting as a result of the interaction between the Caribbean and the South American plates. The Serrania del Interior Range in eastern Venezuela, as well as the Central and Northern ranges in Trinidad were generated as a result of this dextral oblique collision between the Caribbean and South American plates (Algar and Pindell, 1993). In the offshore region, the thrust faults and associated folds were later buried by late Miocene sediments associated with the Orinoco Delta system (Pindell et al., 2005). Earlier phases of deformation associated with the movement of the Warm Springs-Central Range-Caigual strike-slip fault zone have also been suggested by other authors (Dyer and Cosgrove, 1992 and Baab and Mann, 1999). High-pressured mobile shales were deposited during the Miocene (Wood, 2000).

Late Miocene to Early Pliocene:

A transcurrent plate boundary began to develop (Pindell et al., 2005) (See Figure 3.1, curved feature 6). East-west motion was partitioned along the Cariaco-El Pilar fault zones in the west while transpression started to develop toward the east due to reactivation of middle Miocene thrust structures (Pindell et al, 2005). During this time, sediments from the Orinoco Delta were already infilling the Columbus Basin (Leonard, 1983). From late Miocene to early Pliocene a succession of shallow-marine to brackish-water conglomerates and sandstones was deposited (Baab and Mann, 1999).

Late Pliocene to Pleistocene:

Dextral transpression across the region is characterized by the onset of shortening in the Southern Basin of Trinidad (southern part of the Island of Trinidad), transpressional uplift in the Central Range, onset of significant subsidence in the Columbus Channel and eastern offshore areas, and initiation of extensional collapse of the foredeep basin fill toward the Atlantic south of Darien Ridge (Wood, 2000; Pindell and Kennan, 2001; Pindell et al., 2005).

Pliocene to Pleistocene:

During this time the sedimentary infill within the Columbus Basin consists of fluvial-deltaic sands and shales. Dominant processes within the structurally complex Columbus Basin at this time include syndepositional sedimentation, active faulting, high sedimentation rates associated with the Orinoco Delta system and high-frequency sea level changes (Wood, 2000). Three coarsening upward stratigraphic cycles can be identify within the Plio-Pleistocene stratigraphic succession; these cycles were capped by a late Pleistocene transgressive event (Leonard, 1983). The Plio-Pleistocene unit within the Columbus Basin contains most of the discovered hydrocarbon accumulations in this region (Leonard, 1983). Localized sites show evidence of inversion of previously extensional structures, however transtensional deformation continues to be dominant during this time period (Pindell and Kennan, 2001).

A tectonostratigraphic chart for the basin is shown in Figure 2.2.

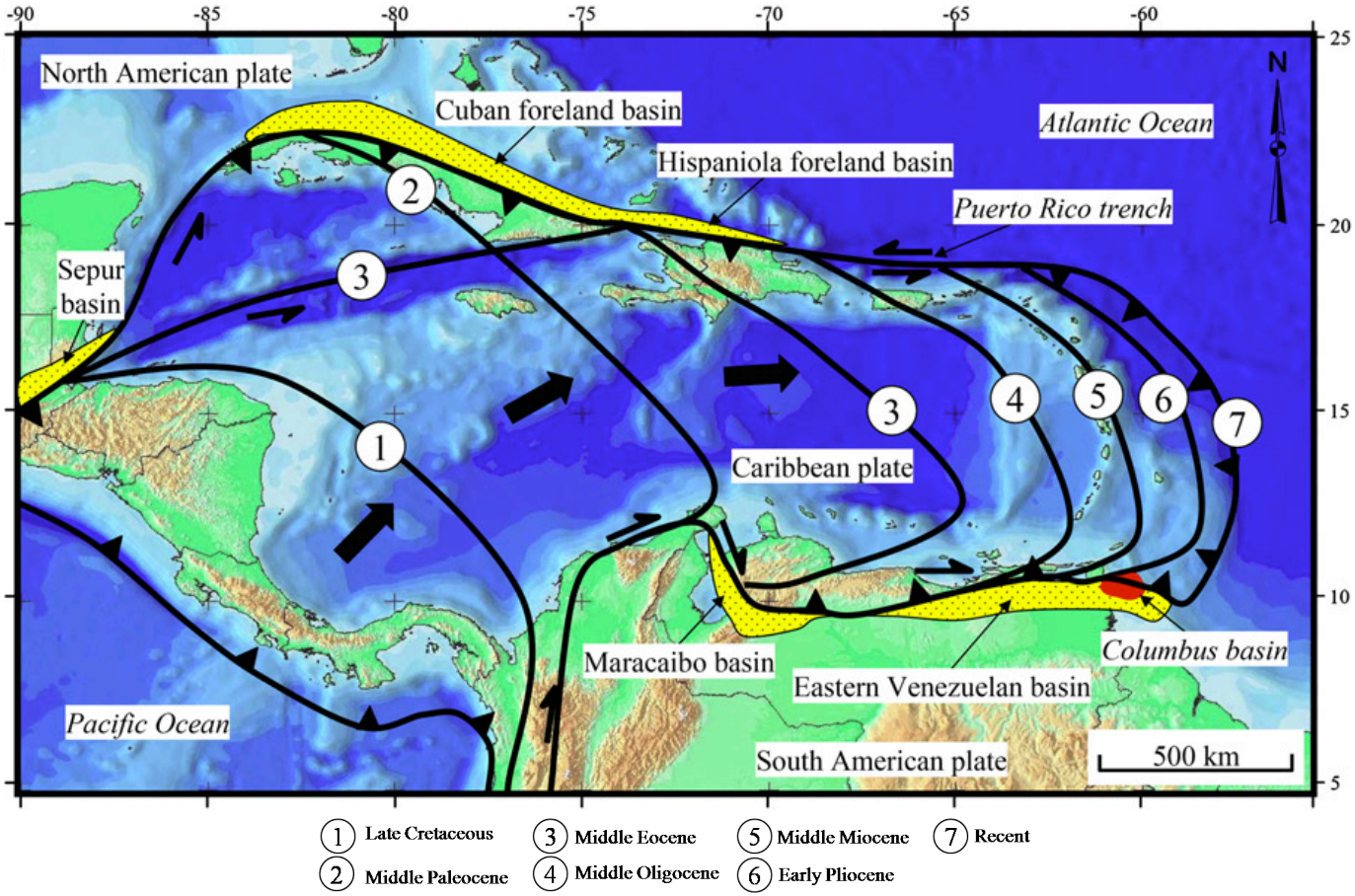

Figure 2.1 Tectonic Evolution of the Caribbean plate with respect to the South America plate. The Caribbean Plate progrades eastward from 250 Km west of the western border of the South American Plate during Late Cretaceous to about 400 Km east of the present location of the Island of Trinidad during the Late-Miocene to Recent time (Garciacaro et al., 2009)

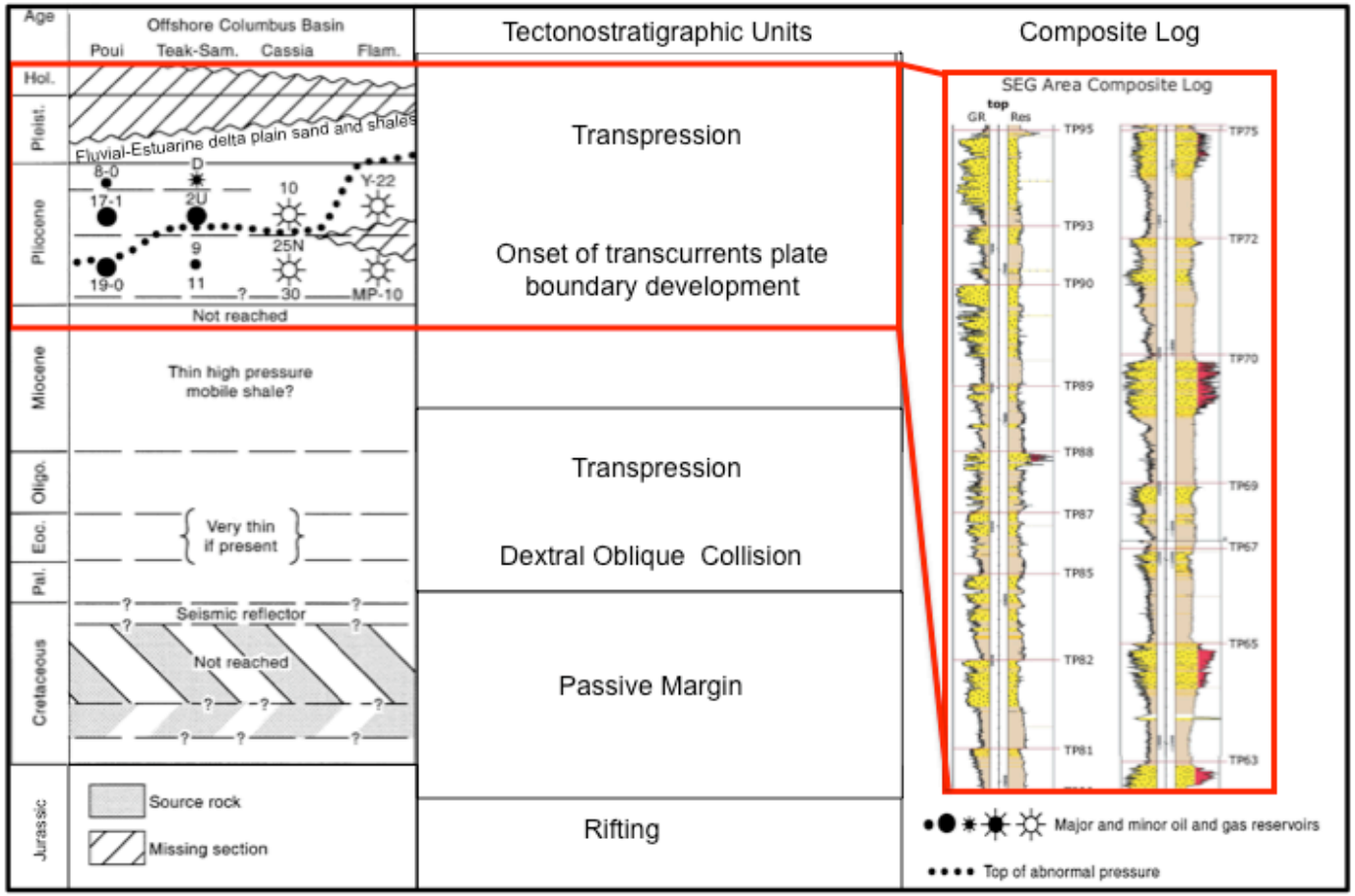

Figure 2.2 Tectonostratigraphic Units within the Columbus Basin. Left column shows the stratigraphy, middle column shows the different units divide by the main tectonic event, and the right column shows a composite log from the southeast Galeota area (southwestern part of the Columbus Basin) (Modified from Wood, 2000 and Sydow et al., 2003)

2.2. EVOLUTION OF THE ORINOCO DELTA

Most of the stratigraphic succession within the Columbus Basin is composed by Orinoco Delta sediments. Therefore, an outline of the development of this delta through time is essential to understand the Columbus Basin evolution. The delta evolution can be summarized as follows:

Middle Eocene

The mouth of the proto-Orinoco river has been recognized during the middle Eocene by several authors in the western part of Venezuela (i.e.: Maracaibo Lake) (Rod, 1981; Stephan, 1985; Kasper and Larue, 1986; Dickey, 1991 in Diaz de Gamero, 1996). By this time the river had a north-south direction and was draining the Colombian Andes to the west and the Guayana highlands to the east (Diaz de Gamero, 1996).

Late Eocene to Middle Oligocene:

After the regional uplift in western Venezuela (end of middle Eocene), the Proto-Orinoco River discharged to the south of its previous mouth in southwestern Venezuela and the northern Llanos Basin of Colombia (Diaz de Gamero, 1996).

Late Oligocene to Early Miocene:

Fluvio-deltaic facies of the proto-Orinoco river were recognized in the western part of the Falcon Basin (Diaz de Gamero, 1996). Foraminifera data suggests that the age of these facies in the Falcon Basin is at the Oligocene-Miocene boundary (Diaz de Gamero, 1996). By this time, the proto-Orinoco River "had a longer course and flowed to the north of its former mouth" (Diaz de Gamero, 1996).

- ***Middle Miocene:***

Diaz de Gamero (1996) established that the actual north-south to east-west shift of the proto-Orinoco river happened during the latest Middle Miocene. By this time, the paleo-Orinoco delta was on the Eastern Venezuela Basin (i.e. Maturin) (Diaz de Gamero, 1996)

- ***Pliocene to Recent:***

From the Pliocene to present, the Orinoco Delta has been prograding and shifting lobes supplying sediments to Trinidad and the Columbus Basin (Diaz de Gamero, 1996).

Figure 2.3 shows a schematic view of a delta in an oblique foreland basin, as it is the case of the Columbus Basin.

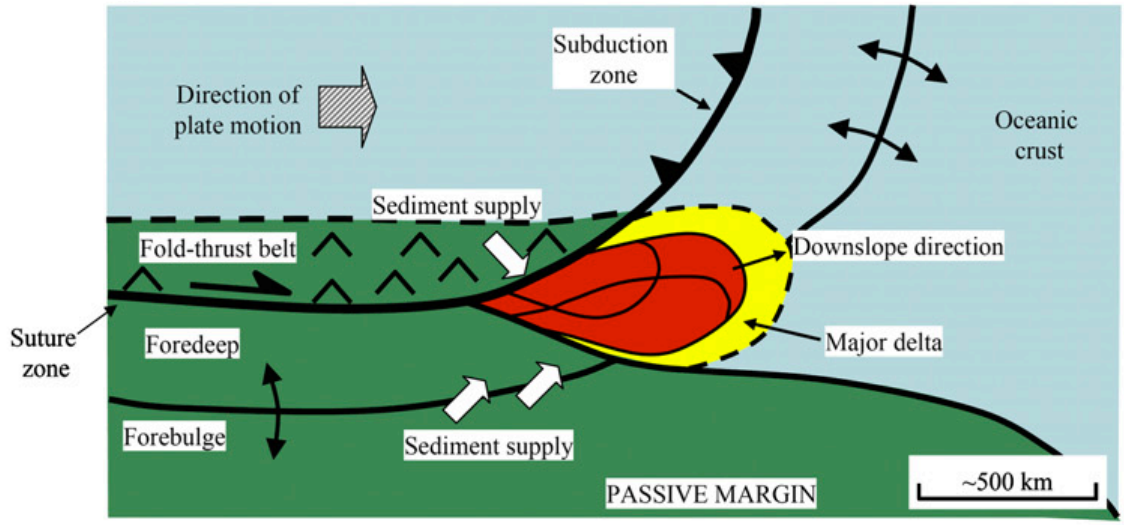

Figure 2.3 Example of evolution of a delta in a oblique foreland basin (Modified from Garciacaro et al., 2009)

2.2.1. Sediment Supply for the Columbus Basin

During the Pliocene to Pleistocene, the Columbus Basin had a sediment accumulation rate of 2 to 6 meters per thousand years with maximum values of 8 meters per thousand years in some depocenters (Wood, 2000).

The Orinoco Delta constitutes the main sedimentary source of the Columbus Basin since the Miocene (Diaz de Gamero, 1996) and 90% of the transported sediments can be tied to the Andes. The Orinoco basin covers about 1.1 $x10^6$ Km^2 of northern South America (Warne et al., 2002), drains about 35% of the Guayana Shield, 15% of the Andes and Coastal mountain ranges, and 50% of the Llanos region (percentages refer to drained surface area in these regions) (Warne et al., 2002). The annual Orinoco Delta sediment discharge is close to 150 x 10^6 metric tons / year and the delta-plain has an approximately area of 22,000 Km^2 (Warne et al., 2002).

The Orinoco Delta system consists of a series of stacked deltaic sequences that began to develop in the Columbus Basin during the early Pliocene. The modern Orinoco Delta is located within a portion of the coastal plain that is subsiding more rapidly than adjacent sectors (Nota, 1958; Brinkman and Pons, 1968 in Warne et al., 2002).

The Guiana Littoral Current also acts as an along shore mechanism that has the capacity to transport as much as 50% of the total Amazon annual sediment discharge to the eastern offshore area of Trinidad and Venezuela, as a consequence the Columbus Basin also receives sediments from fluvial systems located to the south (Amazon, Essequibo and minor fluvial systems) (Eisma et al., 1978 in Warne et al., 2002). The Amazon sedimentary input is mainly composed by fine-grained sediments that are transported as suspended sediment load traveling along the northeastern South American shelf and reaching areas as distant as the Lesser Antilles in the eastern Caribbean (Warne et al., 2002). Once the sediments that are transported from the south as suspended

sediment load reach the Trinidad area, a substantial portion of the sediments is transported landward by waves and tides and deposited along the Orinoco coast and shelf (McClelland Engineers, 1979), an also volumetrically significant portion of sediments is transported through Boca de Serpientes into the Gulf of Paria (Fugro Gulf, 1979; INTEVEP, 1981) and a small portion is transported northeastward along the south coast of Trinidad and then northward along the eastern margin of Trinidad (Koldewijn, 1958 in Warne et al., 2002).

2.3 STRUCTURAL SETTING

There are a series of structural elements that can be observed within the Columbus Basin. In the shelf portion of the basin, northeast-southwest trending anticlines and northwest-southeast orientated down to the northeast normal faults are of common occurrence (Leonard, 1983; Wood, 2000). Near the Darien Ridge northeast to southwest transpressional faults can also be observed. Figure 2.4 shows the main structural configuration within the shelf region of the Columbus Basin

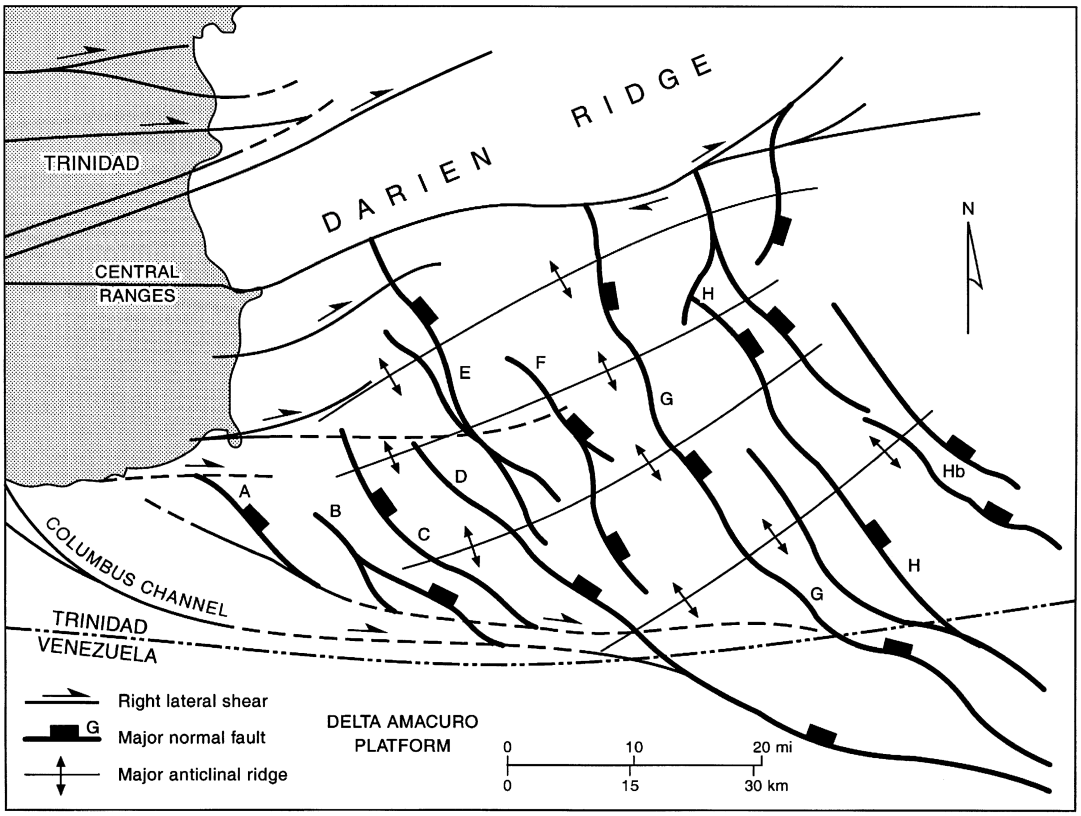

Figure 2.4. Regional Structural Map of the Study Area (Wood, 2000)

In the deep-water blocks to the east, northeast-southwest mud volcano ridges are of common occurrence; these structures are cored by regional transpressional faults. Mud volcano ridges bound mini basins in the deep-water blocks to the east of the shelf break.

There is a greater degree of structural deformation toward the northern portions of the Columbus Basin due to the close proximity to the Caribbean-South American Plate Boundary Zone where transpressional/compressional forces caused more deformation. Toward the south, the basin is dominated by growth fault structures that are common within passive margin configurations, however transpressive faults continue to be present in the deep-water blocks.

2.3.1 Anticlinal Structures:

The anticlines features are characteristically “narrow and steep-sided, commonly thrust-faulted on the flanks, and cut at right angles by later normal faults” (Michelson, 1976 in Leonard, 1983). The genesis of these structures has been associated with the collision of the Caribbean Arc with the South American Plate. This collision was also responsible for the uplift of the Northern Range of Trinidad; the Darien Ridge located in eastern offshore Trinidad represents the eastern and subsurface continuation of the Central Range.

2.3.1 Normal Faulting:

Northwest-southeast growth faults and associated counter regional faults can be observed in the shelf area of the Columbus Basin, as well as in the shelf edge region. These growth fault structures seem to be dominant and denser toward the southern portions of the study area. The genesis associated with the growth faults has bee related to the evolution and development of Plio-Pleistocene shelf edge deltaic systems. Shelf edge deltas have the capacity to increase the sediment load within the shelf break region and thicker stratigraphic succession can increase slope instabilities triggering big scale growth faults. The growth faults become younger to the east, and their throws range from 1,000 ft (305 m) to 10,000 ft (3,050 m). Counter-regional faults occurred downthrown to the larger faults and have offsets of 1,000 ft (305 m). These fault systems are important because they can form growth sediment traps and they can also constitute effective migration pathways for hydrocarbons within the basin (Leonard, 1983).

2.3.3 Mud-Volcano Ridges

The mud volcanoes in the study area can be present as isolated entities that have a variety of shapes and dimensions or as clusters that tend to align in a northeast-southwest

orientation (mud volcano ridges) (Sullivan, 2005). The mud volcano ridges are cored by regional transpressive faults and they are mainly located within the deep-water blocks to the east of the modern shelf break. However, from a plan view perspective, it is evident that the mud volcano ridges are aligned with the main axis of regional anticlines that are located to the west (shelf region) so that they represent the eastern continuation of these structures. Mud volcano ridges represent an important physiographic element within the basin because they can act as barriers that may diverge sediments from the shelf-edge and upper slope towards the basin (Moscardelli et al., 2008). It has been postulated, that individual mud volcanoes and mud volcano ridges were formed as the result of rise overpressures within Miocene mobile shales (Wood, 2000).

2.3.4 Structural Domains

Two structural domains were defined using 2D regional seismic lines. Original seismic lines are a courtesy of GULFREX. Line drawings are done by Davila 2010. Figure 2.5 shows the location of three interpreted lines. Line drawings are shown in figures 2.6, 2.7 and 2.8.

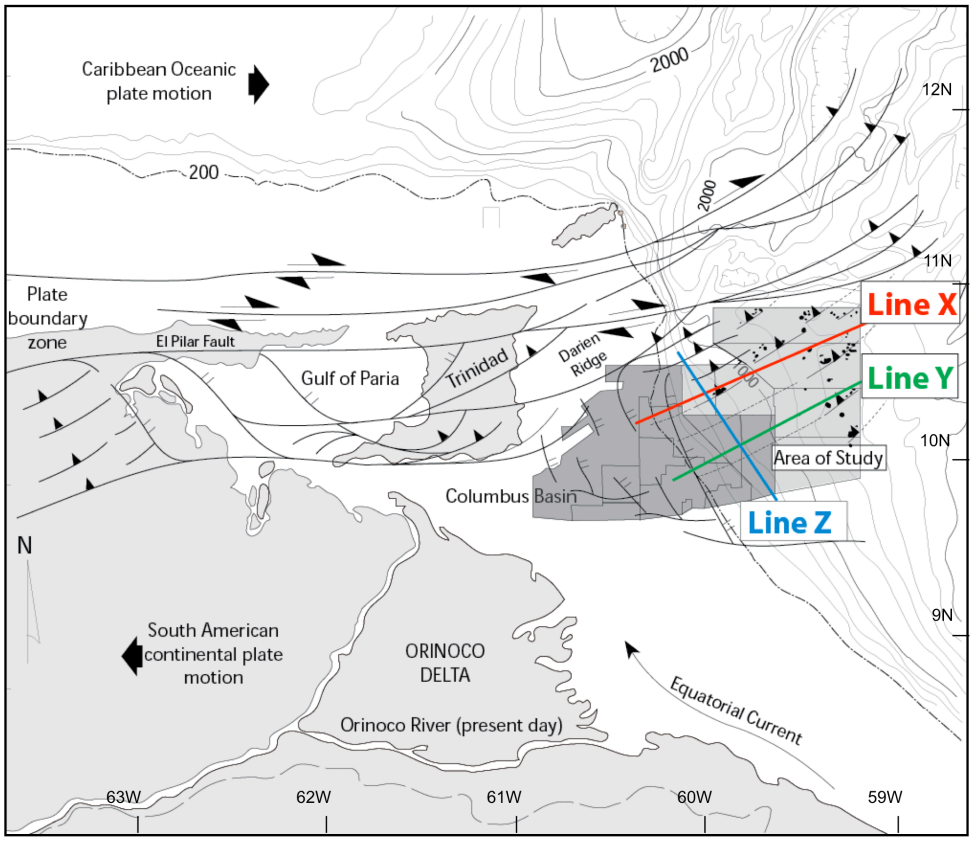

Figure 2.5. Regional Geologic Map of the Study Area (Modified from Wood, 2000). Line X (Figure 2.5) and Line Y (Figure 2.6) illustrate the structural variations along dip for the Northern and Southern Structural Domains, respectively. Line Z (Figure 2.7) illustrates the variation along strike

2.3.4.1 Northern Structural Domain / Transpressive Domain

The northern structural domain (NSD) (Figure 2.6 and 2.8) is dominated by the presence of the following structural elements in order of importance (1) Darien Ridge and associated northeast/southwest transpressive faults, (2) northeast-southwest oriented anticlines, (3) northeast-southwest oriented mud volcano ridges, (4) high angle normal faults associated with the collapsing flanks of mud volcano ridges and (5) northwest-southeast oriented growth faults and counter regional faults with associated roll-over structures.

The Darien Ridge represents the eastern continuation of the Central Range and the northern boundary of the Columbus Basin. The Darien Ridge is a major structural high that in some areas has a horst and graben configuration that is defined by the geometric arrangement of several transpressional faults. The main axis of the Darien Ridge extends into the northeast transitioning into the axis of a mud volcano ridge in the deep-water blocks. It is believed that both, the Darien Ridge and the mud volcano ridge are associated with the same system of transpressional faults but the deformation was more brittle in the shelf area while the higher shale content in the deep-water blocks, as well as the presence of overpressures caused a more ductile deformational style toward the east.

The northeast-southwest oriented anticlines that are located in the shelfal portion of the Columbus Basin were generated as a response to the transpressional forces associated with the Caribbean / South American plate tectonic interactions during the Tertiary. The main axis of these anticlines also seem to geometrically transition toward the northeast into the axis of the deep-water mud volcano ridges suggesting that there is some sort of structural connection between the two (e.g.: underlying transpressional fault?). As it was previously mentioned, there are northeast-southwest regional mud

volcano ridges that are located in the deep-water blocks to the east of the modern shelf break. These ridges seem to be cored by transpressional faults, a series of localized northeast-southwest high angle normal faults can also be seen affecting the flanks of the mud volcano ridges and it is thought that these structures might be associated with gravitational collapses triggered by the steepness of the mud volcano walls.

Finally, there are a series of northwest-southeast growth faults and counter regional faults affecting the shelf and shelf edge region. Growth fault density on the shelf is about 0.65 fault/Km, numerous secondary faults run parallel to the main growth faults distributing the stresses. Big rollover structures and rotated layers characterize the downthrown block of faults. Sediment dragging on the fault plane goes along with block rotation. Counter regional faults are thin-skinned and their origin may be related to layer flexure due the weight of sediment megasequences.

In short, the NSD is dominated by transpressive deformation associated with the Caribbean / South American plate tectonic interaction even though there are still some elements that can also be related to the passive margins (e.g.: growth faults).

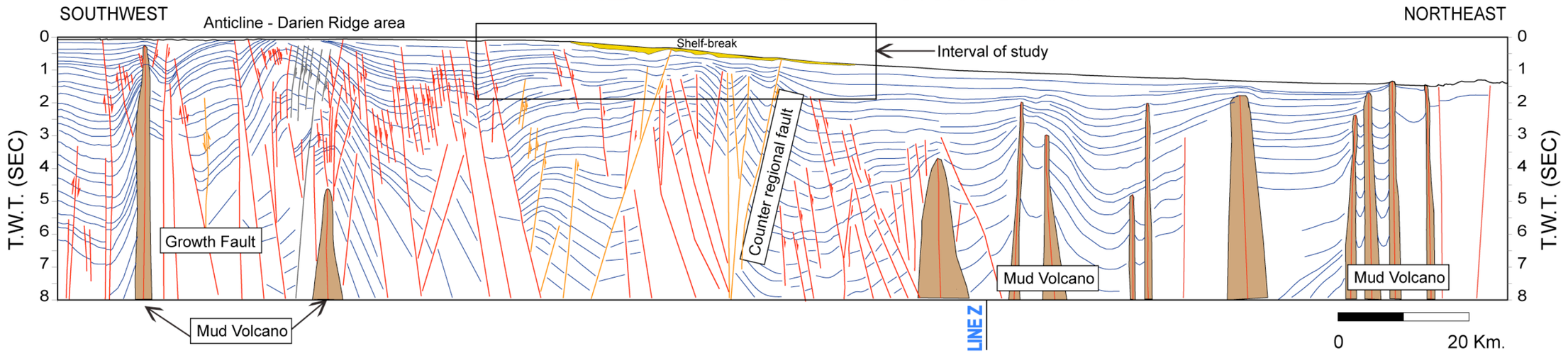

Figure 2.6. Line drawing illustrating the Northern Structural Domain. Figure 2.4 shows the location of this line. Original seismic line courtesy of GULFREX. Line drawing by Davila 2010.

2.3.4.2 Southern Structural Domain / Gravitational Tectonics

The southern structural domain (SSD) (Figure 2.7 and 2.8) is dominated mainly by gravitational tectonics and the most important structural elements in order of importance are (1) northeast-southwest oriented growth faults and counter regional faults, (2) Roll over structures associated with the growth faults, (3) northeast-southwest regional anticlines and (4) northeast-southwest mud volcano ridges.

Growth faults and counter-regional faults can be easily identified on the seismic lines (Figure 2.6). The density and extension of growth faults located in the shelf region of the SSD increase with respect to the NSD. Rollovers are also associated with the growth faults presenting greater amplitudes and a greater degree of compartmentalization on their crests (secondary small-scale normal faults). Of particular importance in this structural domain is the coupling between growth and counter regional faults since these geometric arrangements have the capacity to generate growth fault sediment traps in the outer shelf region. The absence of counter regional faults in certain areas of the shelf break can encourage sediment transport and bypass into deep-water depolocations.

Regional northeast-southwest anticlinal structures are also observable within the SSD and when these structures interact with the rollovers associated with the growth faults they generate anticlines with four-way closures that might become good traps. The main axis of the regional anticlines also follow the trend observed in the NSD transitioning into the axis of mud volcano ridges in the deep-water blocks. It is believe that there is still an important component associated with transpressional deformation in this domain but growth tectonics is definitely the dominant style.

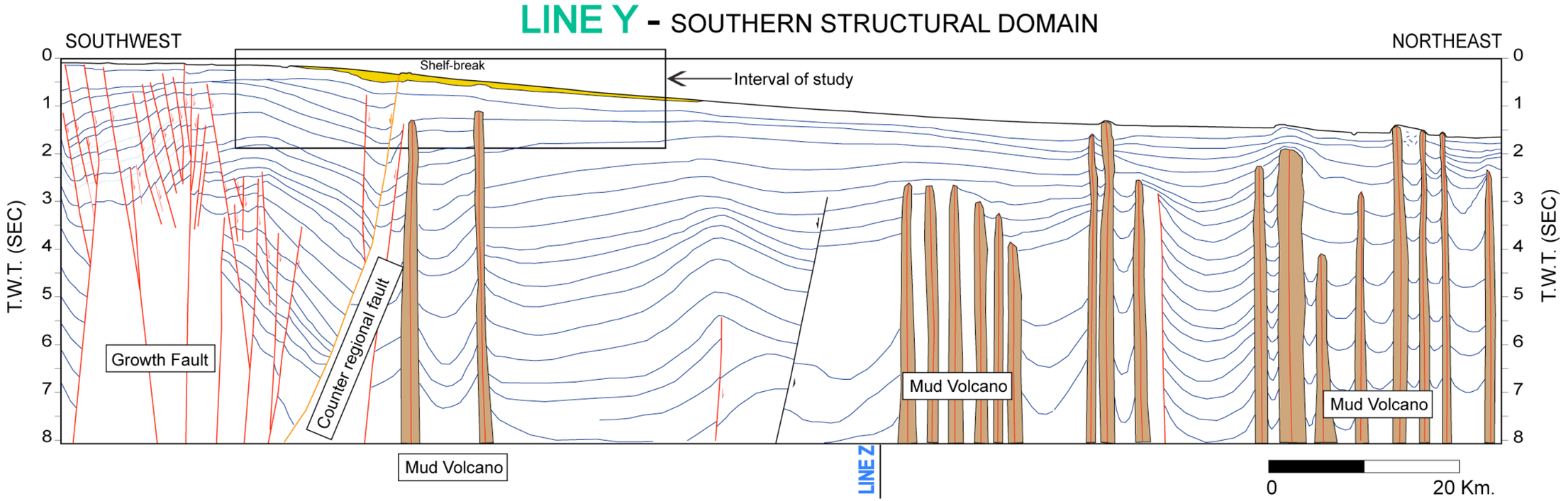

Figure 2.7. Line drawing illustrating the Southern Structural Domain. Figure 2.4 shows the location of this line. Original seismic line courtesy of GULFREX. Line drawing by Davila 2010.

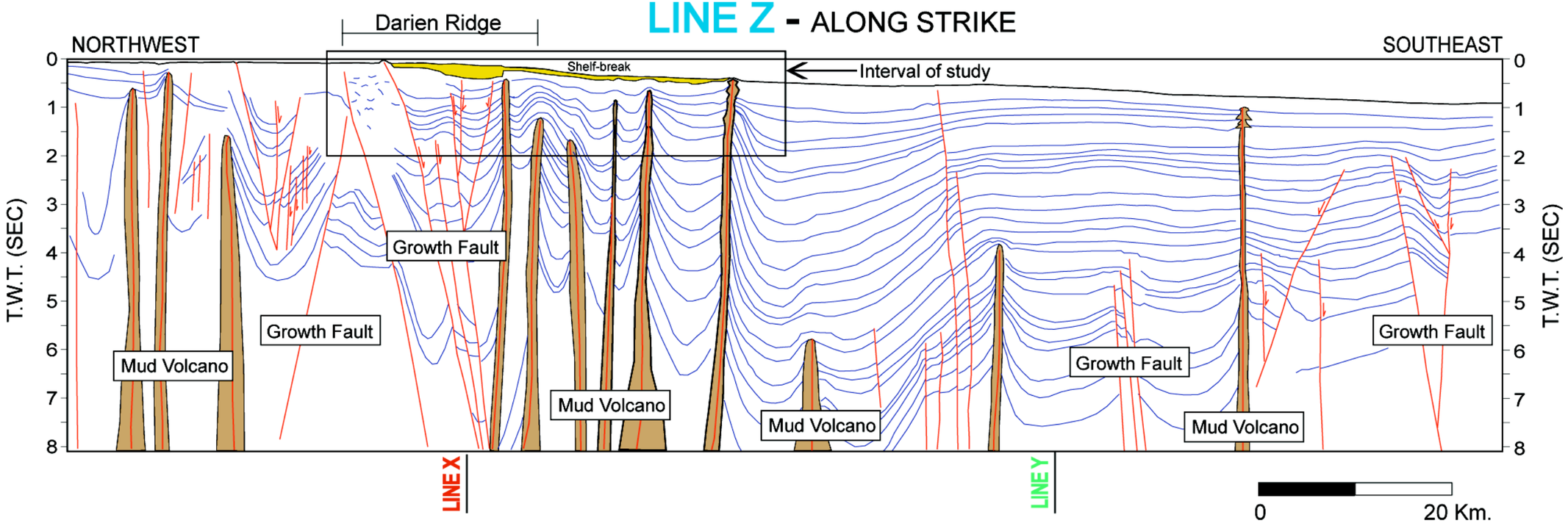

Figure 2.8. Line drawing illustrating the variation along strike in the Columbus Basin. Figure 2.4 shows the location of this line. Original seismic line courtesy of GULFREX. Line drawing by Davila 2010.

Chapter 3: Data Base and Integration

3.1 WELL DATA BASE

3.1.1. Well Logs

Twenty-three wells containing well log suites and biostratigraphic information were available for this study (Fig. 3.1). Gamma-ray curves (GR) were available for 22 of 23 wells, while resistivity curves (R) were available for all wells. Four wells had spontaneous potential (SP) curves and only two wells had sonic curves. Table 3.1 summarizes the type of well log curves that were available as well as the length of the curves and sample intervals. Figure 3.1 shows the location of each well and the layout of the mega-merge 3D seismic survey.

All wells had paper log records, however eight wells also had digital curves available.

	Well name	GR	SP	RES	SONIC	BIO	MIN DEPTH (ft)	MAX DEPTH (ft)	DIGITAL
1	BARRACUDA 1	X		X		X	1,150	11,900	
2	EM1	X		X	X	X	1,400	16,750	X
3	EM3	X		X		X	4,950	15,000	X
4	EMZ-1	X		X		X	1,200	10,000	X
5	EQB-1	X	X	X		X	1,050	15,800	X
6	EQB-2	X	X	X		X	1,100	10,800	
7	LORAN-1	X		X		X	600	11,800	
8	NEQB1	X		X		X	500	13,750	X
9	OILBIRD 1	X		X		X	1,150	14,950	
10	OMEGA-1	X		X		X	550	14,400	X
11	OPR-11		X	X		X	950	14,150	
12	OPR-5	X		X		X	1,550	15,050	
13	REDSNAPPER 1	X		X	X	X	700	13,400	X
14	SEG-4	X		X		X	580	13,700	
15	SEG-7	X	X	X		X	1,000	13,900	
16	SEP1	X		X		X	1,450	13,000	
17	SEQB-1	X		X		X	550	11,900	X
18	SOUTH DARIEN 1	X		X		X	500	11,450	
19	SOUTH DARIEN 2	X		X		X	500	11,250	
20	SEG-1	X		X		X	800	15,000	
21	EL DIABLO-1ST	X		X			1,200	12,900	
22	SDT-2	X		X		X	1,000	16,100	
23	MARLIN 1	X		X			1,900	11,300	

Table 3.1 List of logs available for each well in this study.

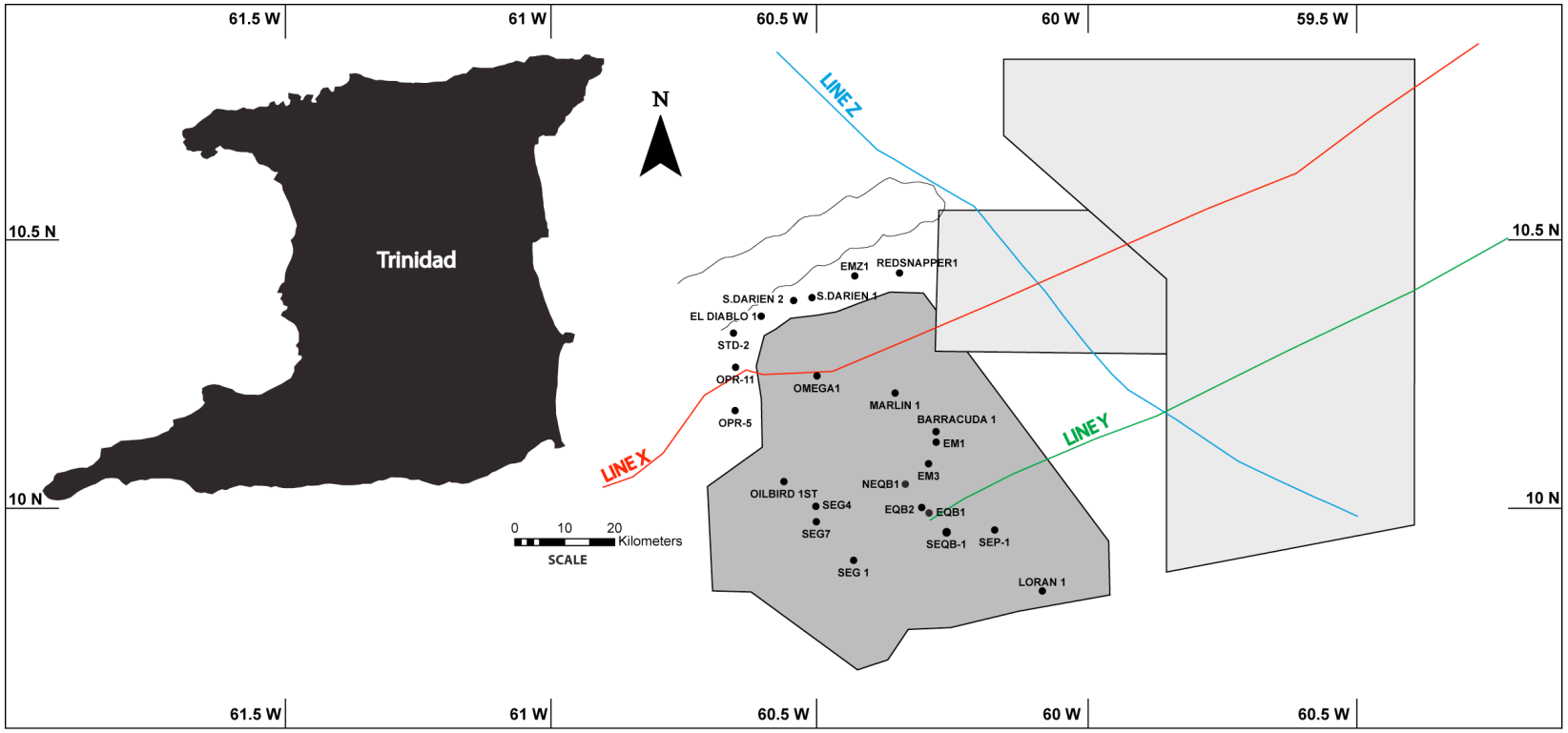

Figure 3.1 Location of the wells and 3D seismic mega-merge layout.

3.1.2. Biostratigraphic Data

Biostratigraphic information, including faunal and floral charts were available for analysis in 21 wells within the study area. The biostratigraphic information was useful to elaborate a detailed interpretation of depositional environments within the study area. The importance of shifts in depositional environments to defining shelf edge locations has been previously discussed, therefore it is important to review the basis for the definition of these depositional settings here.

Palynomorphs, include pollen and spores, as well as dinoflagellate studies were available to the author. Palynomorphs have some limitations when it comes to establish water depths but the presence of pollen and spores can indicate the dominance of marginal marine to continental paleoenvironments. Alternatively, the presence of dinoflagellates indicates a greater influence of marine conditions (Pocknall et. al, 1995). Benthic foraminifera are very good indicators of water depths, certain benthic species and assemblages can be used to identify paleoenvironments ranging from brackish estuaries to deep-water deposits providing relative water depths values.

Pocknall et al. (1995) compiled data from over 40 wells (a study that included all the 23 wells in this thesis work) that were drilled in the Columbus basin since 1965. Analyses of palynomorph abundance, diversity and specific age diagnostic occurrences were made from cuttings, sidewall cores, and conventional core for these wells. In addition faunal data, foraminifera abundance, diversity and age specific faunal were collected dominantly from well cuttings on 30 foot intervals. Palynological samples collected from cuttings were acquired every 90 to 200 feet (Pocknall et al., 1995). Sidewall core and conventional core analysis yielded much better control on the actual distribution of fauna and flora for age control purposes. However, cuttings samples can

provide extremely useful and much more extensive data if properly filtered for downhole contamination and stratigraphic reworking. Documention of casing points allowed for improved credibility of downhole data immediately beneath such points.

Identification of first and last occurrences of biostratigraphic assemblages were of great importance to define paleoenvironments and relevant stratigraphic surfaces. Sudden changes in sea level generated regional unconformities within the basin that were frequently related to the first downhole occurrence of some benthic foraminifera. (Pocknall et al., 2001). Due to their lateral continuity, these unconformities can be correlated and interpreted on neighbor wells along strike, however the presence of northwest-southeast growth faults added an additional level of complexity for the correlations when trying to extend these horizons in the dip direction.

There are several complications that can hinder the paleoenvironmental and age significance of the available biostratigraphic data: (1) Due to active thrusting during the Plio-Pleistocene, biostratigraphic assemblages could have been reworked from higher relief areas (e.g.: Darien Ridge, Northern and Southern ranges of Trinidad, etc) and "misplaced" into younger stratigraphic successions, (2) High energy deltaic systems could have also transported original biostratigraphic assemblages that were "in situ" into more distal locations (allochthonous material) and (3) Thick underconsolidated sequences deposited as a result of high sedimentation rates are of common occurrence within the study area causing downhole caving while drilling and subsequent contamination of the biostratigraphic samples (Pocknall et al. 1995, 2001). As a consequence, a meticulous revision of the foraminifera and palynological data, in conjunction with a detail documentation of the occurrence of casing points and the interpretation of well log motifs were crucial to refine the interpretation of depositional environments in the study area.

3.1.2.1 Depositional Environments

The interpretation of depositional environments was performed by integrating biostratigraphic data and well log motifs (Pocknall et al., 1995). Figure 3.2 shows the main depositional environments that were interpreted in this work, from proximal to distal: (1) Distributary channel and Delta plain, (2) progradational shoreface, (3) Channel/Levee system, (4) basin floor fans and (5) deep-water condensed section (Pocknall et al., 1995 and 2001). In the following section, a brief description of the main characteristics for each paleoenvironmental succession is provided.

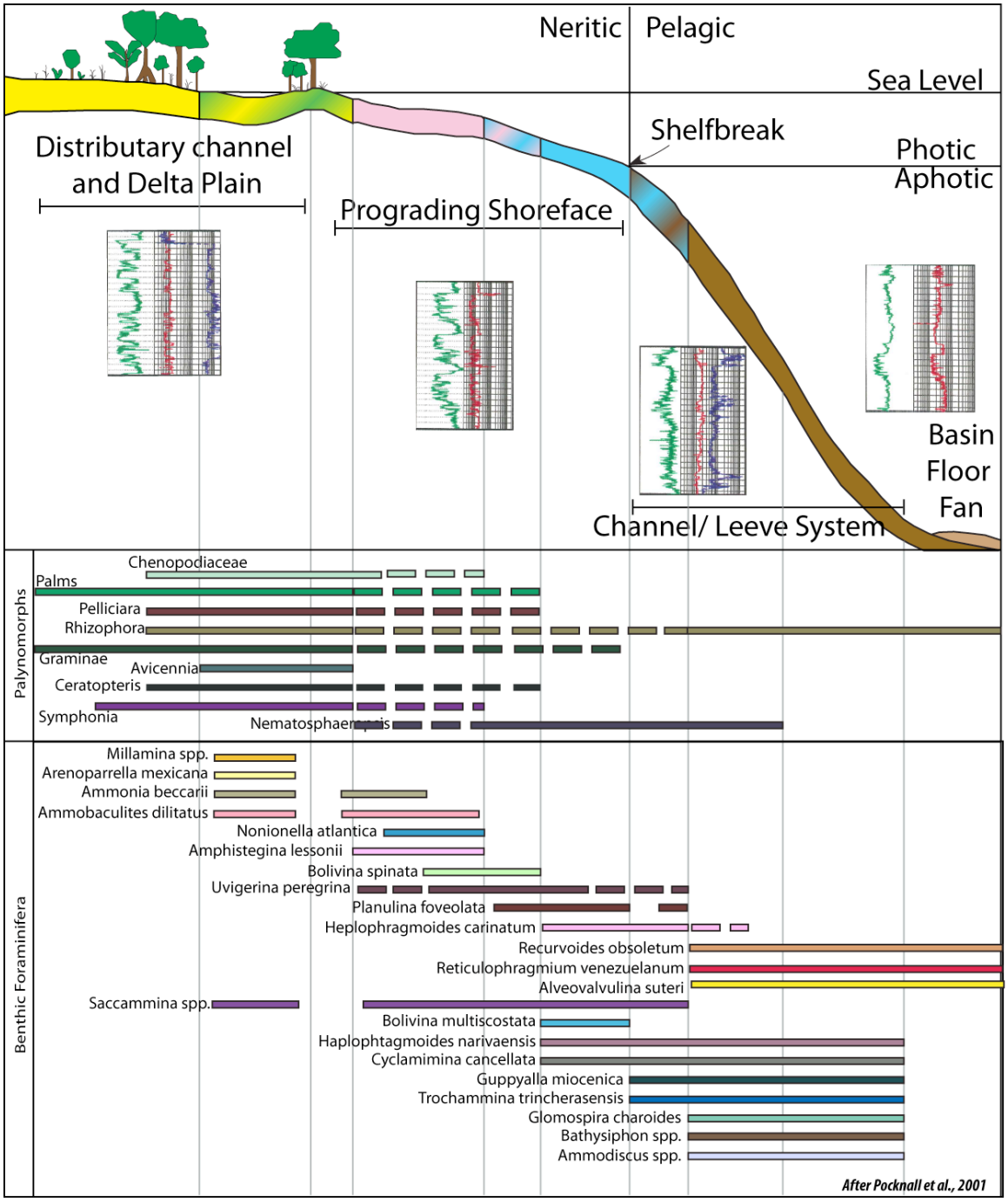

Figure 3.2. Depositional Environments based on foraminifera and palynomorphs data and log motif. The figure illustrates a coastal to deep marine profile and the corresponding palynological data that allowed defining the environments (After Pocknall et al., 1995 and 2001).

3.1.2.1.1 Distributary channel and Delta plain

Reservoirs that are composed of distributary channel and delta plain facies are characterized by presenting high porosity and permeability values. These paleoenvironments are deposited either subaerially or within the zone of tidal influence (Pocknall et al., 1995). Fluvial environments (yellow zone in figure 3.2) comprise active and abandoned channel fills, floodplain, and swamp deposits. Transitional barrier complexes (yellow-greenish zone in figure 3.2) can contain estuarine, lagoonal, beach, marshes and tidal flat environments (Pocknall et al., 1995.

Distributary channel and Delta plain facies tend to preserve palynomorphs that derived from the vegetation growing along the coastal margin and within the immediate vicinity. Some of the associations that are present within these systems include mangrove pollen (derived from *Rhizophora, Avicennia and Pelliceria*), swamp plant pollen (Symphonia and Ceratopteris), swamp marsh grasses (*Gramineae*), palms and chenopodiaceae pollen in addition to benthic foraminifera (*Miliammina telemaquensis, Arenoparrella mexicana, Ammonia beccarii,* and *Ammobaculites dilitatus)*. This biostratigraphic association is indicative of brackish and hypersaline environments, as well as of modern beach and tidal flats (Pocknall et al., 1995).

Blocky and sometimes fining upward well log motifs are common and indicative of stacked braided or meandering fluvial and estuarine channel sands (100 to 300 feet thick), bayhead deltas, or estuarine mouth bars. The sands, within these facies, are well sorted and often unconsolidated (Pocknall et al., 1995).

3.1.2.1.2 Prograding Shoreface

The prograding shoreface facies contain lower, middle, and upper shoreface sub-facies that were deposited below sea level within the zone of wave influence (Pocknall et al., 1995).

Amphistegina lessonii, Nonionella atlantica, and *Bolivina spinata,* and in the most brackish portions *Miliammina* and *Arenoparrella Mexicana,* populate the lower sub-facies (pink zone in figure 3.2). *Amphistegina lessonii* indicates water depths ranging from 60 to 180 feet, characteristic from inner shelf and sandy bottom conditions (Pocknall et al., 1995). The middle shoreface sub-facies (blue-pink zone in figure 3.2) presents a gradual increase in *Uvigerina peregrina* which occurrence is typically related to shelfal conditions where sand deposition and salinity fluctuations are uncommon. The upper shoreface sub-facies (blue zone in figure 3.2) are characterized by the presence of *Bulliminella spp., Planulina foveolata,* and *Bolivina multicostata* which modern corresponding species are often associated with active prograding deltas.

The well log motifs within the prograding shoreface tend to exhibit a coarsening upward pattern indicating increasing sand content as the shoreline progrades basinwards (Pocknall et al., 1995). These prograding shoreface facies are often times composed of stacked sandstone bodies and form the most laterally continuous and thickest reservoir units within the Columbus Basin. The tops of these shoreface-stacked packages are frequently sharply truncated by shale units or by lagoonal muds indicating a temporary and relatively rapid deepening that affects the outer shelf / upper slope area until the next progradational pulse takes place. Deepening or transgressive events inundating the shoreface can be associated with high-frequency sea level fluctuations during the Plio-Pleistocene and/or increased accommodation space associated with the reactivation of growth faults located within the shelf margin region (Pocknall et al., 1995).

3.1.2.1.3 Channel/Leeve system

These facies are deposited in water depths ranging from 600 to 3,000 feet (Pocknall et al., 1995) and include deposits on the slope (brown zone in figure 3.2) and levee channel complexes (brown-blue zones in figure 3.2). Palynomorphs are not common in these facies, with the exception of *Rhizophora* pollen, which is probably present as reworked material. The slope deposits (brown zone) can contain foraminifera that include *Guppyella miocenica, Trochamina trincherasensis,* and *Cyclammina cancellata,* while levee-channel deposits can also contain *Haplophragmoides carinatum, Haplophragmoides narivaensis, Bathysiphon spp.,* and *Reticulophragmium venezuelanum* (Pocknall et al., 1995).

The well log motifs for these facies tend to be serrate showing high frequency intercalations of sand and shale. The sandier intervals tend to show an initial coarsening upward log motif that then reverses into a fining upward log motif toward the top (see figure 3.2). These reservoir types are of high quality and can reach thicknesses in excess of 1,000 feet (Pocknall et al., 1995).

3.1.2.1.4 Basin Floor Fan

Basin floor facies are generally deposited in water depths that are greater than 3,000 feet in the Columbus Basin (Pocknall et al., 1995). Due to reworking caused by transport from the outer shelf and upper slope region, biostratigraphic assemblages within these intervals are a mix of middle to outer neritic foraminifera and *in situ* deep water agglutinates. A distinctive foraminifera assemblage for this facies includes the presence

of *Recurvoides obsoletum, Cyclammina cancellata, Ammodiscus spp*., and *Alveovalvulina suteri*.

Well log motifs for this facies are characterized by the presence of a sharp base that transitions into a blocky to slightly saw-like log motif (Pocknall et al., 1995). These motifs indicate rapidly deposited sand rich sediments. These facies form excellent reservoir/seal relationships in the subsurface in the eastern offshore gas fields of the Columbus Basin (Pocknall et al., 1995).

3.1.2.1.5 Deepwater Condensed Section

These facies are deposited during marine flooding events when most of the active sedimentation processes retreated to the inner shelf (Pocknall et al. 2001). The biostratigraphic assemblages usually contain *Glomospira charoides, Alveovalvulina suteri,* and *Reticulophragmium venezuelanum*. The last two forams are believed to have lived in the paleo Columbus Basin under bathyal conditions (Pocknall et al., 1995). Low resistivity and high-gamma ray characterize well log motifs within these facies (Pocknall et al., 1995).

The following table summarizes the most important aspects of each depositional environment as defined by Pocknall et al. (2001) for the Columbus Basin (See table 3.2).

Facies	Depositional Environment	Log Motif	Reservoir Quality
Distributary channel and Delta plain	Deposited either subaerially or within the zone of tidal influence. Distributary chanel and delta plain: active and abandoned channel fills, floodplain, and swamps. Barrier: estuarine, lagoonal, beach, marshes and tidal flat.	Blocky or occasionally fining upward motif representative of stacked, braided or meandering fluvial and estuarine channel sands (100 to 300 feet thick), bayhead deltas, or estuarine mouth bars.	High porosity and permeability reservoirs throughout the Columbus Basin.
Prograding Shoreface	Deposited while submerged below sea-level and within the zone of wave influence	Coarsening upward sequence. The top of the prograding shoreface complex is often sharply truncated.	Laterally continuous. Thick reservoir units
Channel/Leeve system	Water depths ranging from 600 to 3,000 feet	Serrate, sand-shale log character, fining upward.	High-quality reservoirs with thickness up to 1,000 feet.
Basin Floor Fan	Very deep water (>3,000 feet) near the toe of the continental slope.	Sharp to sharply gradational base in well logs, and consist of several packages, often as thick as 100 feet, each with a blocky to slightly saw-like log motif.	Excellent reservoir/seal relationships.
Deepwater Condensed Section	Deposited during a marine flooding event and possibly a period of quiet sedimentation	Low resistivity logs, high gamma ray shales, and increased abundances of planktic	

Table 3.2 Description of Depositional Environments within the Columbus Basin

3.1.2.2 Age Control

The main age control markers within the Columbus Basin are: (1) extinction of *Grimsdalea Magnaclavata* in the Early Pleistocene, (2) the first appearance of *Alnipollenites verus*, which define the the base of the Pleistocene and it has been called by biostratigraphers in the Columbus Basin as the Pliocene – Pleistocene boundary (Pocknall et al., 2001) and (3) the first appearance of *Globorotalia truncatulinoides* that defines the base of the Pleistocene (Pocknall et al., 1995; Wood, 2000). The occurrences of *Grimsdalea Magnaclavata* and *Alnipollenites verus* have also been reported within the Eastern Venezuelan Basin (EVB) located to the west of the study area. Figure 3.3 shows

the age ranges for palynomorphs and foraminifera indicators for the EVB and since the Columbus Basin represents the eastern continuation of the EVB the same biostratigraphic indicators can be used within the study area to establish age control.

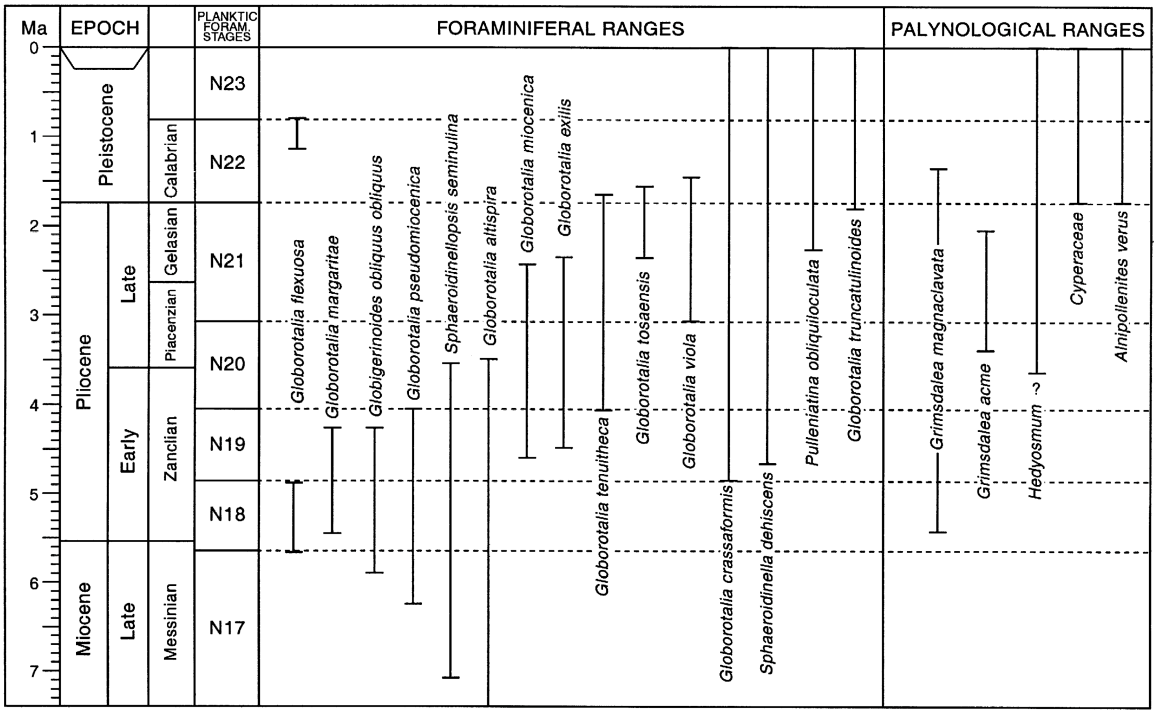

Figure 3.3. Foraminifera and Palynomorph age ranges in the Eastern Venezuela Basin (Wood, 2000)

Grimsdalea magnaclavata was of common occurrence in northern South America during parts of the Late Miocene and Pliocene. The peak occurrence of *Grimsdalea magnaclavata* was from 2.5 to 2.1 Ma (Late Pliocene) and it was extinct (possibly due to climatic changes) somewhere between 2.1 to 2.0 Ma during lowstand conditions (Haq et

al., 1987 in Pocknall et al, 2001). However, Pocknall et al. (2001) have suggested that the extinction of *Grimsdalea magnaclavata* actually occurred around 1.3 Ma in the EVB.

Alnipollenites verus is present in most of the wells that have been drilled in the Columbus Basin. This specie has been associated with the Andean vegetation forest belt (Van der Hammen, 1974 in Pocknall et al., 2001) indicating that there was in fact a change in the Orinoco river trajectory as discussed by Diaz de Gamero (1995). Biostratigraphers have agreed to define the first appearance of *Alnipollenites verus* as the base of the Pleistocene in the Columbus Basin (Pocknall et al., 2001) (See Figure 3.3). It has been reported that *Avicennia* (also indicator of Distributary channel and Delta plain environments) (see figure 3.2) appears at the same time as the Alnus pollen so that both indicators can be used to define the base of the Pleistocene (figure 3.3). The first appearance of *Globorotalia truncatulinoides* also coincides with the base of the Pleistocene and peaks on its abundance have been used to identify a 1.2 Ma flooding event that seals a major period of clastic wedge progradation and reservoir development across the basin (Pocknall et al., 2001).

3.2 DATA INTEGRATION AND INTERPRETATION

3.2.1. Well Log and Biostratigraphic Integration

Four paleoenvironments have been defined in the study area based on the definition of biostratigraphic assemblages and well log motifs (see figure 3.2): (1) Distributary channel and Delta plain, (2) prograding shoreface, (3) Channel/Leeve system and (4) basin floor fans (Pocknall et al., 1995). In addition, Wood (2000) elaborated a chronostratigraphic framework and a sequence stratigraphic interpretation based on well log patterns, depositional facies shifts, biostratigraphic data and location of the wells with respect to the shelf break (her figures 7, 10 and 16). This author used the megadepositional sequence definition as "genetically related strata bounded by regionally unconformable surfaces and their basinwards correlative conformities" to define the sequences (Wood, 2000). Each megasequence can average 10,000 to 12,000 ft in thickness and it usually contains an entire suite of sequence tracts (LST, TST and HST) (Wood, 2000). In this thesis, the original bounding surfaces that Wood (2000) used to define the base and top of individual sequence stratigraphic units were preserved to define the top and base of cycles. However, the use of traditional sequence stratigraphic units is difficult because the identification of traditional system tracts (LST, TST and HST) within the shelf break region (focus of this study) is somewhat cumbersome. For purposes of this net sand distribution analysis it was decided to consider the deltaic portion of the shelf transit cycle, against the marine portion of the shelf transit cycle, since one of our hypotheses is that marine currents bring significant volumes of fine-grained sediments along the margin. For simplicity we will use the nomenclature of T to represent the marine portion of the shelf transit cycle (transgressive

and early highstand, in systems tract nomenclature) and R to represent the deltaic portion of the shelf transit cycle (late highstand and lowstand in systems tract nomenclature).

Figure 3.4 shows the criteria that were used to define the T-R cycles: (1) the base and top of the T-R cycles are define by unconformable surfaces or their basinward correlative conformities as defined by Wood (2000), (2) the marine portions of the cycles were defined by identifying fining upward trends then below wave base coarsening up in the well logs (blue triangles on figure 3.4), (3) the deltaic portions of the cycles were defined by identifying the coarsening upward or blocky trends in the well logs (red triangles on figure 3.4) and (4) the turn around point between the deltaic portions of each cycle and its overlying marine portion was considered to define the transgressive surface (5) the break between the underlying marine portion of each cycle and the overlying deltaic portion of each cycle was considered to be in some instances the lowstand unconformity, and in other instance the regressive surface of marine erosion, depending on the magnitude of shallowing across this boundary.

Once the T-R cycles were picked in each well, several cross-sections (see Figure 3.5 and 3.6) were interpreted to tie the correlative surfaces and unconformities throughout the area. The surfaces were labeled alphabetically from B to P, or younger to older, respectively. For the purpose of this study, only six shelf transit cycles were analyzed within the Pliocene to recent stratigraphic succession. Shelf edge trajectories for each of these six T/R cycles were also mapped (See Section 3.2.3 for more details) and named from younger to older as shelf margins (surfaces) D, E, F, H, J and N.

Cycles between the previous named surfaces were also defined in order to study the long-term relationship of these intervals and were labeled from younger to older as C1, C2, C3, C4, C5 and C6 (See figure 3.6)

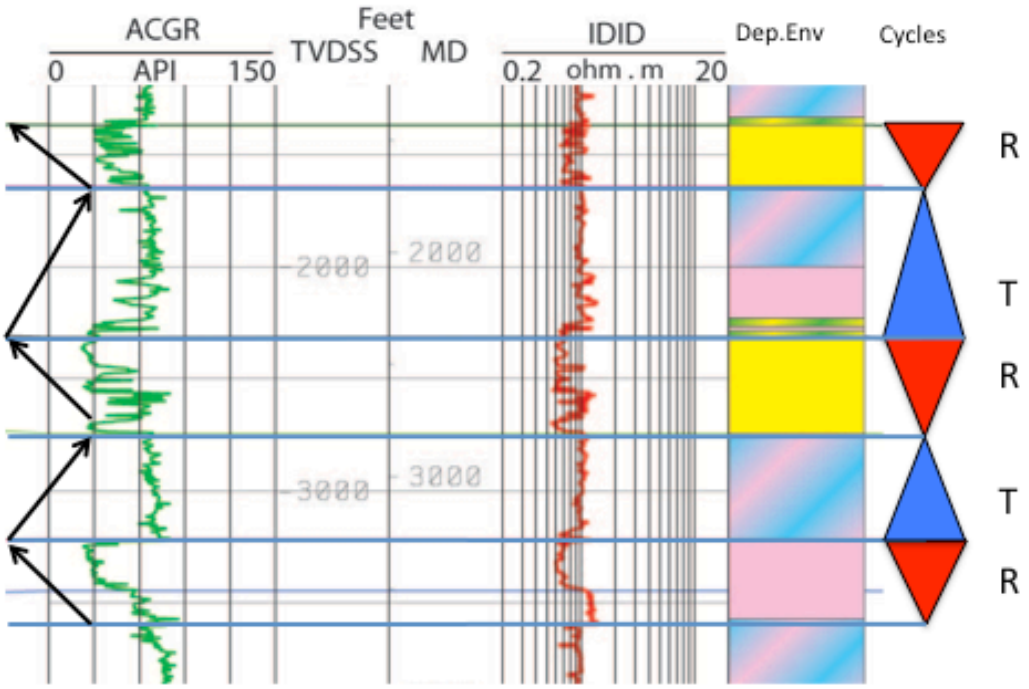

Figure 3.4. Picking of T and R cycles. On the left side, black arrows indicate the log pattern in the gamma-ray log. The next column corresponds to the resistivity log, and the colored column corresponds to the depositional environment, which colors are related to figure 3.2. Finally, blue and red triangles show the extension of the T and R cycles, respectively.

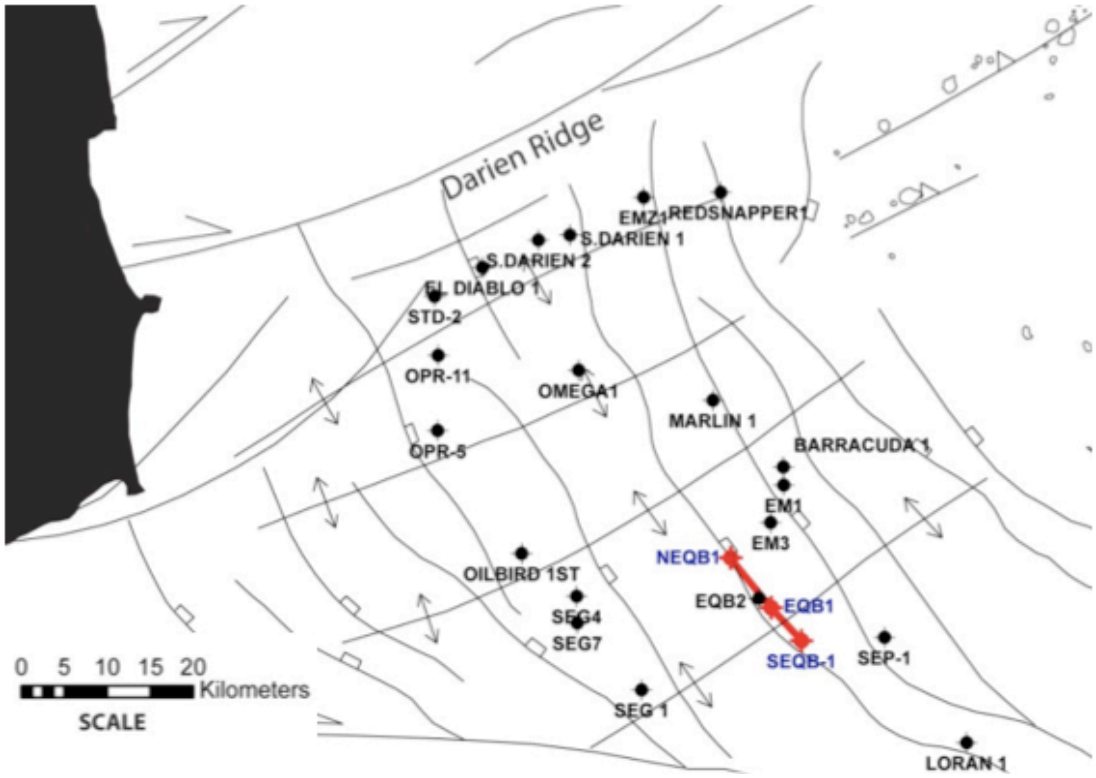

Figure 3.5. Location of the cross-section shown in figure 3.6. The along strike cross-section shows the tie between wells NEQB-1, EQB-1 and SEQB-1.

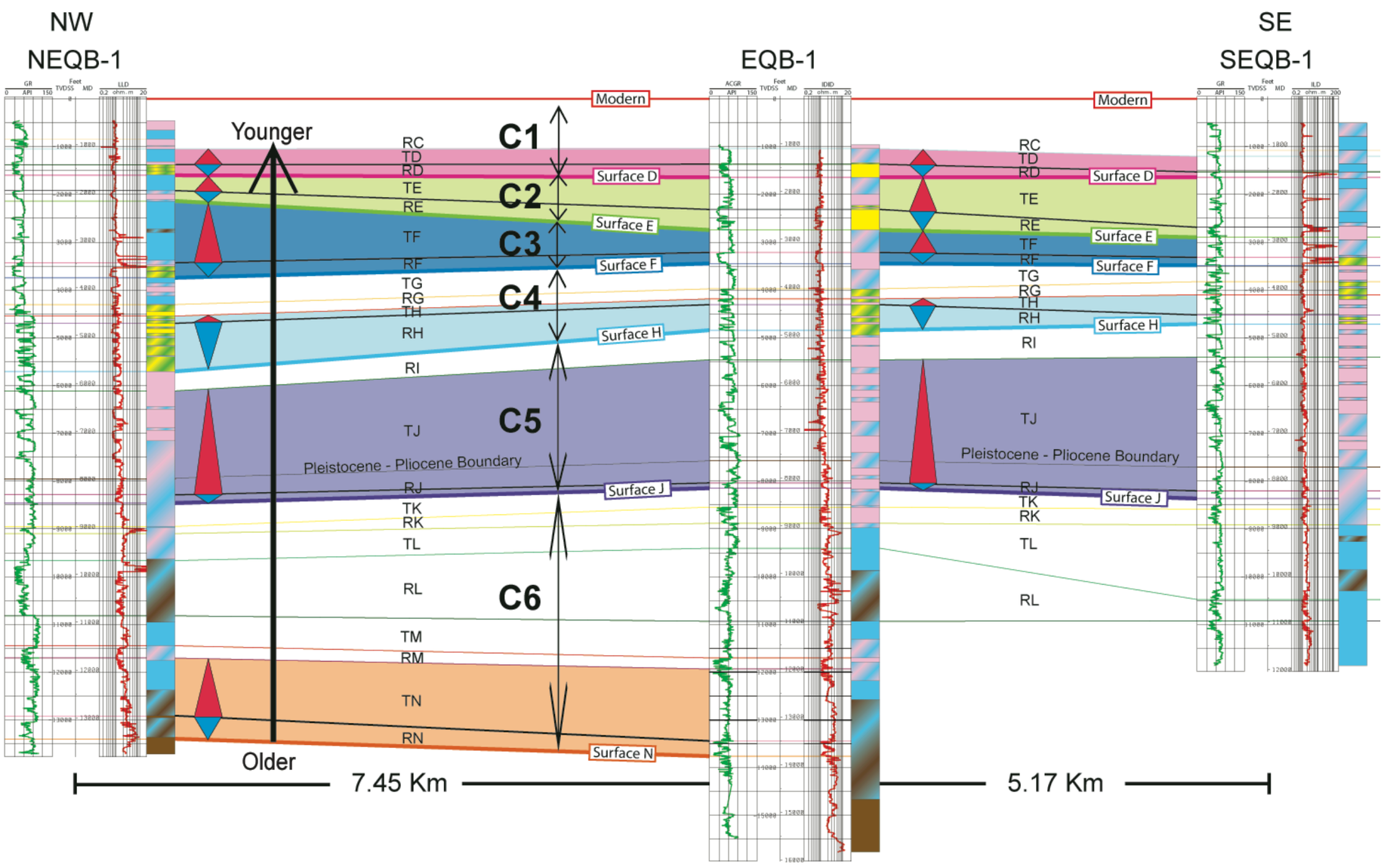

Figure 3.6. Cross-section along strike from wells NEQB1, EQB-1 and SEQB1. Location of this section is shown in figure 3.5. Colored column to the right of each well correspond to the depositional environment interpretation according to key shown in figure 3.2. Colored intervals correspond to the ones analyzed in this research from younger to older: D, E, F, H, J and N. C1 to C6 correspond to long-term cycles.

3.2.2. Calculating Net-to-Gross

The Net-to Gross (NTG) ratio is defined as the ratio between the net sand thickness and the total thickness of a stratigraphic interval as expressed by the following formula.

$$\text{Net-to-Gross Ratio (\%)} = \frac{\text{Net-Sand}}{\text{Total Thickness}}$$

In order to measure the net sand for each interval, a sand cut-off for the gamma-ray logs was chosen. Figure 3.7 shows a partial record of the well NEQB-1, illustrating the sand cut-off selected for the gamma-ray log. Values that are lower than the define cut-off on the gamma ray indicate sand content, these thicknesses are added and included as part of the net-sand measurement. It is important to mention that none of the gamma ray logs were normalized and therefore the sand cut-off values were variable from well to well. Table 3.3 lists the different sand cut-off values that were used by well.

Net-to-gross (NTG) ratios were calculated for the marine and deltaic components of the T-R cycles and then plotted against total thicknesses and net-sand values. The NTG versus total thickness plots seek to understand how sand content vary within T and R cycles and how these variations evolved through time. In addition, NTG trends were mapped for each T-R cycle and analyzed based on the proximity of the wells to the corresponding shelf break. The objective of these maps was to determine if there was a relationship between the proximity to the paleo shelf edge and the sand content, as well as to try to establish potential controlling factors.

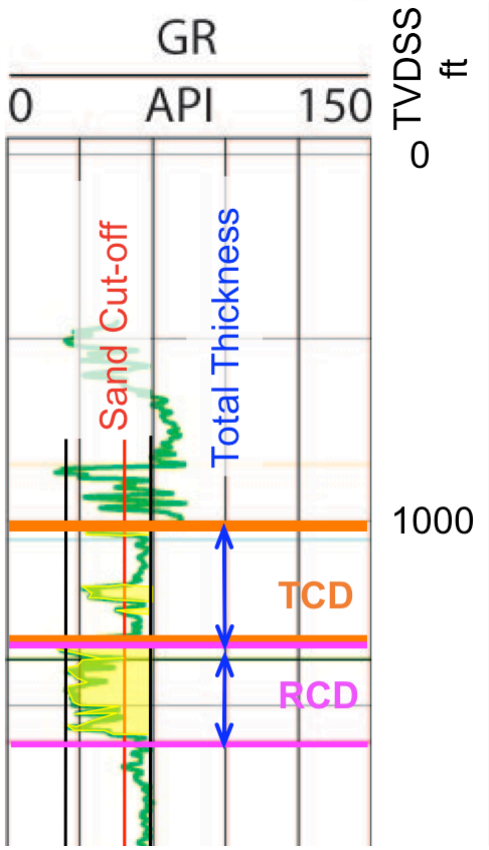

Figure 3.7. Extract of NEQB-1 well log that illustrates the cut-off for determining sand within each interval. Total thickness of each cycle is indicated in blue, while net sand thickness is colored in yellow.

WELL	SAND CUT-OFF (gAPI)	NOTES
STD-2	75	
EL DIABLO ST-1	75	
S.DARIEN 2	55	
S.DARIEN 1	50	65 for Interval N
EMZ1	65	
RED SNAPPER 1	55	
OPR-11	65	
OPR-5	50	
OILBIRD 1	60	
SEG4	60	
SEG7	60	
SEG1	60	
OMEGA 1	65	50 for Interval E
NEQB1	60 for 0 to 4,200 ft	75 for 4,200 ft to 15,000 ft
EQB2	60	
EQB1	60	
SEQB-1	60	
Marlin 1	75	
Barracuda 1	66	
EM1	72	
EM3	75	
SEP-1	72	
LORAN1	70	

Table 3.3 Sand Cut-off values applied for each well to discriminate between sand and shale

3.2.3. Defining the Location of Shelf Edges for each Cycle

The shelf edge region can be defined as the intersecting area between the outer shelf and the upper part of the slope. The shelf edge region can also be recognized by successive increases in slope angles as the outer shelf / upper slope transition occurs and by a rapid deepening in the basinward direction (increase of water depths).

Defining the actual edge of shelf in the series of stratigraphic cycle packages that fill the Columbus Basin is a challenging problem. The density of faulting, abundance of shallow gas impacting seismic imaging, sparsity of well data, large amount of thickening across faults, and thus a subsequent lack of high resolution in biostratigraphic data all combine to leave error within even the most integrated interpretation (see Wood, 2006 and Sydow and Bowman, 2003 for a fuller explanation). In addition, the high sediment supply and aggradational nature of many of the late highstand/lowstand deltaic packages mean that downlap in seismic does not occur on a spatial frequency that leaves one able to identify it easily without significant palinspastic reconstruction of each cycle. We did not have the data necessary to do such a reconstruction for each cycle. Therefore, for purposes of this study, it was decided not to re-invent the wheel but rather to utilize the previous work of Wood (2000), Pocknall et al., (2001), Sydow and Bowman (2003), Bowman (2003), Moscardelli et al. (2006), Maher (2007), and Alvarez (2008) (See Appendix B) as a framework upon which to build and make adjustments to previously defined shelf edge locations. The observations of previous workers were integrated with available well coverage, including log motif and stacking patterns, available biostratigraphic information (see authors mentioned above), regional 2D seismic and 3D seismic (in the shallowest intervals) to arrive at a defensible shelf edge location for each of the cycles under study. Changes in gross depositional settings (ie., deltaic to fully

marine) between wells in the dip direction were used to bound the general location of the shelf edge for any one cycle (See Appendix B6 to B10). In most instances, spacing in the dip direction between control wells is several 10's of kilometers. It was noted by both Wood (2000) and Sydow and Bowman (2003) that the shelf edge of any specific age in this basin is often very close to its time equivalent deltaic aggradational front. This observation, made by the previous authors with substantially more data than available to this thesis, was considered in placement of shelf edge locations.

As part of this research some of the original interpretations were adjusted to increase accuracy for some of the intervals where discrepancies were identified. Figure 3.8 shows a map that compiles the shelf edge locations for the six T-R cycles that were under study as part of this research. The shelf-edge trajectory corresponds to the base of the R cycle (base of the interval). The location of the modern shelf edge was defined by using a compilation map of the seafloor (Sullivan 2005, Moscardelli 2006, Maher 2007, Alvarez 2008. See Appendix B1). Surface D in this study is equivalent to the base of mass transport deposit MTC_1 as defined by Moscardelli et al. (2006) and therefore shelf edge D was defined using this surface (MTC_1) (See Appendix B2).

The shelf edge map shown in figure 3.8 allowed measuring progradational distances between successive intervals. The progradational rates were then compared with aggradational rates that were calculated from the cross sections where the total thickness of each cycle (including T and R units) was taken as the main aggradational value. Last, an ArcGIS database was built that included structural and tectonic interpretations, as well as the shelf edge trajectories for the different intervals and net-to-gross and thicknesses values.

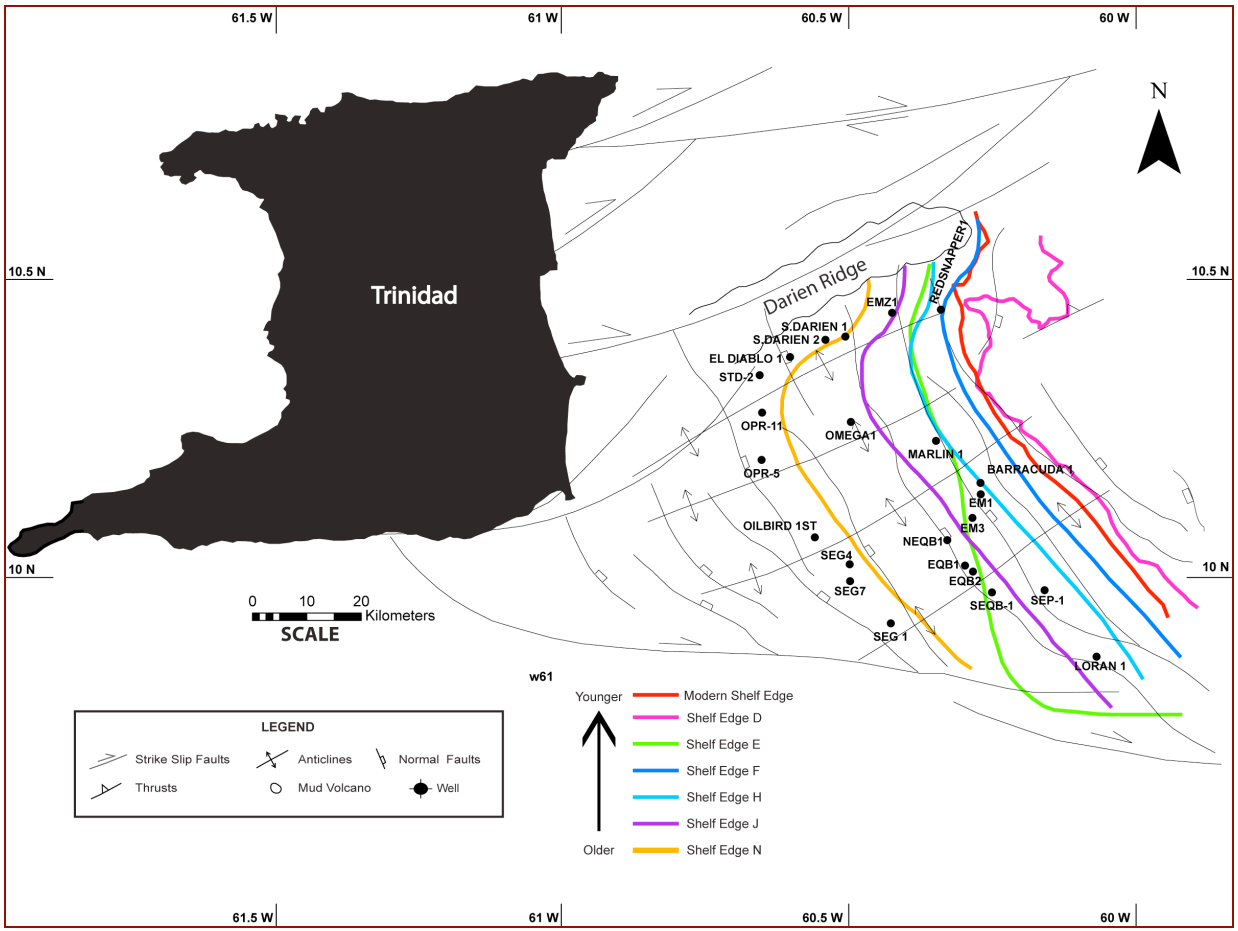

Figure 3.8 Compilation of shelf-edge trajectories. N, J, H, F and E were mapped from well logs, while D and modern shelf-edge were mapped from seismic data. Shelf-edge trajectories migrate NE across the Columbus Basin through time. This migration is closely related to the evolution of the paleo- Orinoco shelf edge delta.

Chapter 4: Sand Distribution along Shelf-edge Deltaic Systems

4.1 SHELF-EDGE TRAJECTORIES ANALYSIS

4.1.1 Age control for cycles used in this research

Table 4.1 shows the age control for the key surfaces interpreted throughout the Columbus Basin and that are used in this study. The chronostratigraphic framework was established by using foraminifera and palynomorph data (see Chapter 3) as interpreted by Wood (2000) to assign age control to the base of the R cycles. More recent work by Moscardelli et al. (2006) established that surface "D" was in fact slightly older than 18,000 yr and not 0.8 my as originally estimated by Wood (2000). Surface "D" is slightly older than the Last Glacial Maximum Lowstand (LGML) surface (Moscardelli et al., 2006). These surfaces define the base of R cycles that have time durations that range between 200k and 1 my (Milankovitch fourth order cycles).

Table 4.1 lists the surfaces and their corresponding age.

SURFACE	AGE
Modern	0 m.y.
"D"	Older than 18,000 yr (Wood, 2000 established 0.8 my)
"E"	1.0 m.y.
"F"	1.3 m.y.
"H"	1.5 m.y.
"J"	1.8 m.y.
"N"	2.0 m.y.

Table 4.1 Age control for cycle of interest in this research. All ages come from Wood, 2000, except for cycle "D", which age is constrained by Moscardelli et al., 2006.

4.1.2 Shelf-edge trajectories through time

Figure 4.1 shows the paleo shelf break location (base of the T-R cycle) of the six T-R cycles that were defined in this work; the map clearly shows that in general shelf-edge trajectories (SETs) migrated northeasterly from older ("N" – orange) to younger ("Modern" – red) across the Columbus Basin (except for shelf-edge trajectory "E"). shelf-edge trajectory "E" defines the only major retrogradational event along the shelf indicating a period of transgression. There is a smaller retrogradational event from shelf-edge trajectory "D" to shelf-edge trajectory "Modern". These retrogradational events could also be explained, as the delta did not reach the previous shelf-break because a diminishment in sediment supply.

This progressive shelf-edge migration is reflecting different periods of progradation and retrogradation across the shelf associated with the evolution of the paleo-Orinoco delta system during Pliocene to Recent time. Figure 4.1 also shows that shelf-edge trajectories are aligned parallel to the strike direction of growth faults within the southern structural domain (SSD) while they deflect to the northeast near the Darien Ridge where transpressive faults are the dominant structural element. It is also worth mentioning that the retrogradational event associated with shelf-edge trajectory "E" (light green trajectory on figure 4.1) reached a more landward position within the SSD where growth faults created more accommodation space allowing for a broader inundation of the outer shelf. The following progradational event from shelf-edge "E" to "D" (Sequence C2) was also more pronounced to the south suggesting that the sediment supply in this region was high enough to prompt a rapid advance of the shelf edge. The changes in orientation associated with Shelf-edge trajectories within the NSD and SSD and the impact that the character of the structures along the margin (e.g: growth faults) has on the creation of additional accommodation space suggest that shelf-edge

trajectories can be strongly influenced by underlying structural variations along the continental margin region.

The distances between successive shelf-edge trajectories were measure along two transects located within the shelf region of the Columbus Basin in order to illustrate the character of the progradational and retrogradational patterns within the Pliocene to Recent stratigraphic succession (figures 4.1 and 4.2). The northern transect was positioned within the NSD where transpressive structures are dominant while the southern transect was located in the SSD where growth and counter regional faults are the dominant structural elements (figure 4.1. red and green-dashed lines, respectively). Progradational distances and cumulative values for shelf-edge trajectories are shown in table 4.2. Because the shelf-edge location for surfaces E, F, J and N were mapped from well logs, there is an error associated to these progradation/retrogradation distances, which range from 5 to 15 kilometers.

				PROGRADATION/RETROGRADATION DISTANCE (KM)			
SEQUENCE	**SURFACE FROM - TO**	**AGE BASE**	**AGE TOP**	**NSD**	**CUM. DIST.**	**SSD**	**CUM. DIST.**
C1	D TO M	0.025*	0	-3	36	-2.9	35.2
C2	E TO D	1.00	0.025	13.5	39	20.5	38.1
C3	F TO E	1.30	1.00	-6.5	25.5	-14	17.6
C4	H TO F	1.50	1.30	6	32	5.9	31.6
C5	J TO H	1.78	1.50	10	26	8.7	25.7
C6	N TO J	2.00	1.78	16	16	17	17

Table 4.2 Shelf-edge progradational distances and cumulative values through time for the NSD and SSD. First three columns list the name of the sequence (see also figure 4.21) and the age of their lower and upper boundary. The remaining columns indicate the progradational or retrogradational distances that were measured along the northern and southern transects (figure 4.1). "M" stands for the modern shelf-edge trajectory. Positive and negative values indicate progradation or retrogradation respectively. Age for surface "D" was assigned arbitrarily for the purpose of this exercise (slightly older than 18ky).

Figure 4.2.a shows the measured progradation distances between successive shelf-edges for both the northern and southern transects while figure 4.2.b shows a cross-plot for age versus cumulative progradational/retrogradational rates.

Figure 4.2.a clearly shows the magnitude of the variabilities associated with the progradational and retrogradational rates of shelf-edge trajectory within the NSD (red bars) and the SSD (green bars). Some of the observations that can be made based on the trends observed in figure 4.2.a are: (1) The rates of progradation for Sequences C6, C5 and C4 in the NSD and SSD are similar showing variations that are less than 1.5 km, (2) There is a significant landward retreat of the shelf-edge associated with the T portion of Sequence C3 (3) The magnitude of the retrogradation in Sequence C3 (from shelf-edge trajectories "F" to "E") was twice as much in the SSD than in the NSD and this difference was tectonically dominated, (4) The progradational episode that followed the Sequence C3 was greater on the SSD than in the NSD and this difference was associated with an increase on sediment supply and the availability of accommodation space on the growth fault domain (SSD) and (5) the magnitude of the last retrogradational event (C1) seems to be equal both in the NSD and SSD.

Figure 4.2.b shows the cumulative progradational/retrogradational values for shelf-edge trajectory through time. Cumulative distances were plotted against the age of

each surface (Wood, 2000 and Moscardelli et al., 2006). The cumulative plot shows that progradational rates for Sequences C6, C5 and C4 were very similar within the SSD and NSD indicating that sediment supply was relatively uniform across the basin as well as its relationship with the available accommodation space within both structural domains. However, for Sequence C3 there is an inversion of the slope and a clear divergence between the cumulative curves indicating the occurrence of a strong retrogradational event that was also more pronounced on the SSD (figure 4.2.b). The continue divergence of the cumulative curves for the next progradational pulse (Sequence C2) and the steeper slope of the cumulative curve associated with the SSD (green curve) also indicates that the progradational rates were greater in the SSD suggesting higher sedimentation rates affecting this area for this time interval. Finally, the last transgressive event (Sequence C1) seems to indicate that the rates at which the shelf-break was migrating landward were again similar both in the NSD and SSD (figure 4.2.b). Variations observed in the cumulative progradational curves are associated with variations on sediment supply, accommodation space (influence by underlying structural controls) and relative sea level fluctuations.

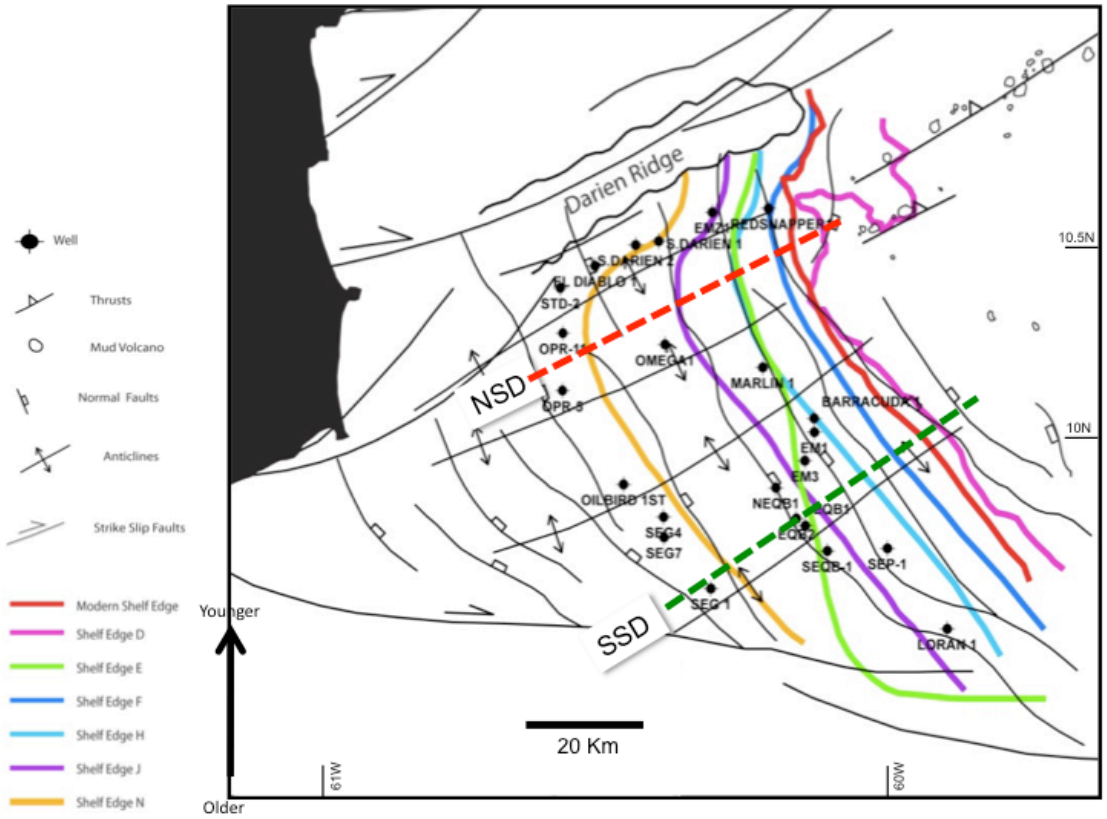

Figure 4.1. Compilation of Pliocene to Recent shelf-edge trajectories along the Columbus Basin. shelf-edge trajectory migrate NE across the Columbus Basin through time. This migration is closely related to the evolution of the paleo-Orinoco shelf edge delta. Two profiles were drawn along dip to illustrate the along strike and along dip variability of shelf-edge trajectory progradation. Red dashed line for Northern Structural Domain and green dashed line for Southern Structural Domain.

Figure 4.2.a Progradational and retrogradational variations along dip within the NSD (red bars) and SSD (green bars) (see figure 4.1 for location). Progradational rates decreased progressively from Sequences C6 to C4 as the paleo Orinoco Delta system approached its most basinwards position (shelf edge delta). Two significant landward shifting (retrogradation) of the shelf-edge occurred during Sequences C3 and C1.

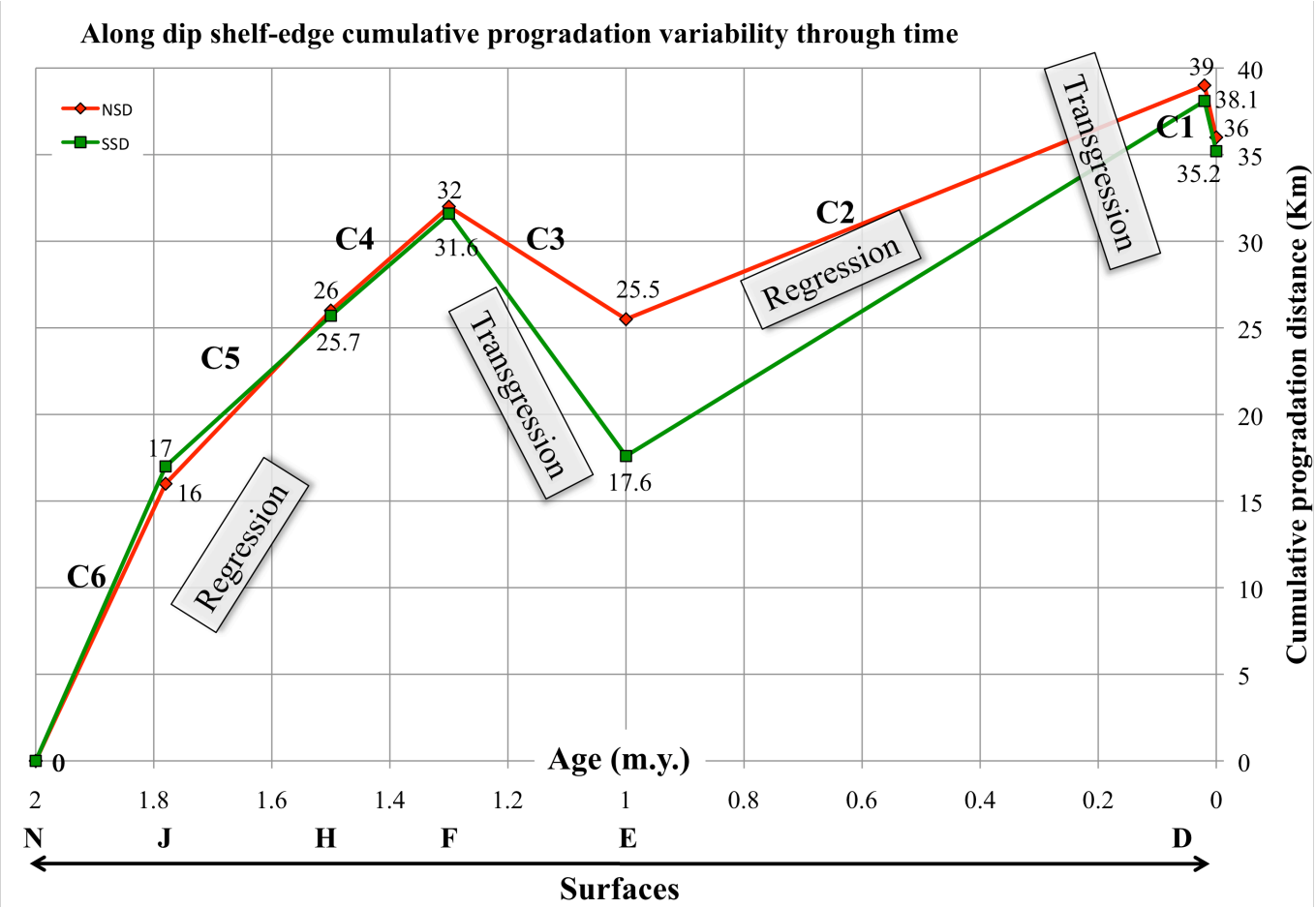

Figure 4.2.b Cumulative progradational rates for the NSD and SSD. See figure 4.1 for location of transects.

4.2 NET TO GROSS MEASUREMENTS AND ANALYSIS

4.2.1. Sand Distribution in the T Cycles

Net sand versus total thickness relationships for the marine cycles or T cycles were plotted as shown in figure 4.3. The cross-plot indicates that total thicknesses vary between 100 and 3,000 ft (30 to 914 m) while net sand values range from 0 to 600 ft. The general trend observed in the cross-plot indicates that there is a positive relationship between total thickness and net sand content (increase sand content associated with thicker intervals) (figure 4.3). However, interval "TN" is an exception to the previous observation since little or nearly zero sand was deposited during this interval. The lack of sand for interval "TN" might be indicating that the deltaic system at this time (oldest interval) was located in a more landward position and that sand delivery was minimum at this time. The cross-plot shows a general trend but it is important to mention that the trendlines fit the data very poorly as reflected by the low R^2 values (figure 4.3). Slope values for individual trendlines are lower than 0.3, indicating that although sand content increases with total thickness, the net-to-gross value is very low, as it would be expected for these marine cycles.

Figure 4.4 shows a cross plot that compiles all the measurements for Net-to-Gross versus Total Thickness for the six T intervals identified in each T-R cycle. According to this cross-plot, net-to-gross values never exceed 60% and there seems to be a general trend and threshold suggesting that net-to-gross values are inversely proportional to total thickness (figure 4.4).

During transgression, sand is generally reworked and spread along strike in the basin. Sand content, in these units, is often times constrained to the proximal parts of the

system where some fluvial/deltaic influence might still be present. Appendix A contains the table with all the net sand, total thickness, and net-to-gross ratios.

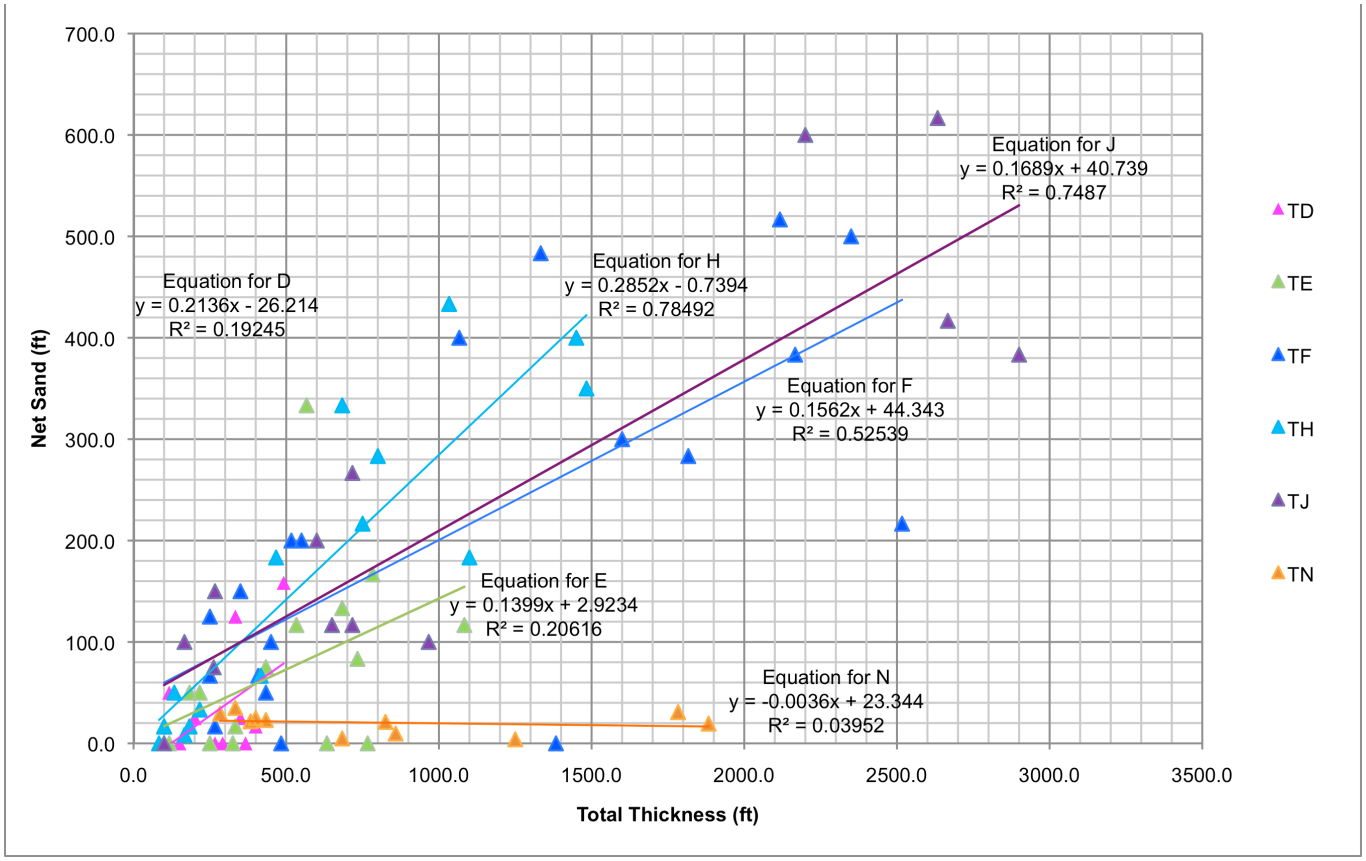

Figure 4.3 Crossplot Net Sand vs. Total Thicknesses for the T intervals. Net sand values range from 0 to 600 ft, while total thickness range from 100 to 3,000 ft. Trendlines fit the data very poorly as reflected by the R^2 values. Slopes are lower than 0.3, indicating that although sand content increases with total thickness, the net-to-gross values are very low.

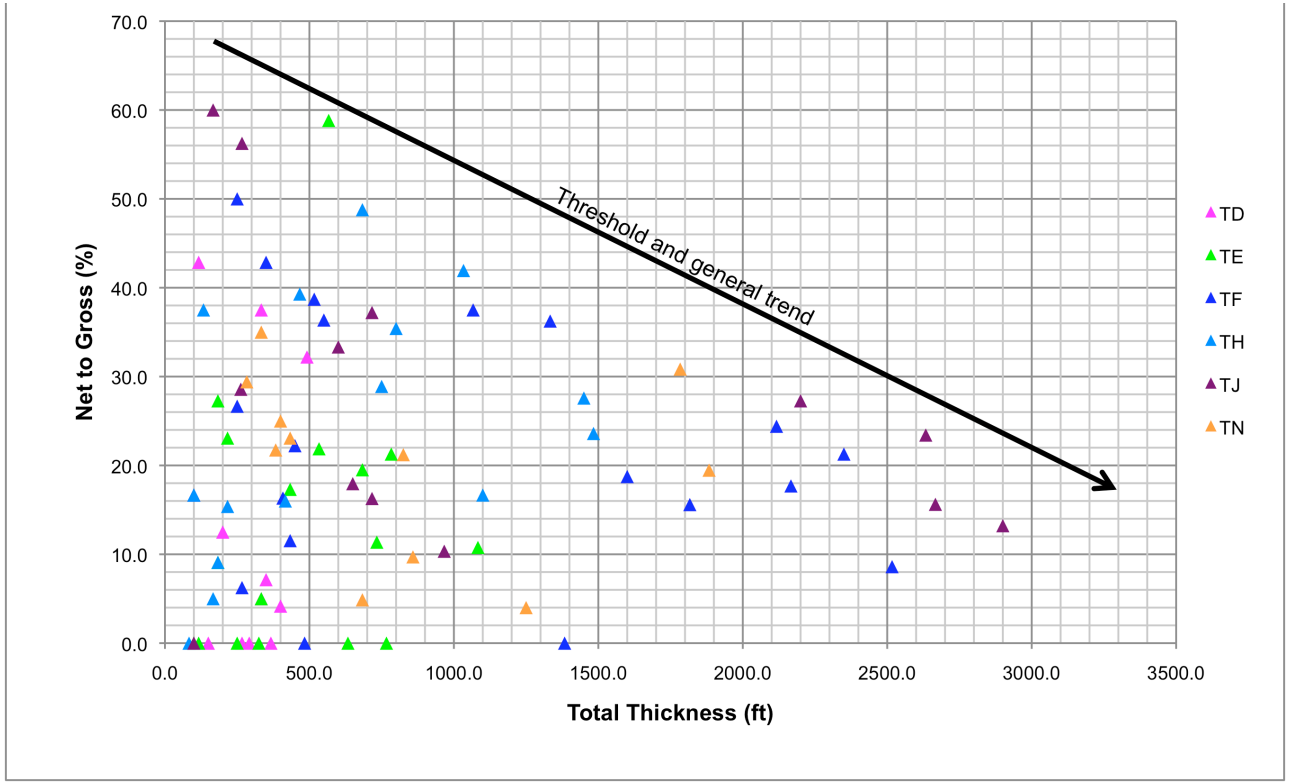

Figure 4.4 Crossplot Net-to-Gross vs. Total Thickness for the T intervals. Total thicknesses vary from 100 to 3,000 ft (30 to 9800 m). Net-to-gross values never exceed 60%, and there is a general trend suggesting that net-to-gross is inversely proportional to total thickness.

Net-to-gross distribution maps for intervals “TD” to “TN” are shown in figures 4.5 to 4.10. Contours were not possible to make because the data do not show a defined pattern. However, distribution maps were made to analyze local variation on the sand accumulation.

In the NTG distribution maps, near the Darien Ridge, all intervals show NTG values higher than 10% and up to 60%. During transgression sediments retrograde and are probably trapped against this ridge, but also there might be a local sand source from the Darien ridge itself that cannot be determined.

The well Omega-1, which is located within the Columbus Channel show NTG values that are lower than 10% for all T intervals except for “TE” where values can reach 17%. The Columbus Channel is a pathway for sediments, and it is possible that during times of transgression coarser sediments manage to be transported through this conduit reaching more outer shelf positions.

On the upper slope region (east of corresponding shelf-edge), only few wells show sand content in intervals “TE”, “TJ” and “TN” where the NTG ratios are lower than 27%.

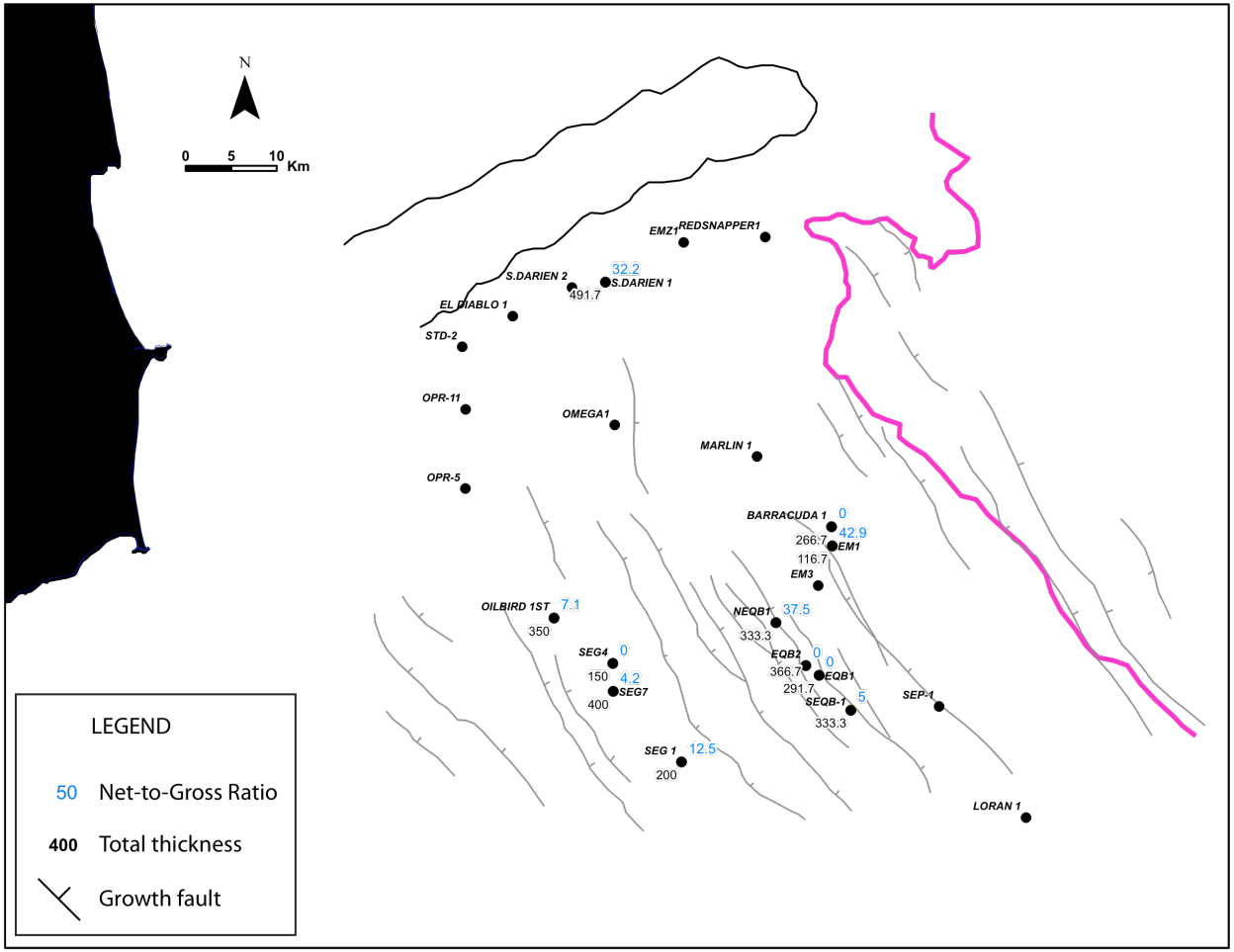

Figure 4.5. Net-to-gross distribution in T interval “TD”. NTG ratios in blue, Total Thickness in black. Normal faults as thin gray lines.

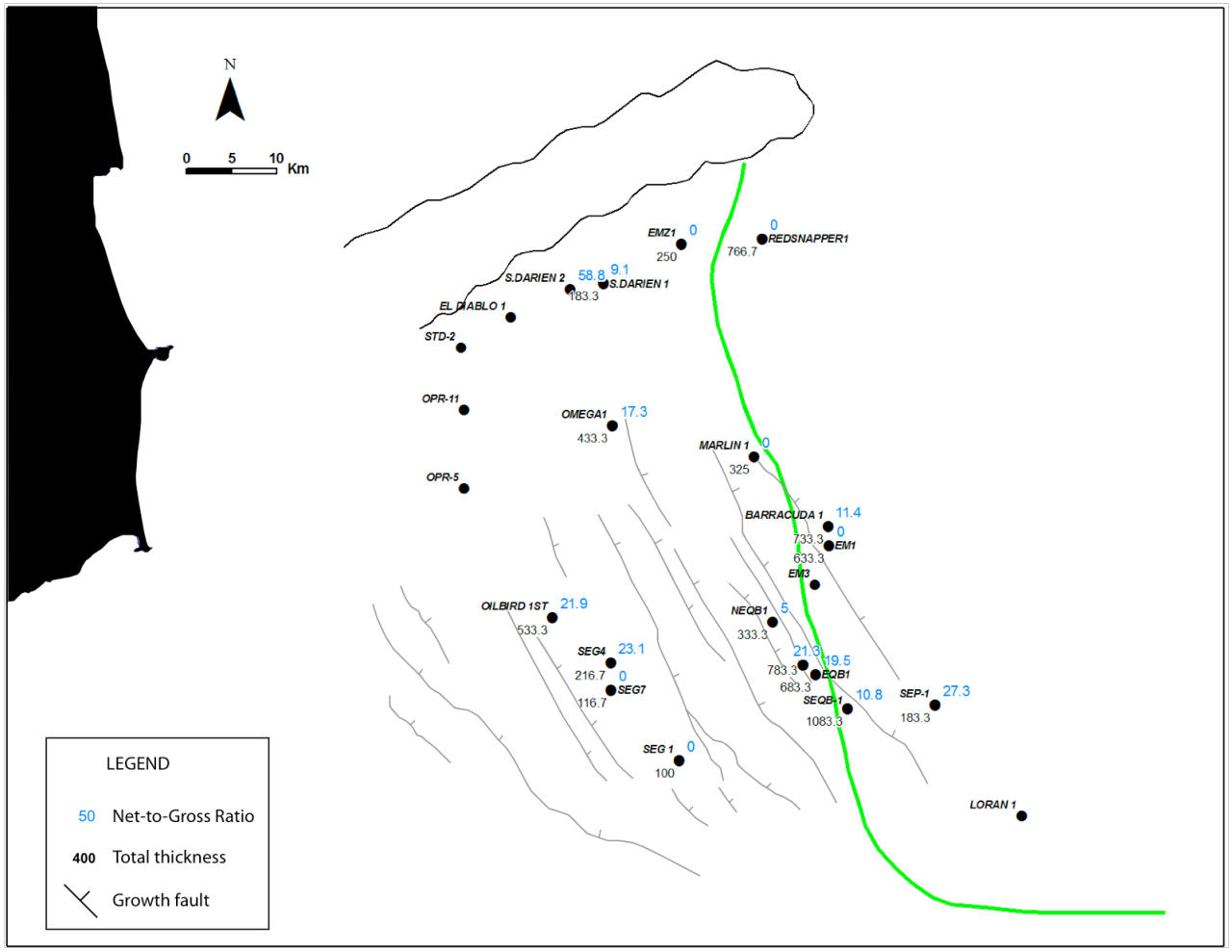

Figure 4.6. Net-to-gross distribution in T interval “TE”. NTG ratios in blue, Total Thickness in black. Normal faults as thin gray lines.

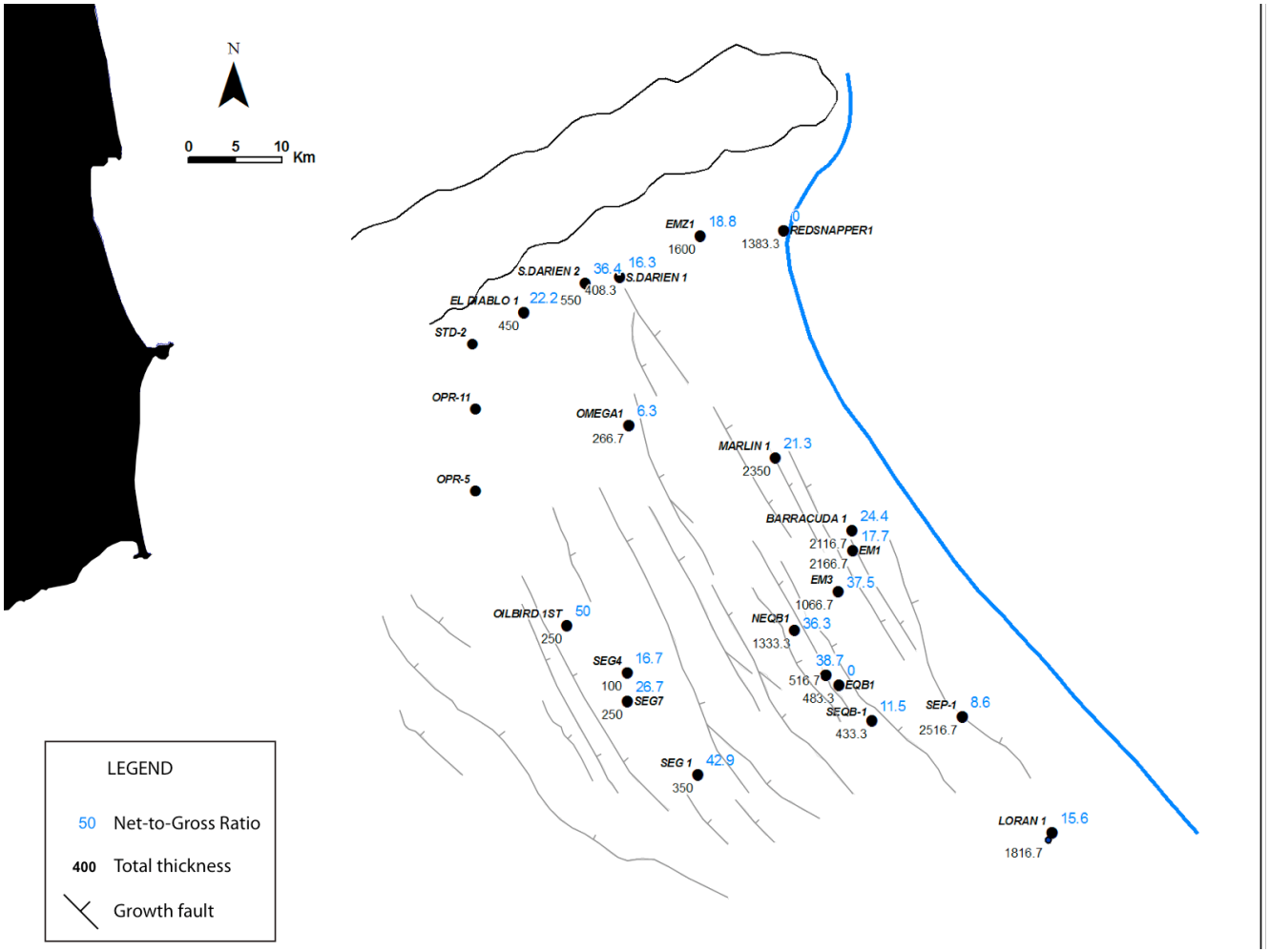

Figure 4.7. Net-to-gross distribution in T interval “TF”. NTG ratios in blue, Total Thickness in black. Normal faults as thin gray lines.

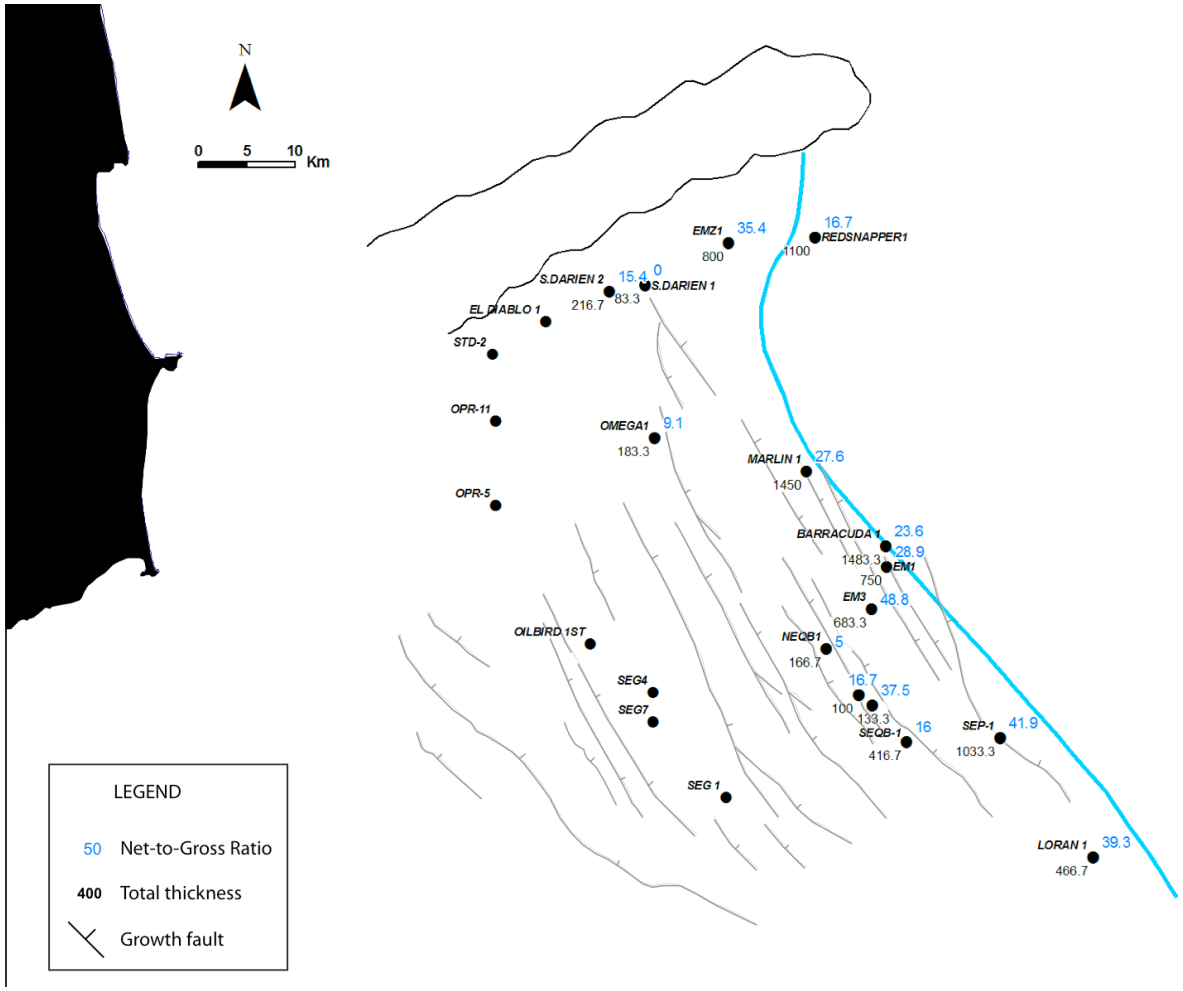

Figure 4.8. Net-to-gross distribution in T interval “TH”. NTG ratios in blue, Total Thickness in black. Normal faults as thin gray lines.

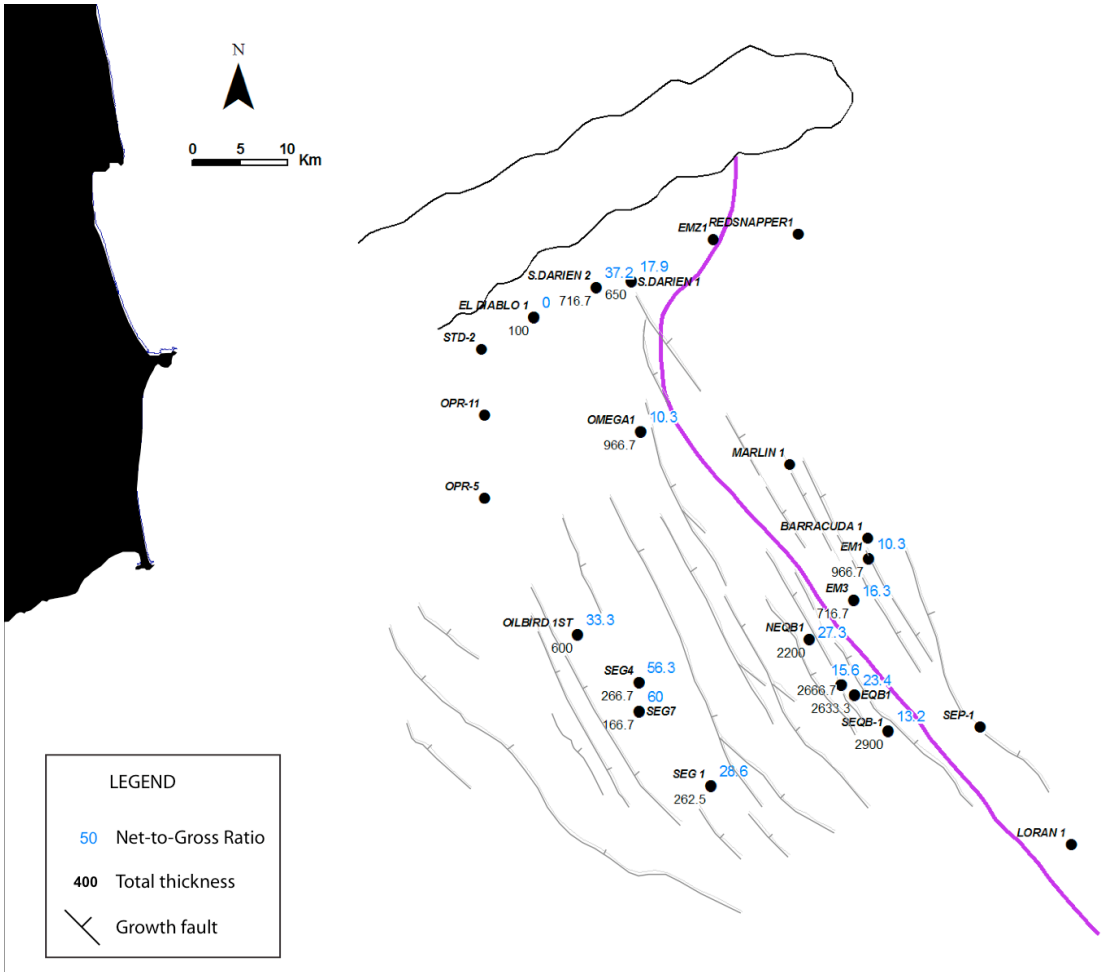

Figure 4.9. Net-to-gross distribution in T interval “TJ”. NTG ratios in blue, Total Thickness in black. Normal faults as thin gray lines.

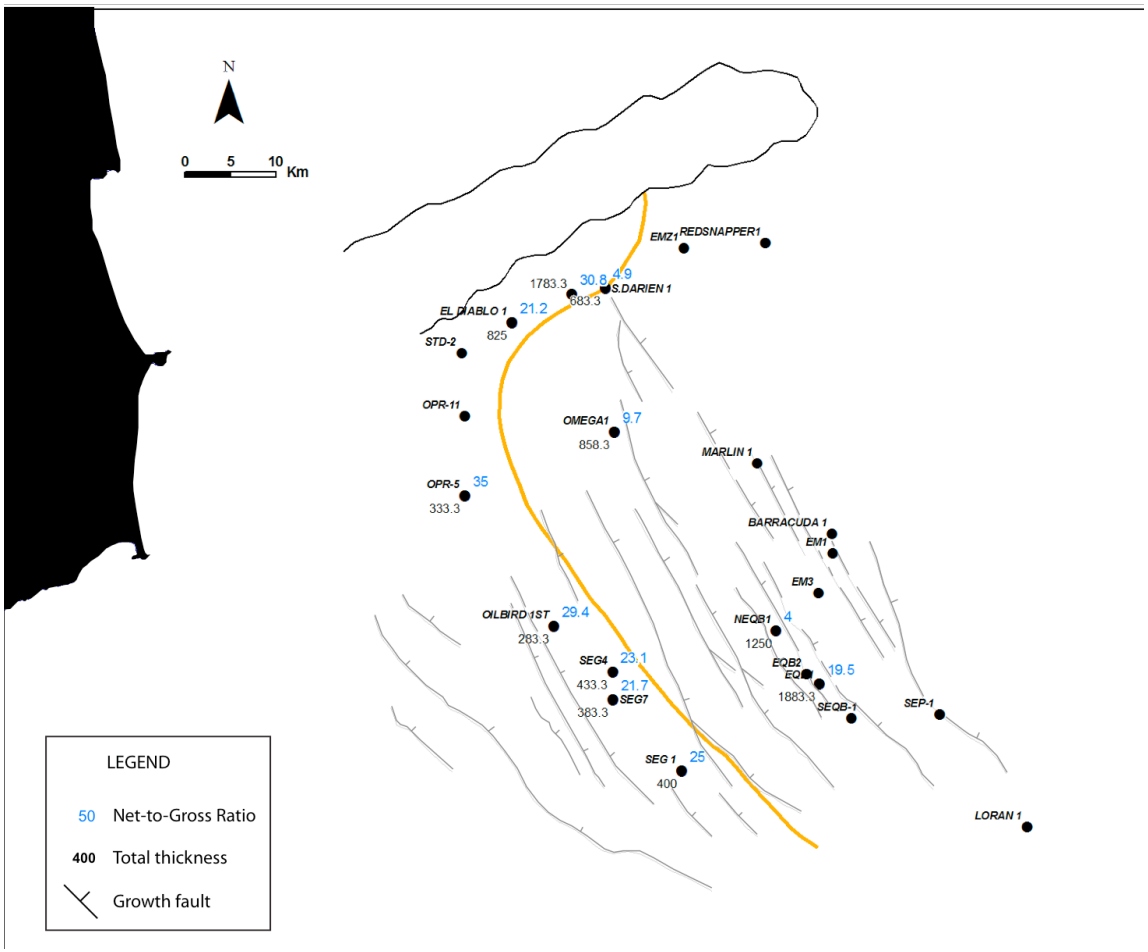

Figure 4.10. Net-to-gross distribution in T interval “TN”. NTG ratios in blue, Total Thickness in black. Normal faults as thin gray lines.

4.2.2. Sand Distribution in the R Cycles

Net sand versus total thickness relationships for the R cycles were plotted in figure 4.11. The cross-plot shows that for the majority of the data points the total thickness values range from 100 to 600 ft. The only exception is associated with data points contained within cycle "RH" where total thickness values range from 240 to 1320 ft. Net sand predominantly ranges from 20 to 420 ft, however higher values are also observed within cycle H.

For R cycles "RD", "RE", "RF" and "RH" the trendlines show a fair to good correlation with R^2 values ranging from 0.35 to 0.84. Net sand and thickness relationships have a positive correlation for most R cycles, except for R cycle "RN" where the relationship between these parameters is inverse. Similarly to the T cycle for the "N" T-R cycle, the inverse correlation between net sand and thickness can be explained by the relative location of shelf-edge "N" with respect to the basinwards position of the wells and the inland location of the paleo inner-shelf Orinoco delta.

The cross plot that is shown in figure 4.11 compiles all the total thickness versus net-to-gross measurements for each of the R cycles that were identified within the six T-R cycles. NTG values seem to be widely distributed within these cycles with most of the data points showing variations from a minimum of 35% to a maximum of 90%. This high variability depends on the existence or not of sedimentary fairways and bypass zones, the capacity to retain sediments near the shelf break (sediment traps) and the character of the sedimentary source.

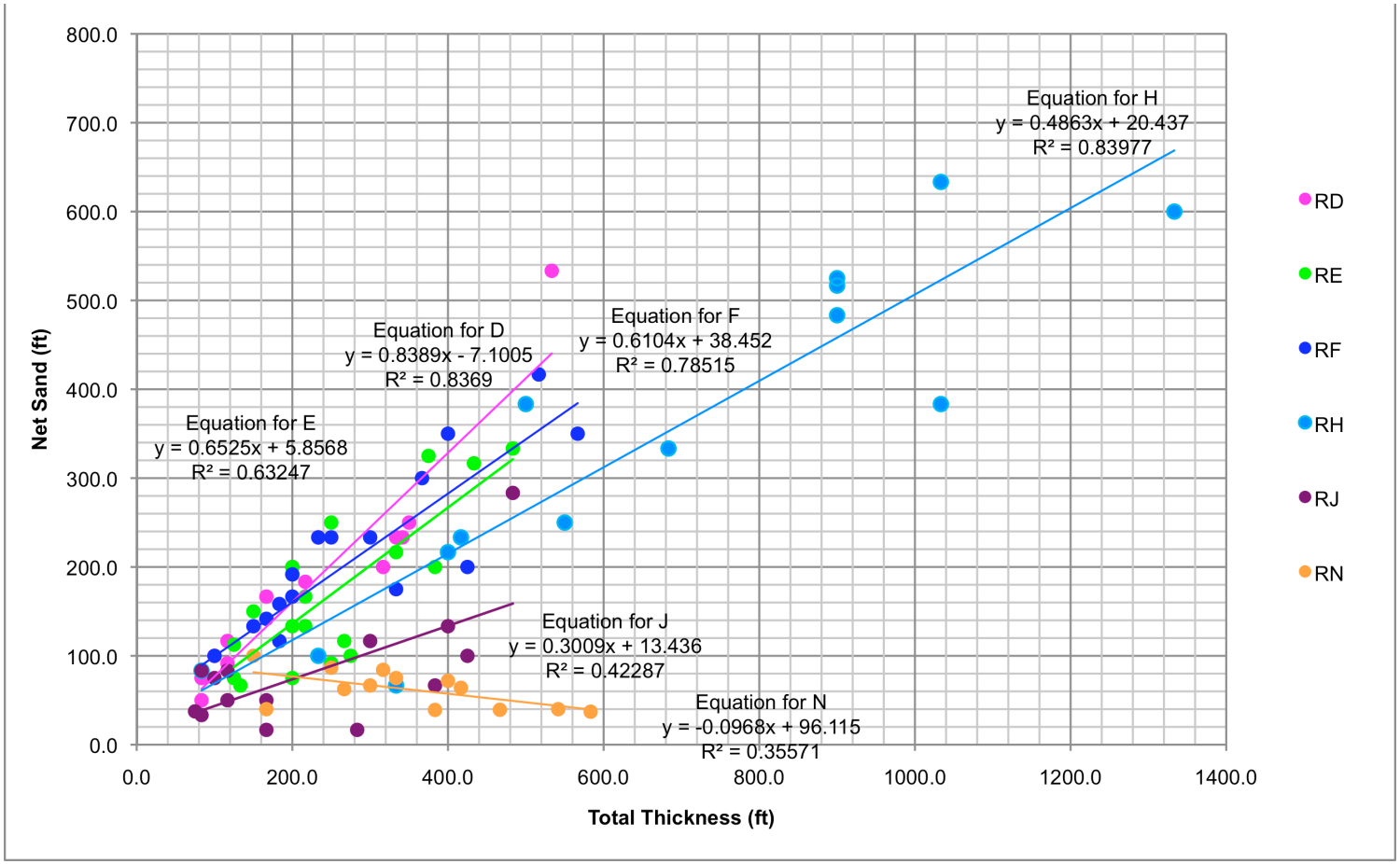

Figure 4.11. Net-Sand versus Total Thickness for R cycles

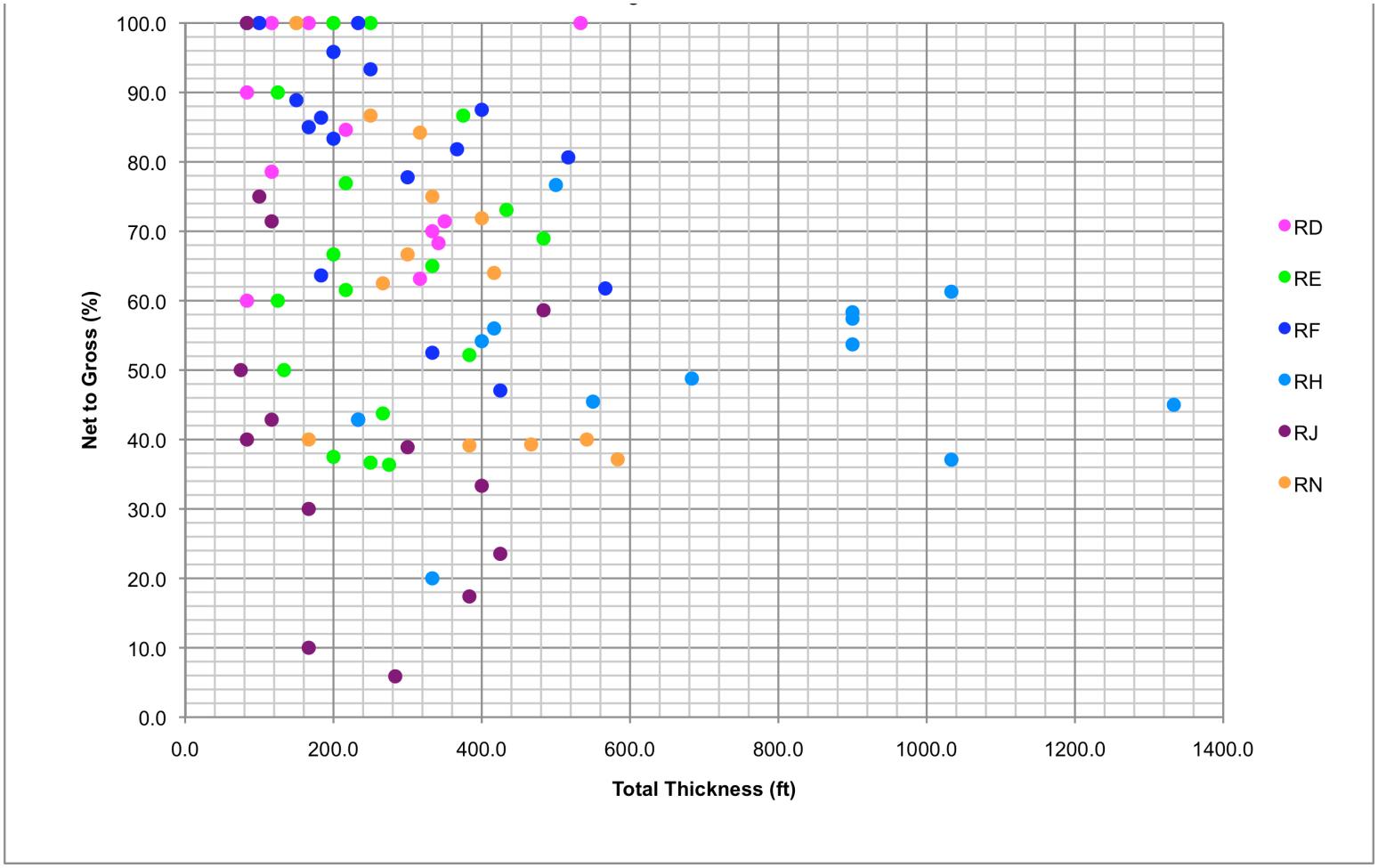

Figure 4.12. Net-to-gross versus Total Thickness for R cycles

Figures 4.13 to 4.18 show a series of NTG maps that were generated for each of the R cycles associated to the T-R cycles (contouring varies in intervals of 10). An attempt of mapping the NTG values through the ArcGIS contouring tool was made, but since the data population is very low and it is widely distributed, contouring was not reliable. Instead, contours were drawn by hand, which allowed the incorporation of the influence of the regional structures in the distribution of the NTG percentages.

In general, NTG contours are aligned NW-SE in the SSD where the accumulation of sediments is highly influenced by the NW-SE oriented growth and counter regional faults (figures 4.13 to 4.18). In the SSD the growth and counter regional faults form localized areas of accommodation that are associated with individual fault compartments. It has been observed that within these growth-fault compartments, NTG values increase northeasterly as the thickness of the sedimentary wedge decreases and the distance from the growth fault increases (figure 4.27). In contrast, the NTG contours deflect to a NE-SW orientation near the Darien Ridge where the lack of accommodation space near the structural high prevents the accumulation of coarse-grained sediments. Most of the NTG values that have been observed near the Darien Ridge are lower than 60%, except for the values within the R cycle RD. The relatively lower NTG values near the Darien Ridge for most of the T-R cycles might be indicating that this area was most likely acting as a bypass zone with poor sand preservation. The anomalous higher NTG values related to the last R cycle RD could be instead associated with the last glacial lowstand maximum episode and with the presence of exceptionally high sedimentation rates in this area at this time.

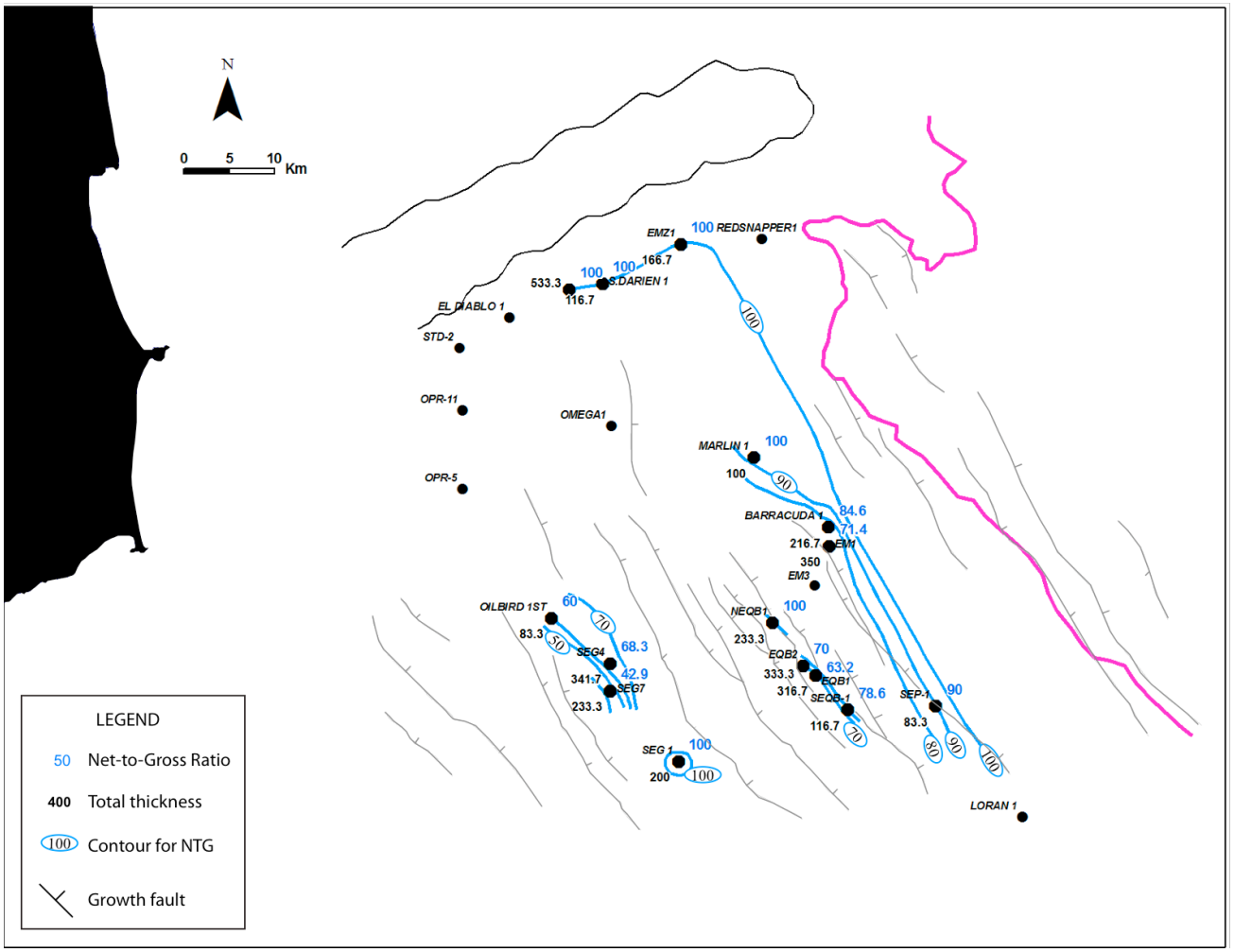

Figure 4.13. Net-to-gross map for R cycle “RD”. NTG ratios in blue, Total Thickness in black.

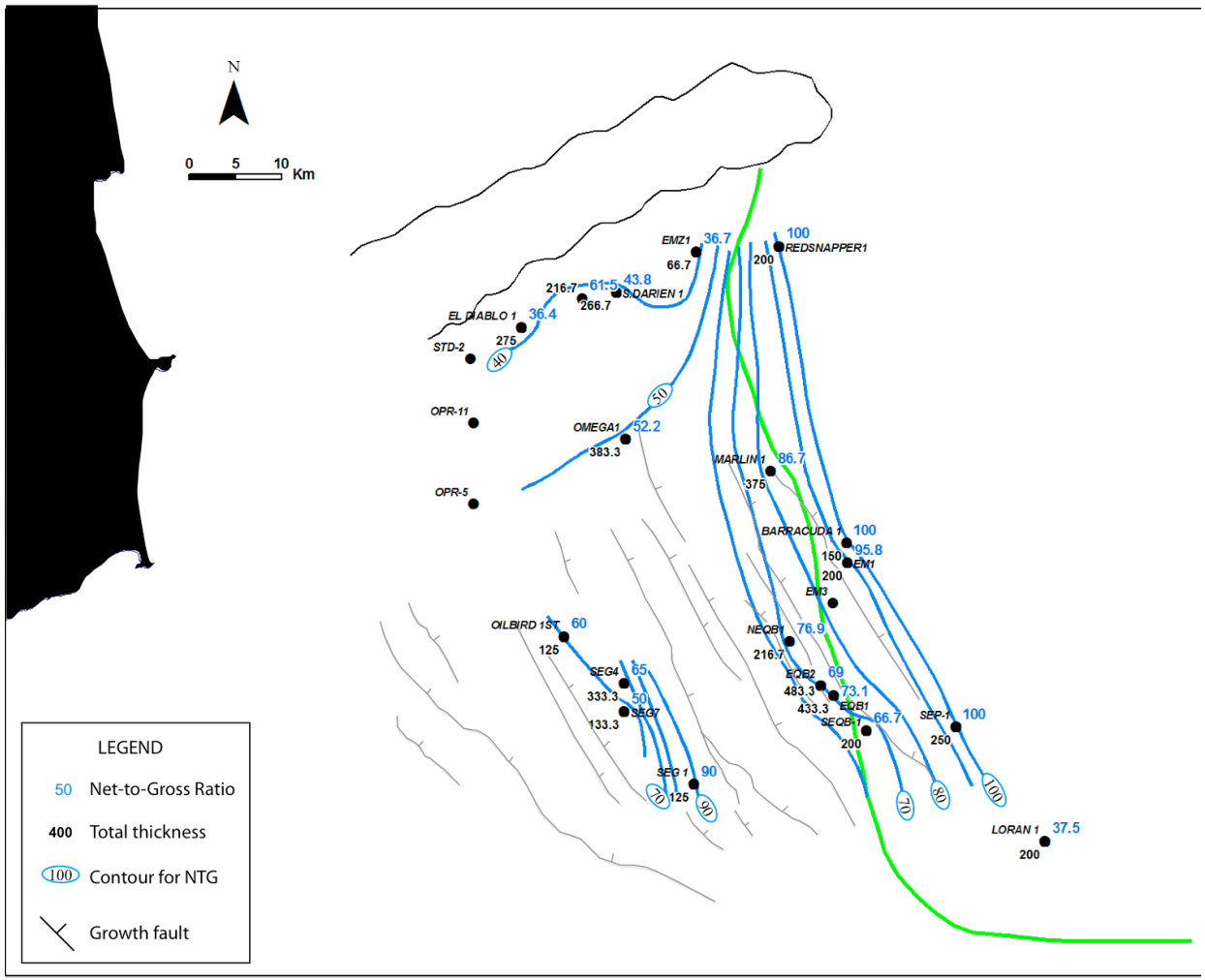

Figure 4.14. Net-to-gross map for R cycle “RE”. NTG ratios in blue, Total Thickness in black.

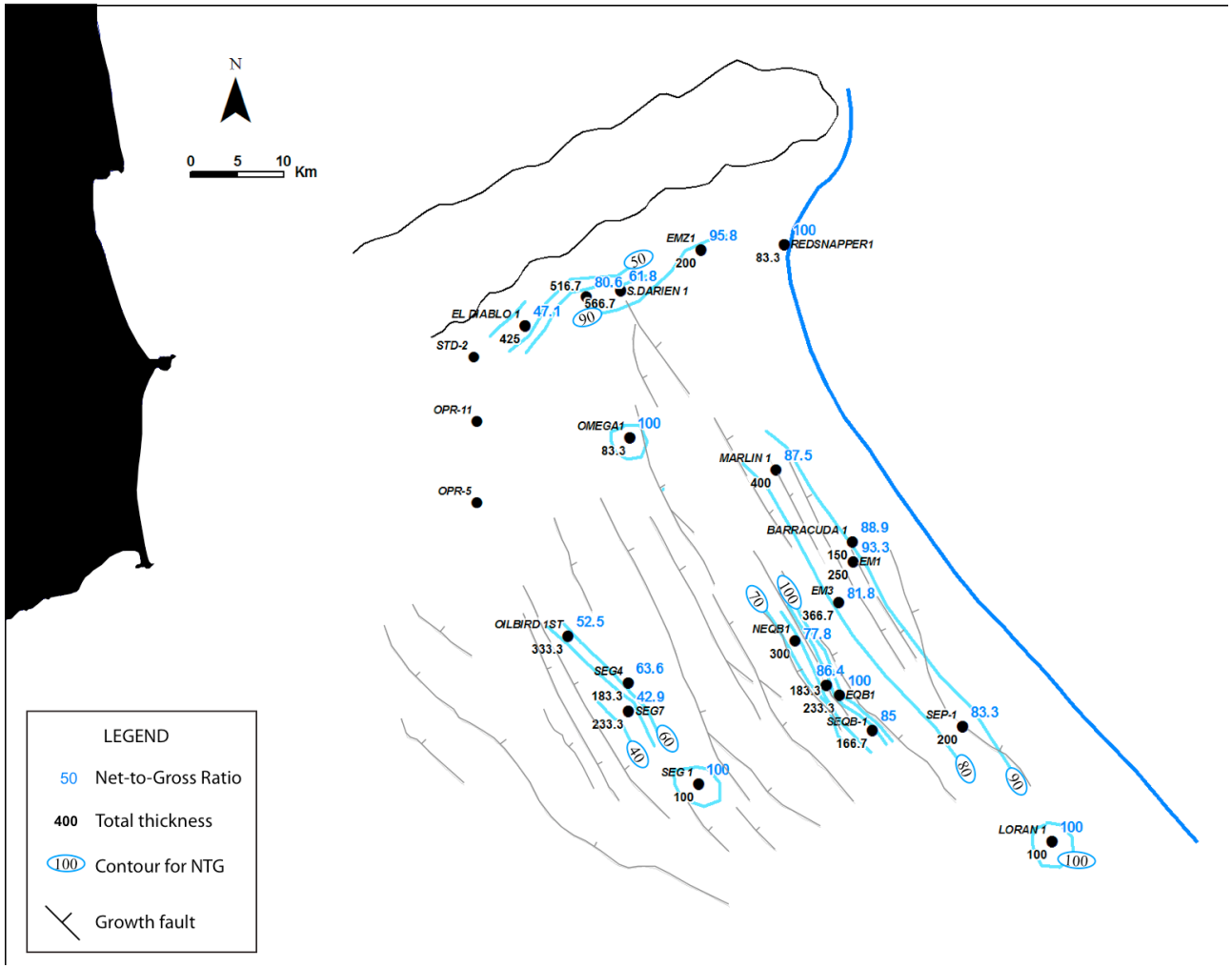

Figure 4.15. Net-to-gross map for R cycle “RF”. NTG ratios in blue, Total Thickness in black.

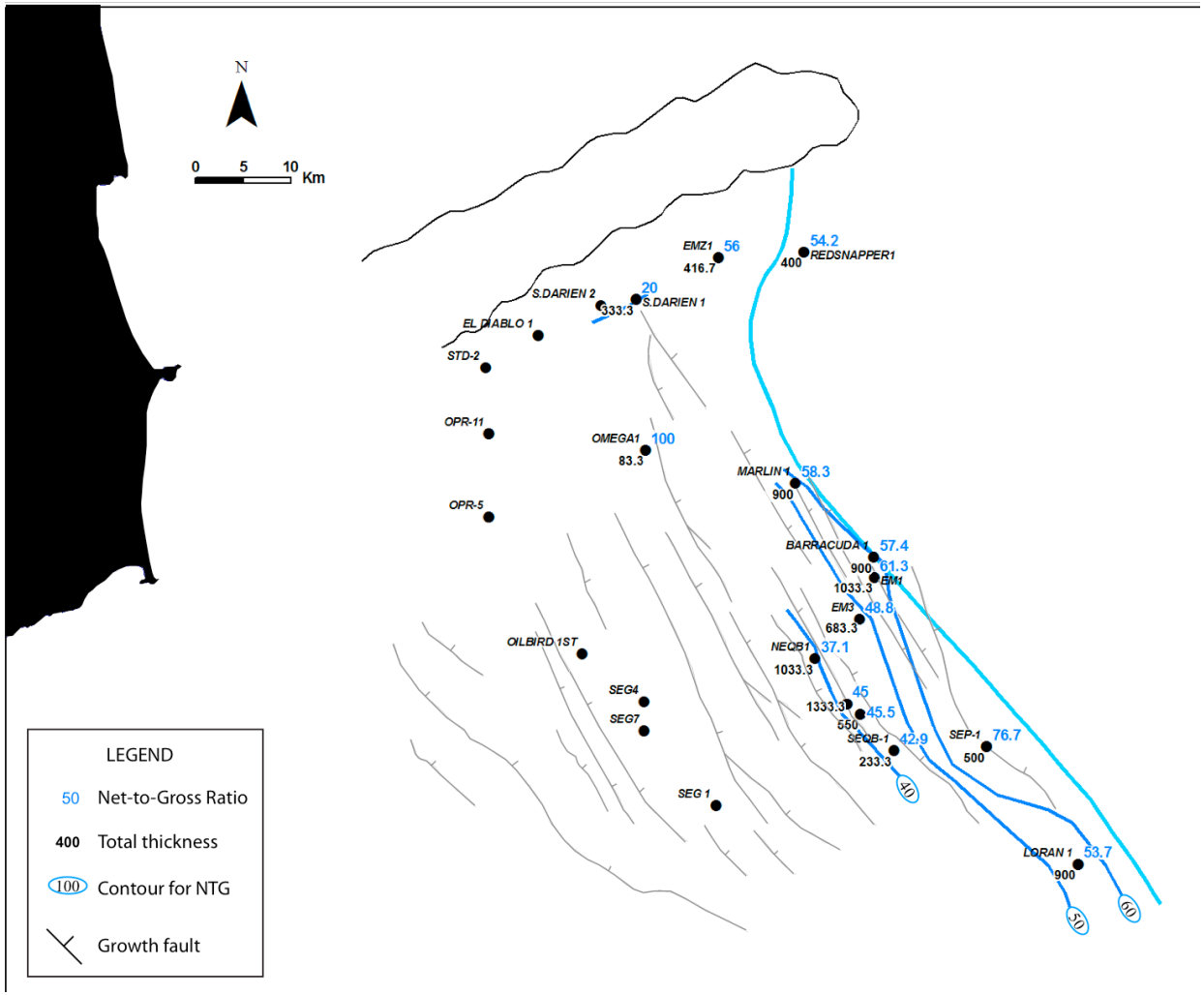

Figure 4.16. Net-to-gross map for R cycle “RH”. NTG ratios in blue, Total Thickness in black.

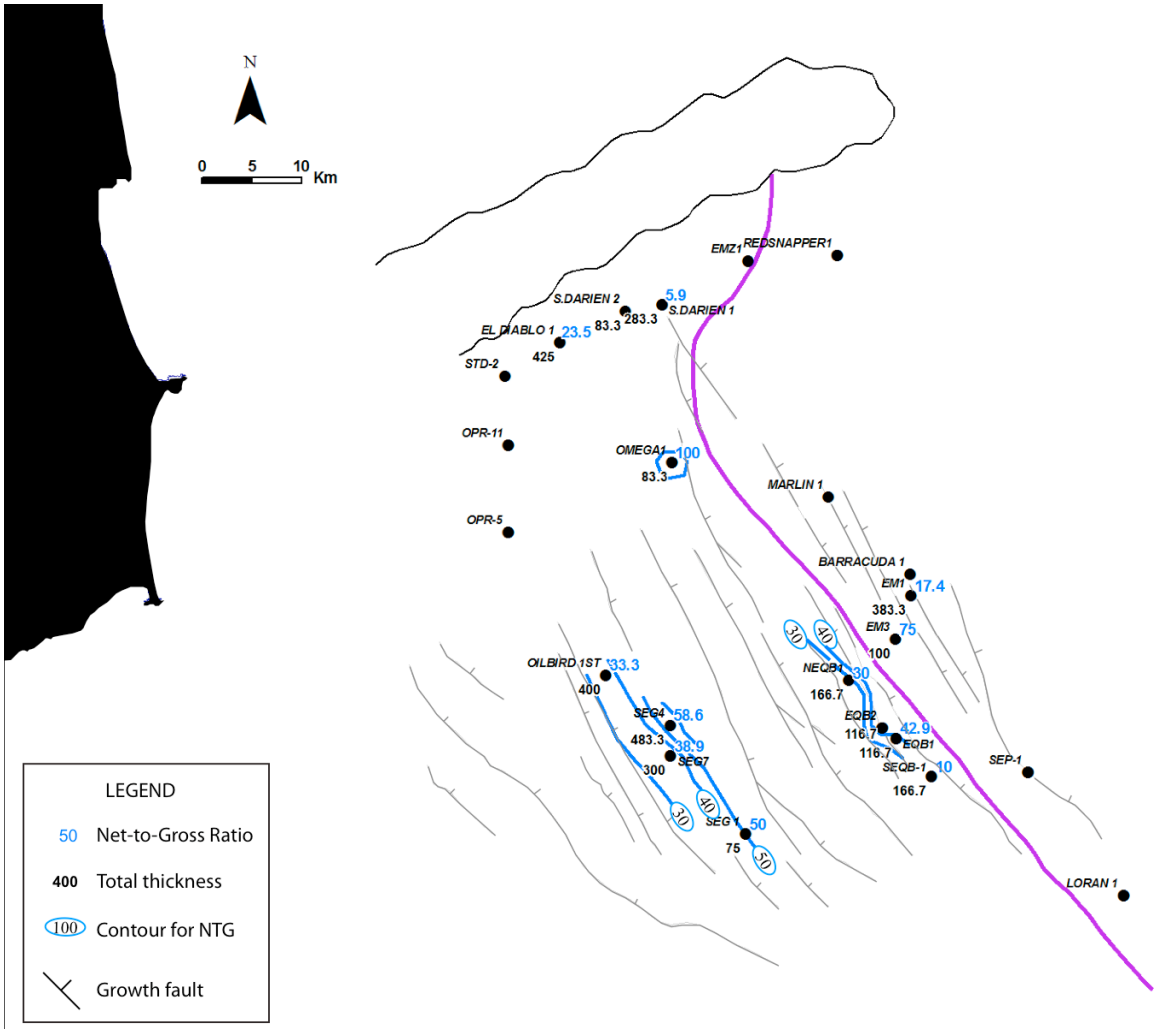

Figure 4.17. Net-to-gross map for R cycle “RJ”. NTG ratios in blue, Total Thickness in black.

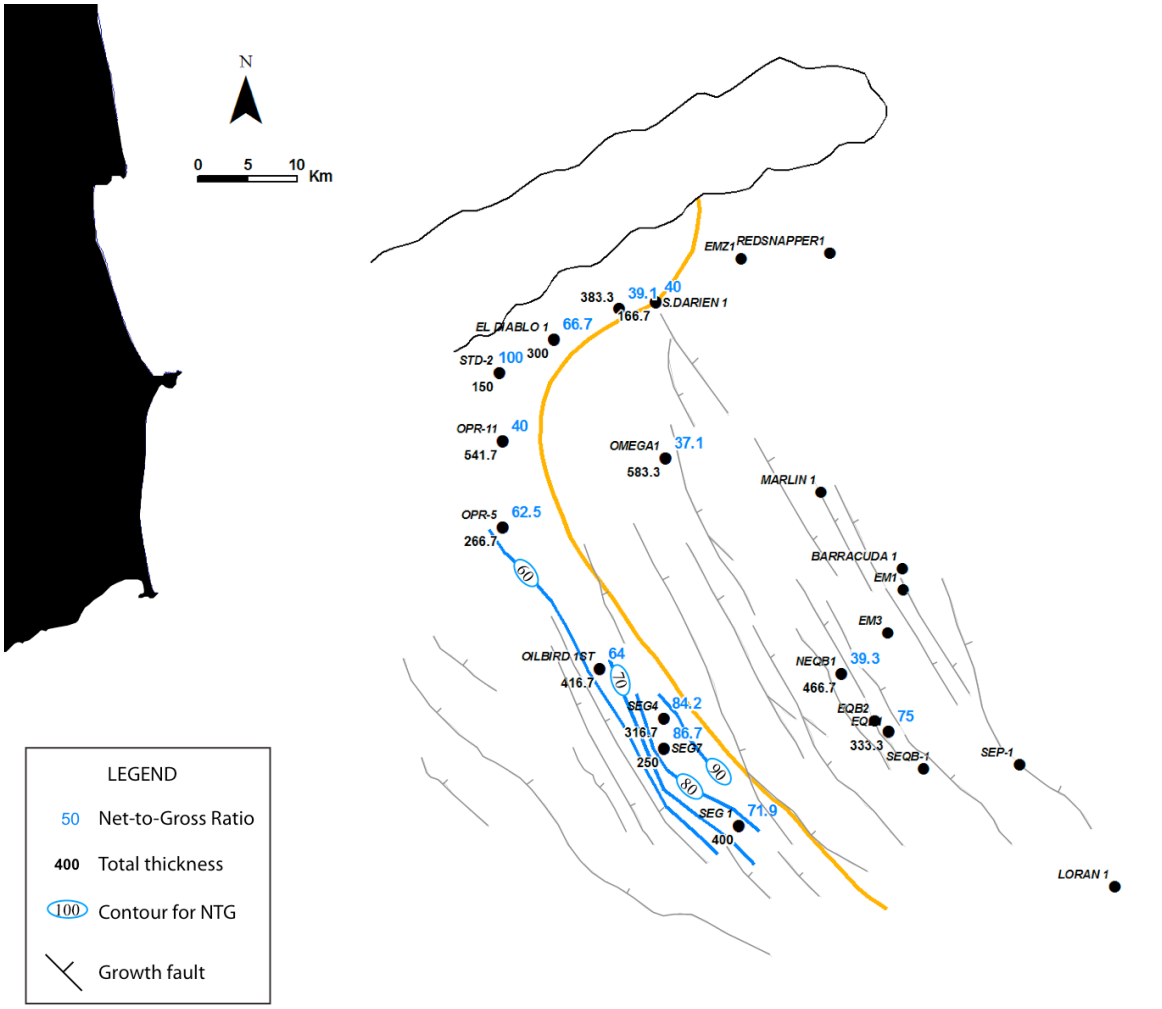

Figure 4.18. Net-to-gross map for R cycle “RN”. NTG ratios in blue, Total Thickness in black.

4.3 RELATIONSHIP BETWEEN SHELF EDGE TRAJECTORIES, SAND DISTRIBUTION AND T-R CYCLES

4.3.1 Net-to-gross values variability regarding shelf-edge position

Figure 4.19 shows a crossplot of NTG versus distance to corresponding shelf-edge for each of the R cycles measured (distances were measured from the wells to the mapped shelf edges, see figure 4.1). The crossplot shows a general trend that indicates that the NTG ratios increase as the time equivalent shelf-edge is approached (figure 4.19). However, NTG values are also controlled by the influence of local structures.

The NTG increase associated to the proximity to the shelf edge is related to the additional accommodation space that was created along the margin by growth and counter-regional faults (sediment traps) and by the presence of paleocanyons. Figure 4.20 is an isopach map of the last T-R cycle (D) that shows how the geometric arrangement of the growth and counter-regional faults facilitated the creation of a compartment that is parallel to the shelf edge trajectory and to the strike of the faults. This compartment defines a growth fault sediment trap on the upper part of the slope that had the capacity to sequestered sediments in this region. Interestingly, the isopach map also shows how there is an area (point) of sediment bypass that coincides with the southern end of the counter regional fault and through which sediments are fed into deep-water depolocations (Moscardelli et al. in prep).

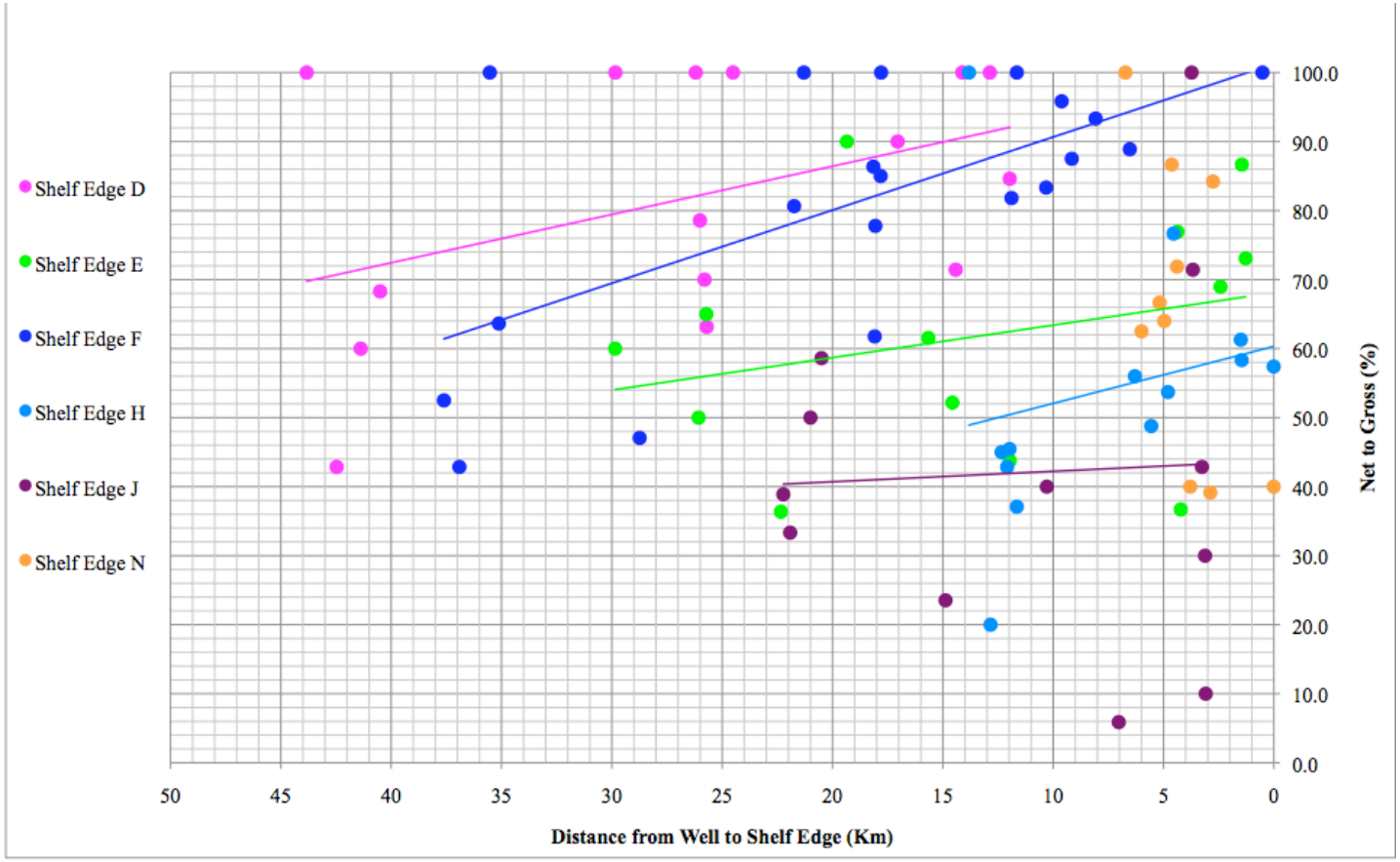

Figure 4.19. Net-to-gross ratios versus Distance from well to Shelf-edge for R cycles.

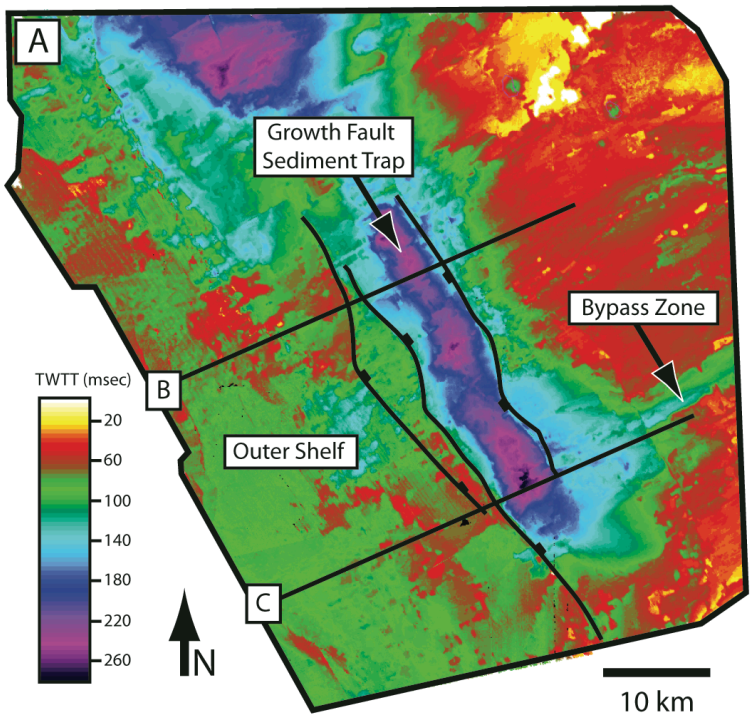

Figure 4.20. Isochron map showing greater thickness trapped between normal and counter-normal fault in the SSD of the Columbus Basin. (From Moscardelli et al., in prep)

4.3.2 Shelf-edge aggradation and progradation rates

Aggradation and progradation rates were computed for each sequence C1 to C6 defined in the well log cross-section shown in figure 3.6 and 4.21 within individual wells. Figure 4.21 shows a cartoon that schematically illustrates how the measurements were taken. The aggradational value associated to a cycle was equivalent to the total thickness of individual T-R cycles (including the ones not analyzed in this study, if they were present in each C1 to C6, such as: TG/RG, TI/RI, TK/RK, TL/RL and TM/RM. See

figure 4.21) while the progradational rates were measured from the location of the well to the shelf break of the cycle top (see figure 4.21). Ideally, progradational rates should be measure between successive clinoform rollover points, however the low seismic resolution in this case did not allow to resolve these geometries in the study area. The well location provides with a fix point of reference for all the cycles and therefore it can be used to compare progradational rates between the different intervals (figure 4.21).

Five sequences were measured and analyzed:

1) C2 (from surface E to D)

2) C3 (from surface F to E)

3) C4 (from surface H to F)

4) C5 (from surface J to H)

5) C6 (from surface N to J)

Figure 4.22 shows the crossplot showing the relationships between progradational versus aggradational values for each cycle. The cross-plot shows that progradation is more dominant for sequences C2 (green data points) and C3 (dark blue data points) where aggradational rates stay below 500 m while progradational rates range from 1 to 45 km. On the other hand, aggradational rates tend to be higher than progradational rates for sequences C4 (light blue data points), C5 (purple data points) and C6 (orange data points) with aggradational rates that can reach a maximum of 2500 m for sequence C5 (see figure 4.22).

Sequences that are dominated by aggradation (C4, C5 and C6) may indicate that there was more accommodation space available within the shelf and therefore less sand delivery towards the basin since most sand was trapped within more shelfal positions. Conversely, sequences where progradation was dominant (C2 and C3) may suggest a greater chance of sand delivery into deep water locations since sand delivery systems to

the shelf-edge might have been more effective. Based on these criteria, intervals deposited from time F to E (from 1.3 m.y. to 1 m.y.) (Sequence C3 = T-R cycle "F") and from E to D (1 m.y. to ≈20,000 years) (Sequence C2 = T-R cycle "E") had a better chance to bypass sediments through the shelf-edge areas and therefore to create wider basin floor fans downslope. On the other hand, during times where higher aggradational rates were dominant (Sequences C4, C5 and C6) sands might have been preferentially trap within the shelf (e.g.: growth fault sediment traps) (figure 4.22). These observations have obvious implications for hydrocarbon exploration.

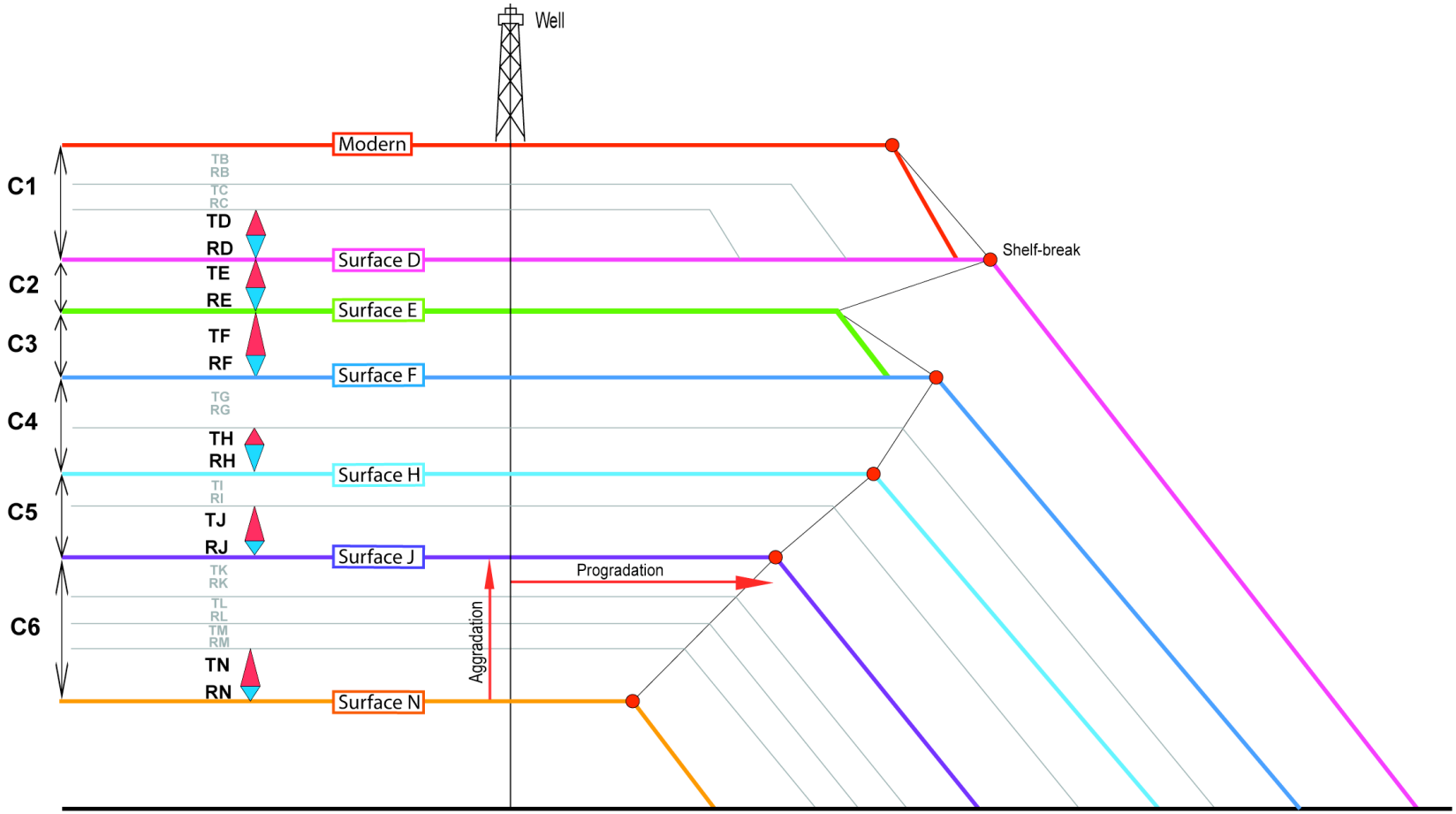

Figure 4.21. Schematic diagram of shelf-edge trajectories in a profile view. This was the methodology used to measured aggradation and progradation rates from each well.

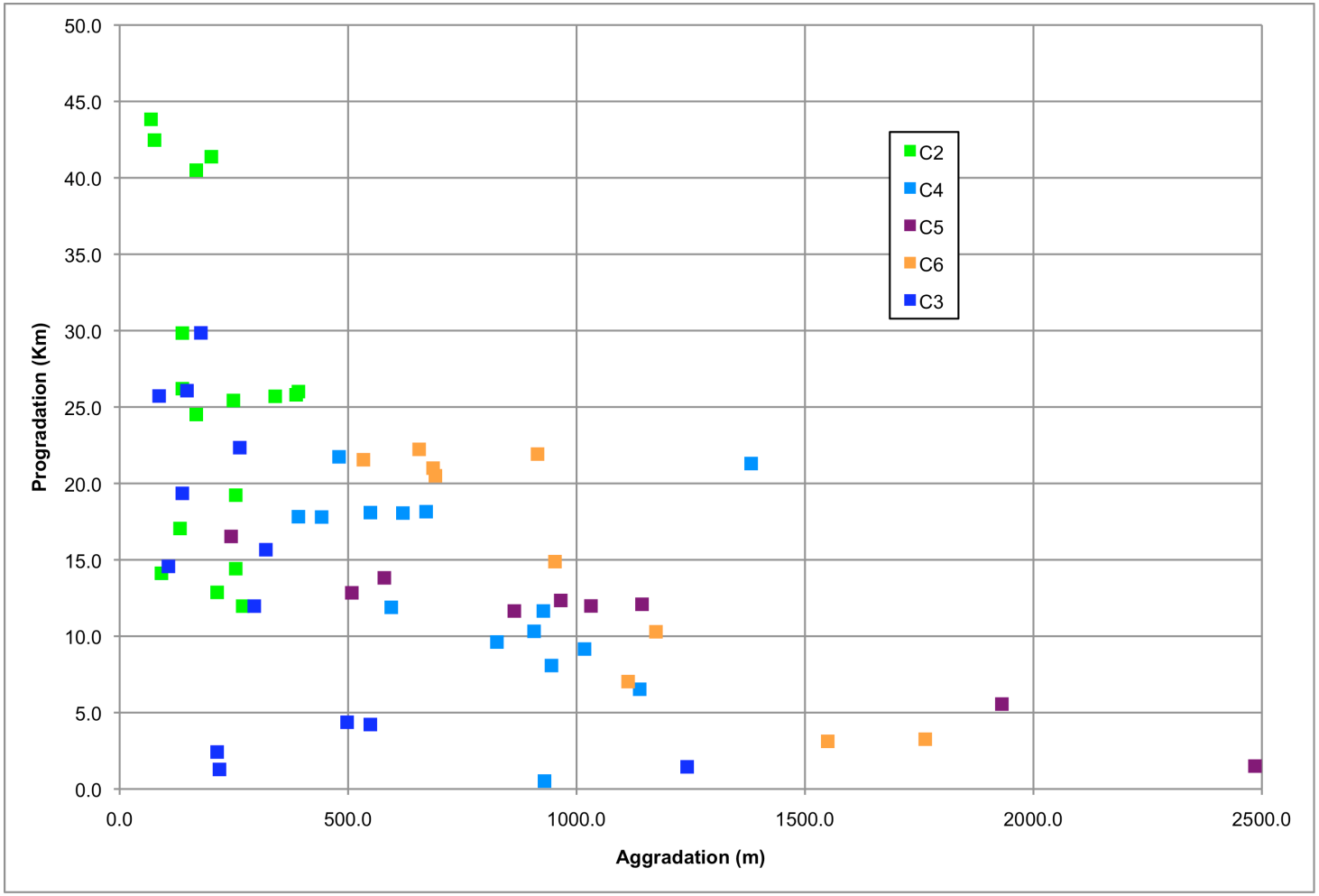

Figure 4.22. Aggradation vs. Progradation crossplot for sequences C2 to C6 defined in figure 4.21 and 3.6

4.3.3 Long Term Comparison of Aggradational vs. Progradational rates

Carvajal et al. (2009) published a comprehensive work that seek to compile and compare information from different continental margins around the world with the objective to understand the role of sediment supply in the growth of ancient shelf margins. The sequences studied by Carvajal et al. (2009) comprised time scales that were greater than 1–2 m.y., while in this work time scales for individual T-R cycles vary between 200 K to 1 m.y. Similarly to observations that were made in section 4.2.1 of this work, Carvajal et al. (2009) concluded that continental margins where progradation was dominant were more prone to allow for the delivery of sand into deep-water depolocations.

In order to compare the results of this research with those presented by Carvajal et al. (2009), we decided to use the whole succession from surface N to surface D (Adding all the sequences C2, C3, C4, C5, C6) as one aggradational value for each well. Only 8 of 23 wells showed all sequences C2 to C6. Progradational distances were measured from the shelf-edge N to the shelf-edge D along profiles that intersected the wells in discussion (see table 4.3). Then, these values were plotted as data points in the original aggradational versus progradational plot presented by Carvajal et al. (2009) (see figure 4.23). Ages for surfaces N and D are 2 m.y. and 25,000 years, respectively; therefore the sequence between these two surfaces comprised a cycle of time scale of 1.975 m.y., which is comparable to the sequences used by Carvajal et al (2009) in their study.

Table 4.3 summarizes these measurements.

No	Well	Aggradation (m)	Progradation (Km)	Aggradation Rate (m/m.y.)	Progradation Rate (Km/m.y.)
1	OILBIRD 1	1959	36.4	992	18
2	SEG4	1499	37.6	759	19
3	SEG7	1352	38	684	19
4	SEG1	1265	38.6	641	20
5	NEQB1	3699	38.5	1873	19
6	EQB1	3796	38.7	1922	20
7	S.DARIEN 2	2355	29	1192	15
8	S.DARIEN 1	2602	26	1317	13

Table 4.3 Aggradation versus Progradation rates for a sequence of 1.97 m.y. measured between surfaces N and D.

Figure 4.23 shows a crossplot of aggradation vs. progradation rate from Carvajal et al. (2009). The wells in table 4.3 are also plotted and labeled from 1 to 8 accordingly.

In the figure the blue squares are referred to the Orinoco Delta in three of its basins: Eastern Venezuela Basin (EV), Columbus Basin (CB) and Plataforma Deltana (PD). The single point from the Columbus Basin corresponds to the Pleistocene sequence reported by Sydow et al. (2003) (See also table 1 in Carvajal et al., 2009).

Six of the eight wells show progradation rates between 18 and 20 Km per m.y., which indicates that the eastern offshore Trinidad is a slow prograding margin, according to the classification done by Carvajal et al. (2009).

Aggradation rates are between 640 and 1900 meters per m-y. These relatively high shelf-edge aggradation rates might be indicative of high accommodation space and/or high subsidence rates (Carvajal, et al., 2009). Subsidence rates can reach high values in growth-fault depocenters that can accumulate large sediment volumes and therefore decrease the sediment volume that would prograde and bypass to deep-water deposits (Carvajal et al., 2009).

In long-term scale (1-2 m.y.) the Orinoco Delta seems to behave as an aggradational delta that increases sediment storage due to growth fault and high subsidence rates. However, in the short-term scale, the Orinoco delta seems to behave as a rapid progradational delta, for the younger sequences C2 and C3, where sediment bypass is more likely to occur; and as a rapid aggradational (slow prograding) margin for the older intervals C4, C5 and C6.

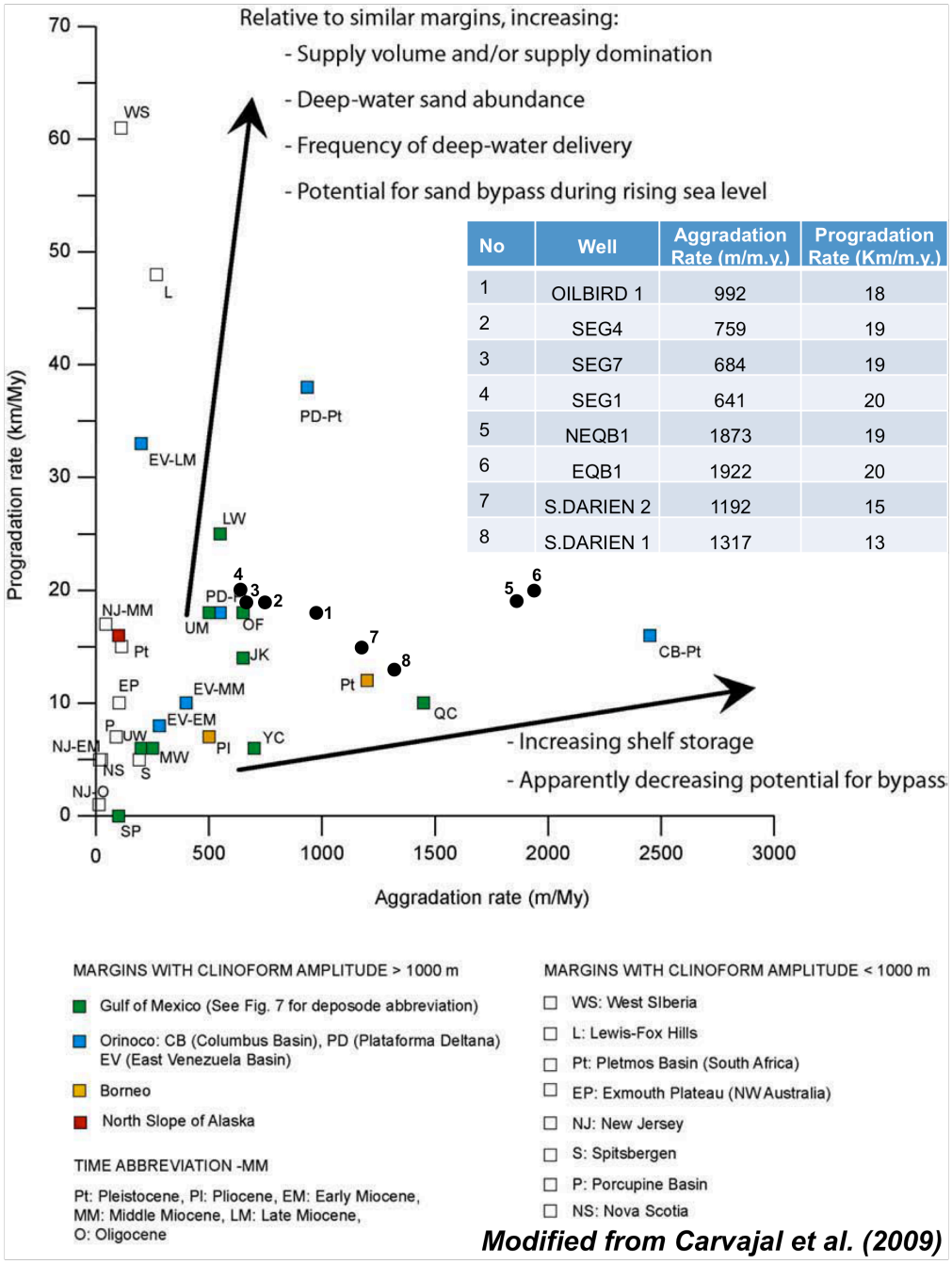

No	Well	Aggradation Rate (m/m.y.)	Progradation Rate (Km/m.y.)
1	OILBIRD 1	992	18
2	SEG4	759	19
3	SEG7	684	19
4	SEG1	641	20
5	NEQB1	1873	19
6	EQB1	1922	20
7	S.DARIEN 2	1192	15
8	S.DARIEN 1	1317	13

Figure 4.23. Comparison of aggradation vs. progradation rates from data used in this research with data used by Carvajal et al (2009)

4.4 INTEGRATION WITH PREVIOUS SEISMIC DATA ANALYSIS

Alvarez (2008) mapped three key horizons across the 3D seismic mega-merge volume. She tied the well to the seismic using a time-depth conversion from a synthetic seismogram done for the whole log of the RedSnapper well with a neighbor seismic volume in block 4ab.

The 3D seismic mega-merge volume has a length of 1 second; therefore, only surfaces D, E, F and G were recognized based on previous well picks loaded in the database of the project. These picks were not refined and hence some contradictions are found with the new tops defined in this research study.

Because this volume is a merge from different surveys, and the details of how this merge was done remain unclear, different amplitudes are observed within the merge

In order to tie these surfaces with the well logs (and the new picks), sonic logs from EM-1 well along with the 3D mega merged-volume were used to compute synthetic seismogram for each individual interval using SynTool software package from LandMark. The synthetic seismogram correlation indexes were very low for each interval, ranging between 20 and 45%. A fair correlation index in the industry would be higher than 65% for single intervals.

Figure 4.24 show an example of the seismogram and the correlation index is annotated on the bottom. Positive amplitude generally characterized the abrupt change in sand bodies (i.e. top of the R intervals).

Based on the new synthetic seismogram we assessed the correlation with the seismic and especially on the western part of the area some misties were found with maximum of 100 ms, which will represent 75 meters of error (i.e.: 1 ms = 0.75 m).

However, these maps were used to understand the regional trend in accommodation space and dominant structures and features within the basin.

Figure 4.25 and 4.26 show the correlation between the isochron map from the seismic data and the NTG map from the well data for two of the measured T-R cycles: T-R cycle "E" and T-R cycle "F".

The seismic maps show a regional trend of the accommodation space. Greater thicknesses are trapped against the faults. Thickness decrease when moving away from the western bounding fault towards the east, this trend is observed in successive fault blocks. Faults created mini-basins, which act as depocenters. Sediments prograde and start to fill the mini-basin until it stalls and then prograde toward the next mini-basin created by the next pair of faults. Near the Darien Ridge, thicknesses decrease parallel the structure. The Columbus channel is also observed in both maps, which serves as a conduit for sediments to move from the inner shelf towards the basin.

When comparing the seismic maps with the net-to-gross maps NTG values decrease as the Darien Ridge is approached. The contours for the rest of the basin follow the strike of the growth faults. NTG ratios increase locally as moving away from the western bounding fault, while as confirmed by the seismic maps, the total thickness decrease. Figure 4.27 shows a cartoon that explained this issue.

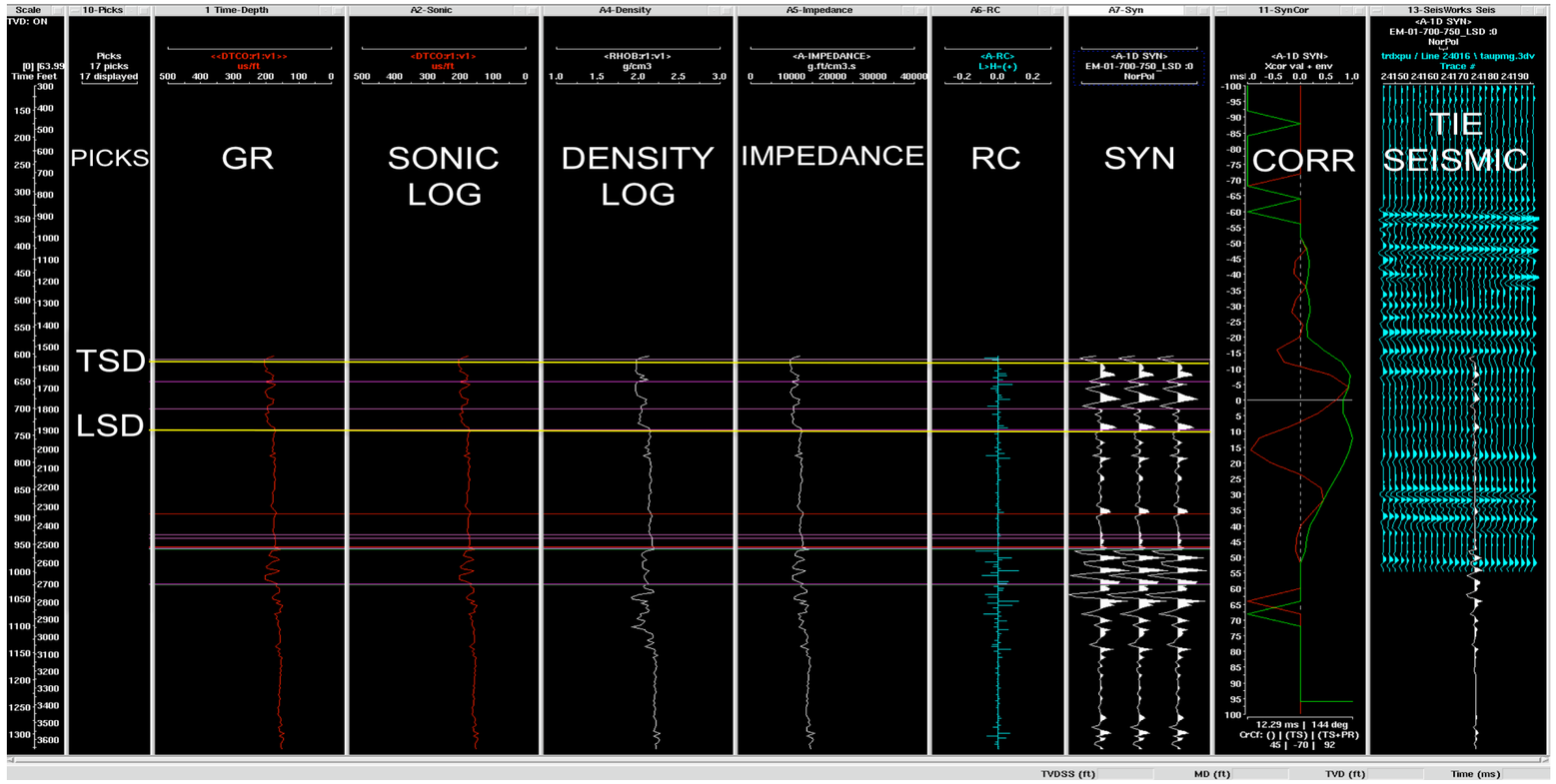

Synthetic Seismogram from: EM-01.
Interval: LSD 700-750 ms.
Survey: 3D mega-merge seismic volume

Correlation Coefficient: 45%

Figure 4.24. Example of Synthetic Seismogram from well EM-01 for specific surface RD (LSD in figure). Columns from left to right contain: Pick names, gamma-ray log, sonic log, density log, impedance (computed), reflection coefficients (RC), synthetic seismogram, correlation between synthetic seismogram and seismic, tie with seismic trace from 3D mega-merge seismic volume. The correlation coefficient is 45%, however graphically the correlation column is showing a poor correlation.

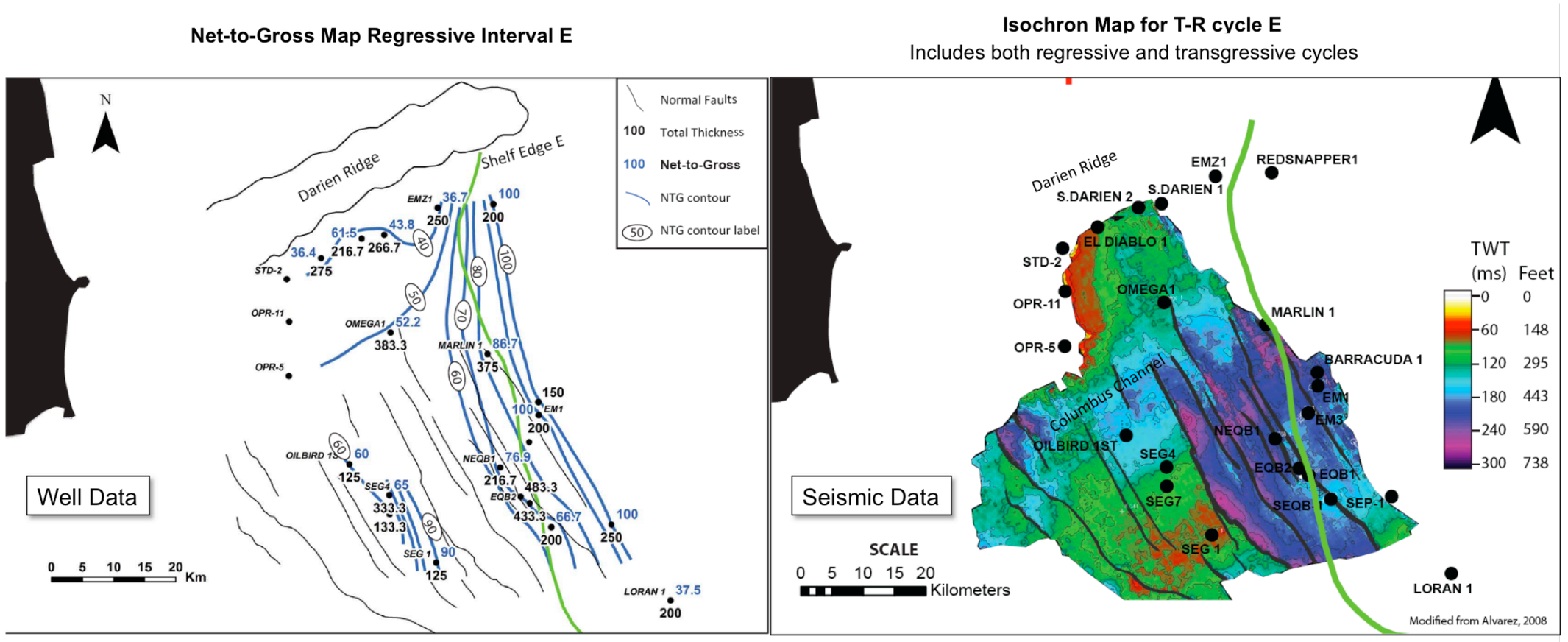

Figure 4.25. Correlation between net-to-gross map for R cycle RE and isochron map T-R cycle “E”.

Net-to-Gross Map Regressive Interval F

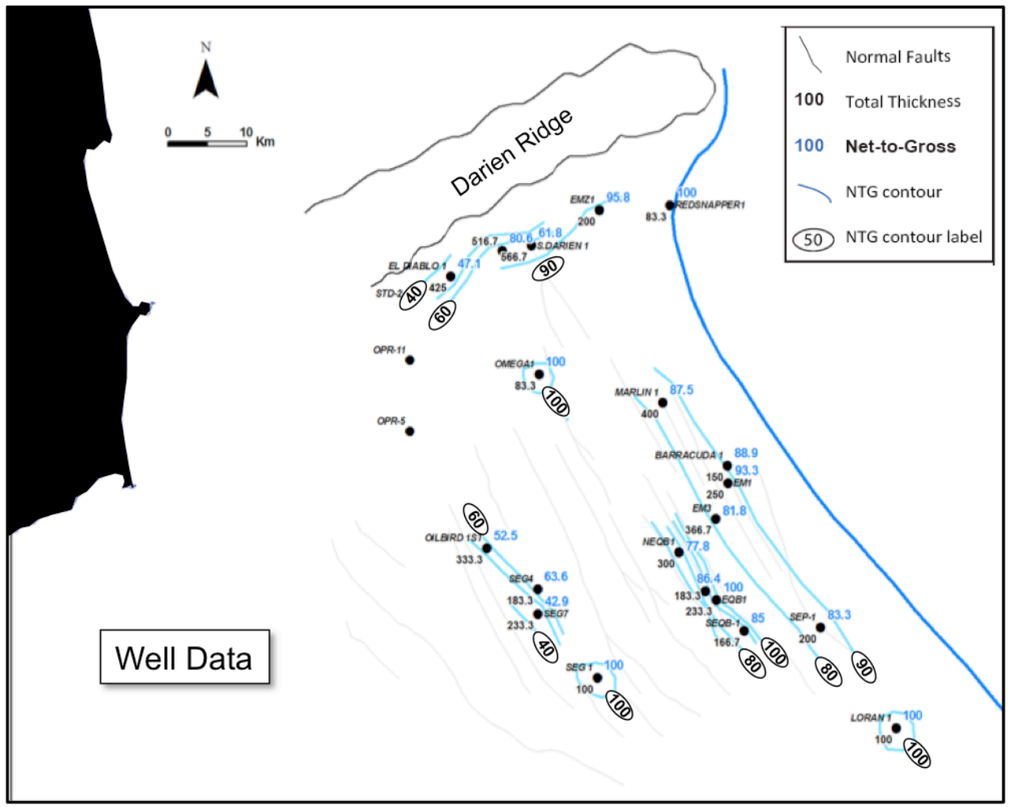

Isochron Map for T-R Cycle F
Includes both regressive and transgressive cycles

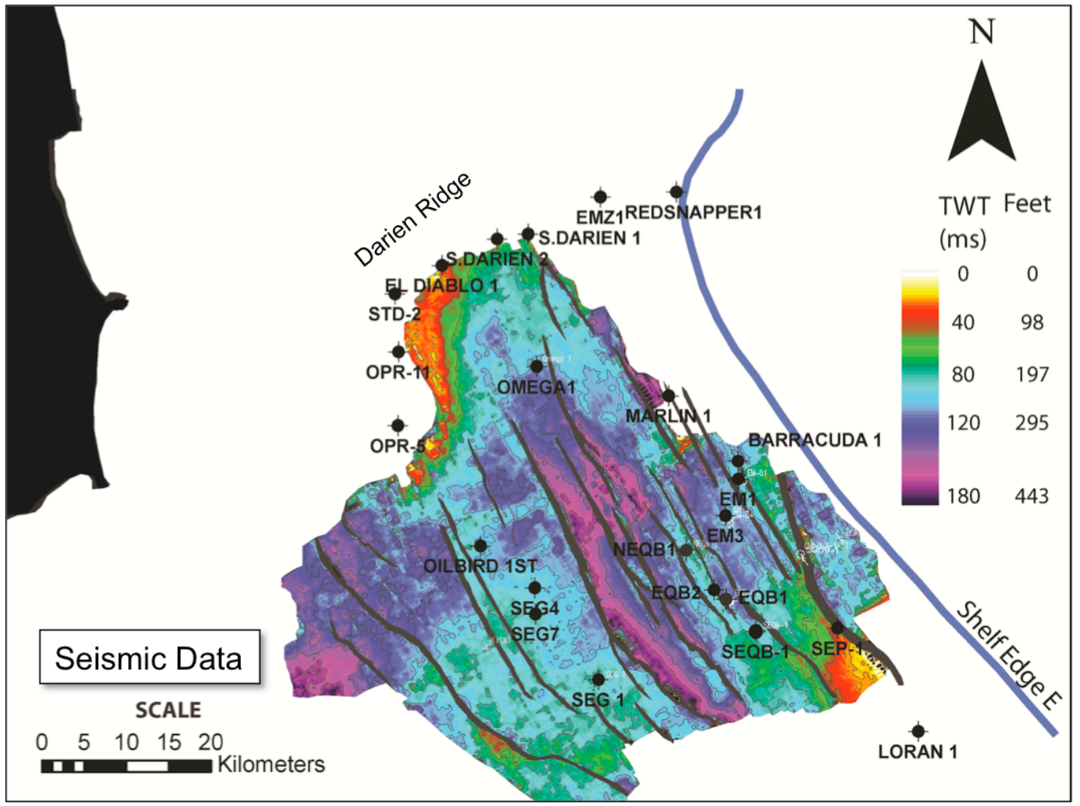

Figure 4.26. Correlation between net-to-gross map for R cycle RF and isochron map for T-R cycle “F”.

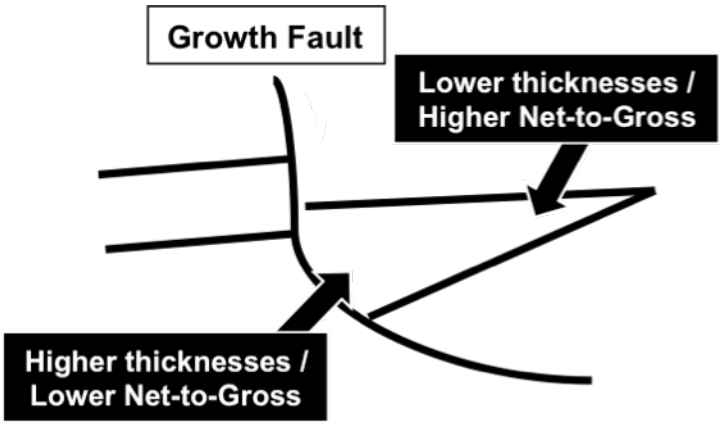

Figure 4.27 Diagram showing the relationship between Net-to-gross ratio an total thickness in a mini-basin created by a growth fault.

4.4 SUMMARY AND DISCUSSION

Sand distribution within R and T cycles shows a very different scenario for each one. When analyzing both cycles, T cycles have NTG values lower than 60% whereas for R cycles most of the values range from 35% to 100%.

The relationship between net sand and total thicknesses for both cycles shows the same trend: net sand increase as total thickness increase. However, trendline slopes reveal that for T cycles the highest slope value is 0.3; while for R cycles slopes range between 0.3 and 0.83, indicating a higher sand content during R cycles which is expected when the sea-level is falling. For T-R cycles "D" and "E", T cycles show very low sand content while for their R cycles, NTG ratios are very high. This may be evidence of basinwards sand bypass during R cycles.

Both net-to-gross maps for R and T cycles show that the growth faulting controls the distribution of sand.

Within the Columbus Channel, the well Omega-1, show very low NTG ratios during T cycles and very high net-to-gross ratios during their counterpart R cycles. The Columbus Channel is a pathway for sediments, and it is possible that during transgression sediments go through and reach more proximal parts as the channel serves as a conduit that connect the outer shelf with the inner shelf.

Near the Darien ridge, all cycles show NTG ratios higher than 10% and up to 60% for T cycles, while for R cycles these values are generally lower than 60%, except for D, but they tend to decrease as the ridge is approached. During transgression sediments retrograde and are probably trapped against this ridge. It is not possible to assess how much of the sand is fed locally from the Darien Ridge.

During R cycles, all NTG maps show contours increasing locally within a fault block. The NTG ratios increase as moving away from the downthrown side of the western bounding fault and as they approach the hanging-wall of the eastern bounding fault, while at the same time total thicknesses diminish. This is consistent with the trend observed for the seismic maps where thicknesses diminish as moving away from the downthrown side of the fault. This model suggests that sediments are infilling the mini-basins created by the growth faults.

4.5 NEW MODEL PROPOSED FOR THE COLUMBUS BASIN

Wood (2000) shows a possible explanation to create these mini-basins. Figure 4.28 shows the illustration of the timing of formation (from oldest to youngest) of various aspects of typical megasequence across the gas trend area from Cassia field, Offshore Trinidad.

The author proposed that a typical sequence of fault initiates with a normal fault (See figure 4.27 - G Fault) that extends and terminates glide plane F in depth. The sediment wedge to the northeast of the fault begins to be rotated about counter regional glide plane G". As a consequence, a shelf break is created and sediments start to accumulate landward of the underlying mobile shale. Due to the weight of sediments and as a response to continued extension, mobile shales are forced eastward, and the next fault (H Fault) initiated the same cycle. Afterward, accommodation space is filled and the shelf break progrades eastward. On the fault plane H, sediments are being dragged by the fault. The process repeats itself until there is no shale to withdraw.

Figure 4.28 shows that the thickness of each cycle is greater near the western bounding fault (G fault) and decrease as the eastern bounding fault (H Fault) is reached. In section 4.3 an observation was made from the comparison between the seismic map and the NTG map, where the relationship between NTG and thickness seems to be inversely proportional, as it is also illustrated by figure 4.27.

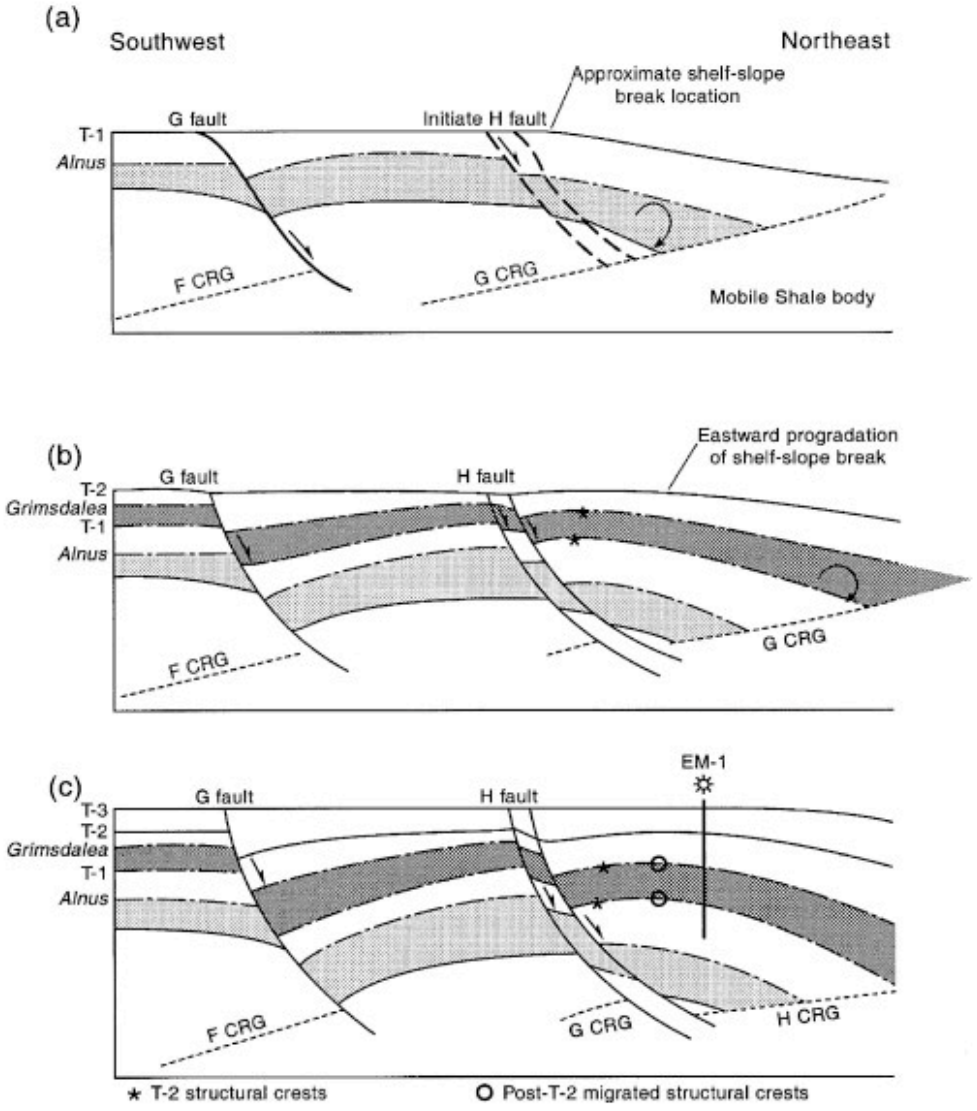

Figure 4.28. Illustration of the timing of formation (from oldest to youngest, a to b to c, respectively) of various aspects of a typical megasequence across an area from Cassia field within the Columbus Basin (Wood, 2000).

As explained in Chapter 3, at least 50% of the sediments in the Columbus Basin come from the Amazon River.

The Amazon River supplies mainly fine-grained sediments that have been transported by the Guiana Current, which runs north-south along the western coastline of South America (from Amazon River to Orinoco Delta). Figure 4.29 shows a satellite image of planktonic distribution in the water column, which reflects the suspended sediments transported by the Guiana Current. The potential of this current to transport sediments is clearly appreciated and therefore reworking and redistribution of sediments in the Columbus Basin, the Eastern Venezuelan Basin and the North Coast Marine Area (NCMA) of Trinidad and Tobago is likely to occur.

This current is transporting sediments in the direction of the growth faulting in the Columbus Basin, when it reaches the proximal part of the fault wedge (figure 4.26) fine sediments are mixed with sandy and shaly sediments from the Orinoco Delta. On the thicker part of the wedge (on the downthrown side of each western bounding fault), larger accommodation space allowed the current to redistribute the sediments and clean the sand in the section, leaving the finer sediments to settle down, therefore lowering the NTG ratio. On the other hand, in the distal part of the fault wedge, where the accommodation space is smaller, the water column is reduced and the sand is reworked and being trapped in the thinner part of the fault wedge.

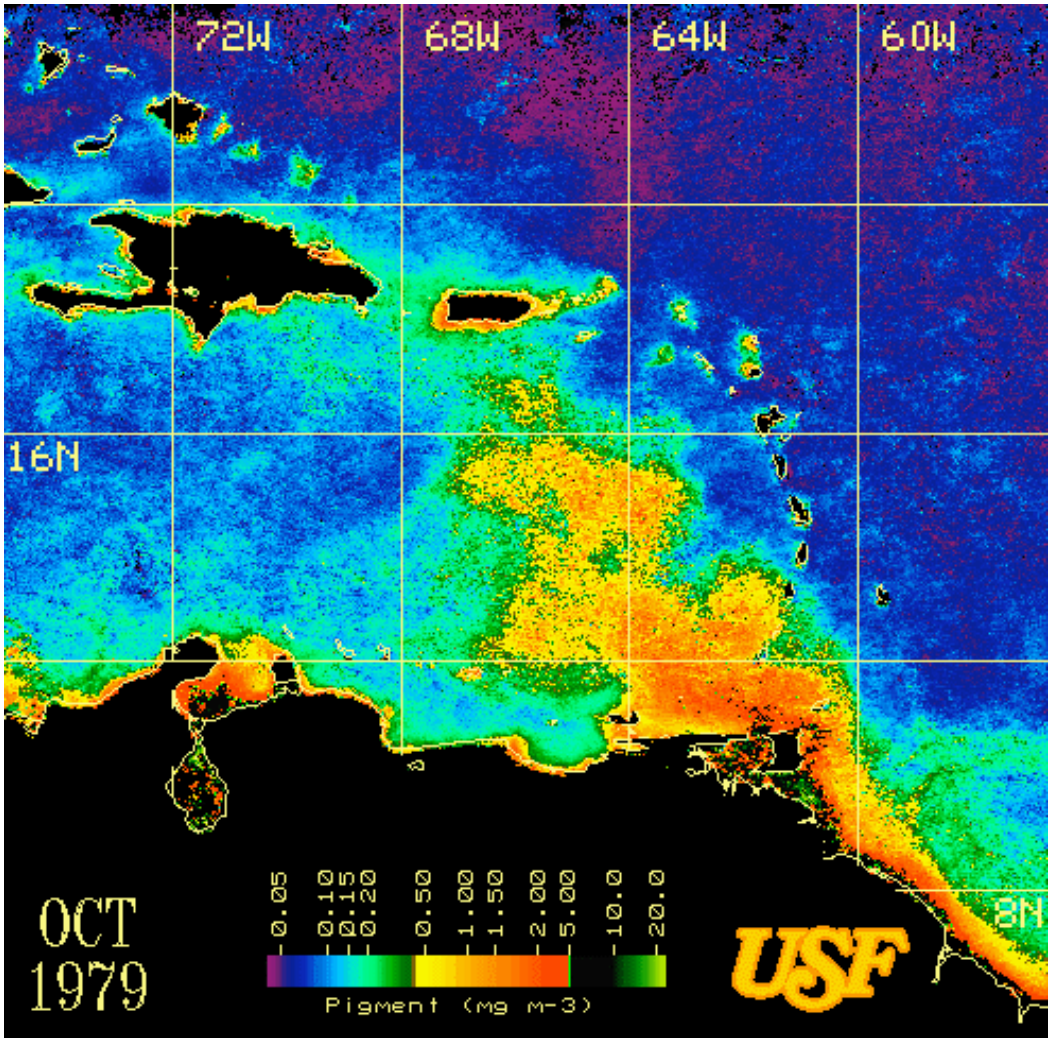

Figure 4.29. Satellite image of Suspended Sediment – Fluid Muds strong salinity fronts associated with the plume discharged in the eastern Caribbean Sea for October 1979, showing the spatial extent of the Orinoco River plume (USF, 1979).

Chapter 5: Conclusions

The shelf-edge connects the outer shelf with the deep-water basin and therefore represents a very efficient method of sand delivery toward the basin. In the Columbus Basin, the shelf-edge zone is a highly complex are due to high accommodation space interacting with different depositional processes. Several wells have been drilled within the Pliocene-Recent sequence, where over 60 pay zones have been identified within shelf-edge reservoir units.

The Columbus Basin exhibits along-strike structural variations due to the presence of the Darien Ridge in the Northern Structural Domain and normal growth and counter-normal faults in both the Northern and Southern Structural Domains. These underlying structures are controlling the geometries, accommodation space and sand distribution of these shelf-edge deltaic units.

This research analyzed in detail six T/R cycles identified within the Pliocene to Recent stratigraphic succession, from older to younger are labeled T-R cycles: N, J, H, F, E, and D. During this time, shelf edge trajectories migrate northeasterly across the Columbus Basin. This migration is associated with the evolution of the paleo-Orinoco Delta system through time. Shelf edge orientations and geometries are strongly influenced by the underlying structural controls that are present in the NSD and SSD.

Different progradation rates have been observed both along strike and dip in the shelf-edge trajectories in plan view. Progradation distances decrease from time of surface N to time of surface F in a similar magnitude in both NSD and SSD. The transgressive event E seems to be twice larger in the SSD vs. NSD.

NTG values within T cycles never exceed 60% and they seem to be inversely proportional to total thickness, whereas for R cycles NTG are highly variable, ranging from 35% to 90%.

There is an increase of net-to-gross within the R cycles of each T/R cycle as the shelf break is approached. Additional accommodation space associated with growth and counter regional faults (sediment traps) and structurally control paleocanyons favored the thickening of the stratigraphic successions near the shelf break.

NTG maps and isochron maps from the seismic indicated that the NTG are controlled by the underlying structures. In the NSD the NTG ratios decrease as the Darien Ridge is approached and in the SSD the NTG are locally controlled by the growth faults.

The growth faults created mini-basins that serve as depocenters, where thickness decreases when moving away from the western bounding fault and at the same time NTG ratio increase. The Guiana current is believed to play an important role in the redistribution and reworking of sand in the Columbus Basin. In the mini basins, the fault wedge shows larger accommodation space near to the western bounding fault, hence the Guiana current is allowed to clean the sand by bringing finer sediments that later would settle down and would lower the NTG ratio. In the distal part of the fault wedge (thinner part) the NTG is higher and this may be caused by the smaller accommodation space that make the current to rework the sand.

Aggradation and progradation distances were computed for each interval and the results suggest that the younger Sequences C2 (T-R cycle E) and C3 (T-R cycle F) show a stronger progradational trend than the older C4, C5 and C6. This strong progradational trend might indicate delivery of sand basinwards, while for the older intervals; the aggradational trend suggests a increase in sediment storage.

In long-term scale (1-2 m.y.) the Orinoco Delta seems to behave as an aggradational delta that increases sediment storage due to growth fault and high subsidence rates. However, in the short-term scale, the Orinoco delta seems to behave as a rapid progradational delta, for the younger sequences C2 and C3, where sediment bypass is more likely to occur; and as a rapid aggradational (slow prograding) margin for the older intervals C4, C5 and C6.

Appendices

APPENDIX A

CYCLE	TD			RD		
WELL	TT	TS	NTG	TT	TS	NTG
STD-2						
EL DIABLO ST-1						
S.DARIEN 2				533.3	533.3	100.0
S.DARIEN 1	491.7	158.3	32.2	116.7	116.7	100.0
EMZ1				166.7	166.7	100.0
RED SNAPPER 1						
OPR-11						
OPR-5						
OILBIRD 1	350.0	25.0	7.1	83.3	50.0	60.0
SEG4	150.0	0.0	0.0	341.7	233.3	68.3
SEG7	400.0	16.7	4.2	233.3	100.0	42.9
SEG1	200.0	25.0	12.5	200.0	200.0	100.0
OMEGA 1						
NEQB1	333.3	125.0	37.5	233.3	233.3	100.0
EQB2	366.7	0.0	0.0	333.3	233.3	70.0
EQB1	291.7	0.0	0.0	316.7	200.0	63.2
SEQB-1	333.3	16.7	5.0	116.7	91.7	78.6
Marlin 1				100.0	100.0	100.0
Barracuda 1	266.7	0.0	0.0	216.7	183.3	84.6
EM1	116.7	50.0	42.9	350.0	250.0	71.4
EM3						
SEP-1				83.3	75.0	90.0
LORAN1						

Table A.1. Total Thickness (TT), Total Sand (TS) and NTG (Net-to-Gross) values for Cycles RD and TD

CYCLE	TE			RE		
WELL	TT	TS	NTG	TT	TS	NTG
STD-2						
EL DIABLO ST-1				275.0	100.0	36.4
S.DARIEN 2	566.7	333.3	58.8	216.7	133.3	61.5
S.DARIEN 1	183.3	16.7	9.1	266.7	116.7	43.8
EMZ1	250.0	0.0	0.0	250.0	91.7	36.7
RED SNAPPER 1	766.7	0.0	0.0	200.0	200.0	100.0
OPR-11						
OPR-5						
OILBIRD 1	533.3	116.7	21.9	125.0	75.0	60.0
SEG4	216.7	50.0	23.1	333.3	216.7	65.0
SEG7	116.7	0.0	0.0	133.3	66.7	50.0
SEG1	100.0	0.0	0.0	125.0	112.5	90.0
OMEGA 1	433.3	75.0	17.3	383.3	200.0	52.2
NEQB1	333.3	16.7	5.0	216.7	166.7	76.9
EQB2	783.3	166.7	21.3	483.3	333.3	69.0
EQB1	683.3	133.3	19.5	433.3	316.7	73.1
SEQB-1	1083.3	116.7	10.8	200.0	133.3	66.7
Marlin 1	325.0	0.0	0.0	375.0	325.0	86.7
Barracuda 1	733.3	83.3	11.4	150.0	150.0	100.0
EM1	633.3	0.0	0.0	200.0	191.7	95.8
EM3						
SEP-1	183.3	50.0	27.3	250.0	250.0	100.0
LORAN1				200.0	75.0	37.5

Table A.2. Total Thickness (TT), Total Sand (TS) and NTG (Net-to-Gross) values for Cycles RE and TE

CYCLE	TF			RF		
WELL	TT	TS	NTG	TT	TS	NTG
STD-2						
EL DIABLO ST-1	450.0	100.0	22.2	425.0	200.0	47.1
S.DARIEN 2	550.0	200.0	36.4	516.7	416.7	80.6
S.DARIEN 1	408.3	66.7	16.3	566.7	350.0	61.8
EMZ1	1600.0	300.0	18.8	200.0	191.7	95.8
RED SNAPPER 1	1383.3	0.0	0.0	83.3	83.3	100.0
OPR-11						
OPR-5						
OILBIRD 1	250.0	125.0	50.0	333.3	175.0	52.5
SEG4	100.0	16.7	16.7	183.3	116.7	63.6
SEG7	250.0	66.7	26.7	233.3	100.0	42.9
SEG1	350.0	150.0	42.9	100.0	100.0	100.0
OMEGA 1	266.7	16.7	6.3	83.3	83.3	100.0
NEQB1	1333.3	483.3	36.3	300.0	233.3	77.8
EQB2	516.7	200.0	38.7	183.3	158.3	86.4
EQB1	483.3	0.0	0.0	233.3	233.3	100.0
SEQB-1	433.3	50.0	11.5	166.7	141.7	85.0
Marlin 1	2350.0	500.0	21.3	400.0	350.0	87.5
Barracuda 1	2116.7	516.7	24.4	150.0	133.3	88.9
EM1	2166.7	383.3	17.7	250.0	233.3	93.3
EM3	1066.7	400.0	37.5	366.7	300.0	81.8
SEP-1	2516.7	216.7	8.6	200.0	166.7	83.3
LORAN1	1816.7	283.3	15.6	100.0	100.0	100.0

Table A.3. Total Thickness (TT), Total Sand (TS) and NTG (Net-to-Gross) values for Cycles RF and TF

CYCLE	TH			RH		
WELL	TT	TS	NTG	TT	TS	NTG
STD-2						
EL DIABLO ST-1						
S.DARIEN 2	216.7	33.3	15.4			
S.DARIEN 1	83.3	0.0	0.0	333.3	66.7	20.0
EMZ1	800.0	283.3	35.4	416.7	233.3	56.0
RED SNAPPER 1	1100.0	183.3	16.7	400.0	216.7	54.2
OPR-11						
OPR-5						
OILBIRD 1						
SEG4						
SEG7						
SEG1						
OMEGA 1	183.3	16.7	9.1	83.3	83.3	100.0
NEQB1	166.7	8.3	5.0	1033.3	383.3	37.1
EQB2	100.0	16.7	16.7	1333.3	600.0	45.0
EQB1	133.3	50.0	37.5	550.0	250.0	45.5
SEQB-1	416.7	66.7	16.0	233.3	100.0	42.9
Marlin 1	1450.0	400.0	27.6	900.0	525.0	58.3
Barracuda 1	1483.3	350.0	23.6	900.0	516.7	57.4
EM1	750.0	216.7	28.9	1033.3	633.3	61.3
EM3	683.3	333.3	48.8	683.3	333.3	48.8
SEP-1	1033.3	433.3	41.9	500.0	383.3	76.7
LORAN1	466.7	183.3	39.3	900.0	483.3	53.7

Table A.4. Total Thickness (TT), Total Sand (TS) and NTG (Net-to-Gross) values for Cycles RH and TH

CYCLE	TJ			RJ		
WELL	TT	TS	NTG	TT	TS	NTG
STD-2						
EL DIABLO ST-1	100.0	0.0	0.0	425.0	100.0	23.5
S.DARIEN 2	716.7	266.7	37.2	83.3	33.3	40.0
S.DARIEN 1	650.0	116.7	17.9	283.3	16.7	5.9
EMZ1						
RED SNAPPER 1						
OPR-11						
OPR-5						
OILBIRD 1	600.0	200.0	33.3	400.0	133.3	33.3
SEG4	266.7	150.0	56.3	483.3	283.3	58.6
SEG7	166.7	100.0	60.0	300.0	116.7	38.9
SEG1	262.5	75.0	28.6	75.0	37.5	50.0
OMEGA 1	966.7	100.0	10.3	83.3	83.3	100.0
NEQB1	2200.0	600.0	27.3	166.7	50.0	30.0
EQB2	2666.7	416.7	15.6	116.7	83.3	71.4
EQB1	2633.3	616.7	23.4	116.7	50.0	42.9
SEQB-1	2900.0	383.3	13.2	166.7	16.7	10.0
Marlin 1						
Barracuda 1						
EM1	966.7	100.0	10.3	383.3	66.7	17.4
EM3	716.7	116.7	16.3	100.0	75.0	75.0
SEP-1						
LORAN1						

Table A.5. Total Thickness (TT), Total Sand (TS) and NTG (Net-to-Gross) values for Cycles RJ and TJ

CYCLE	TN			RN		
WELL	TT	TS	NTG	TT	TS	NTG
STD-2				150.0	150.0	100.0
EL DIABLO ST-1	825.0	175.0	21.2	300.0	200.0	66.7
S.DARIEN 2	1783.3	550.0	30.8	383.3	150.0	39.1
S.DARIEN 1	683.3	33.3	4.9	166.7	66.7	40.0
EMZ1						
RED SNAPPER 1						
OPR-11				541.7	216.7	40.0
OPR-5	333.3	116.7	35.0	266.7	166.7	62.5
OILBIRD 1	283.3	83.3	29.4	416.7	266.7	64.0
SEG4	433.3	100.0	23.1	316.7	266.7	84.2
SEG7	383.3	83.3	21.7	250.0	216.7	86.7
SEG1	400.0	100.0	25.0	400.0	287.5	71.9
OMEGA 1	858.3	83.3	9.7	583.3	216.7	37.1
NEQB1	1250.0	50.0	4.0	466.7	183.3	39.3
EQB2						
EQB1	1883.3	366.7	19.5	333.3	250.0	75.0
SEQB-1						
Marlin 1						
Barracuda 1						
EM1						
EM3						
SEP-1						
LORAN1						

Table A.6. Total Thickness (TT), Total Sand (TS) and NTG (Net-to-Gross) values for Cycles RN and TN

APPENDIX B

elements that can also be related to the passive margins (e.g.: growth faults).

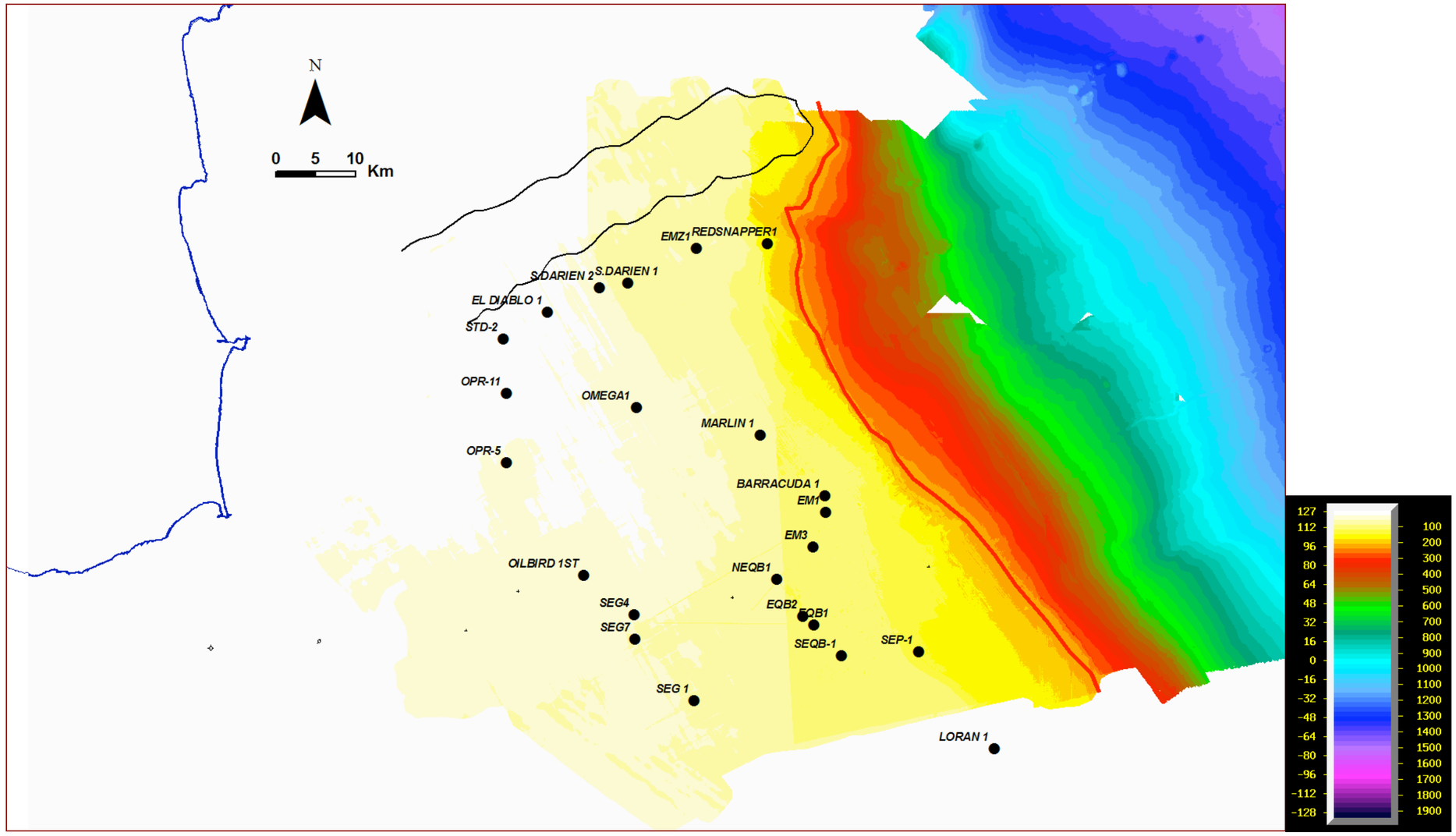

Figure B.1 Seafloor map compiled from Sullivan (2005), Moscardelli (2006); Maher (2007); Alvarez (2008). Thick red line corresponds to the modern shelf-edge

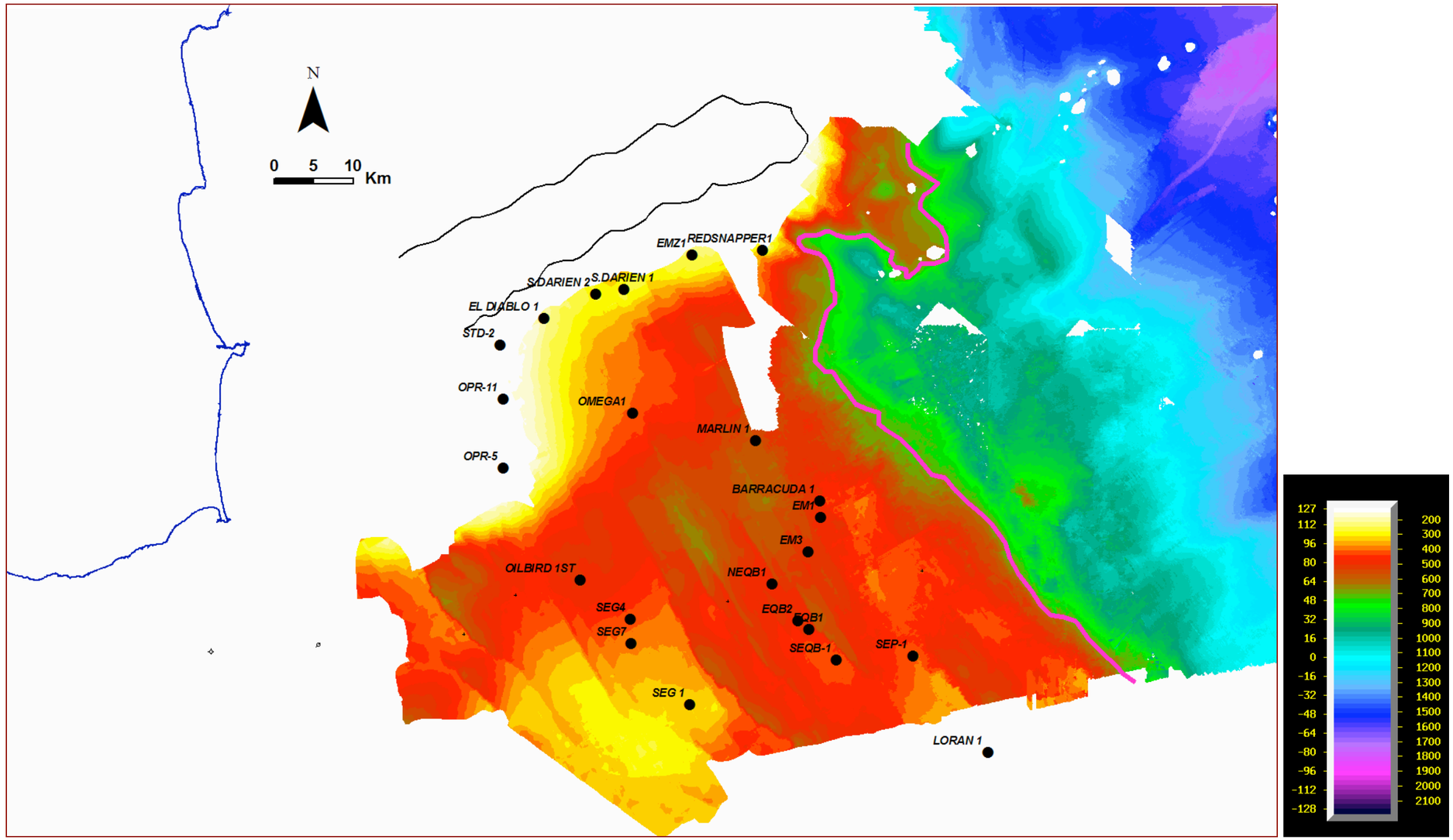

Figure B.2 Surface D map compiled from Moscardelli (2006) and Alvarez (2008). Thick magenta line corresponds to the shelf-edge D

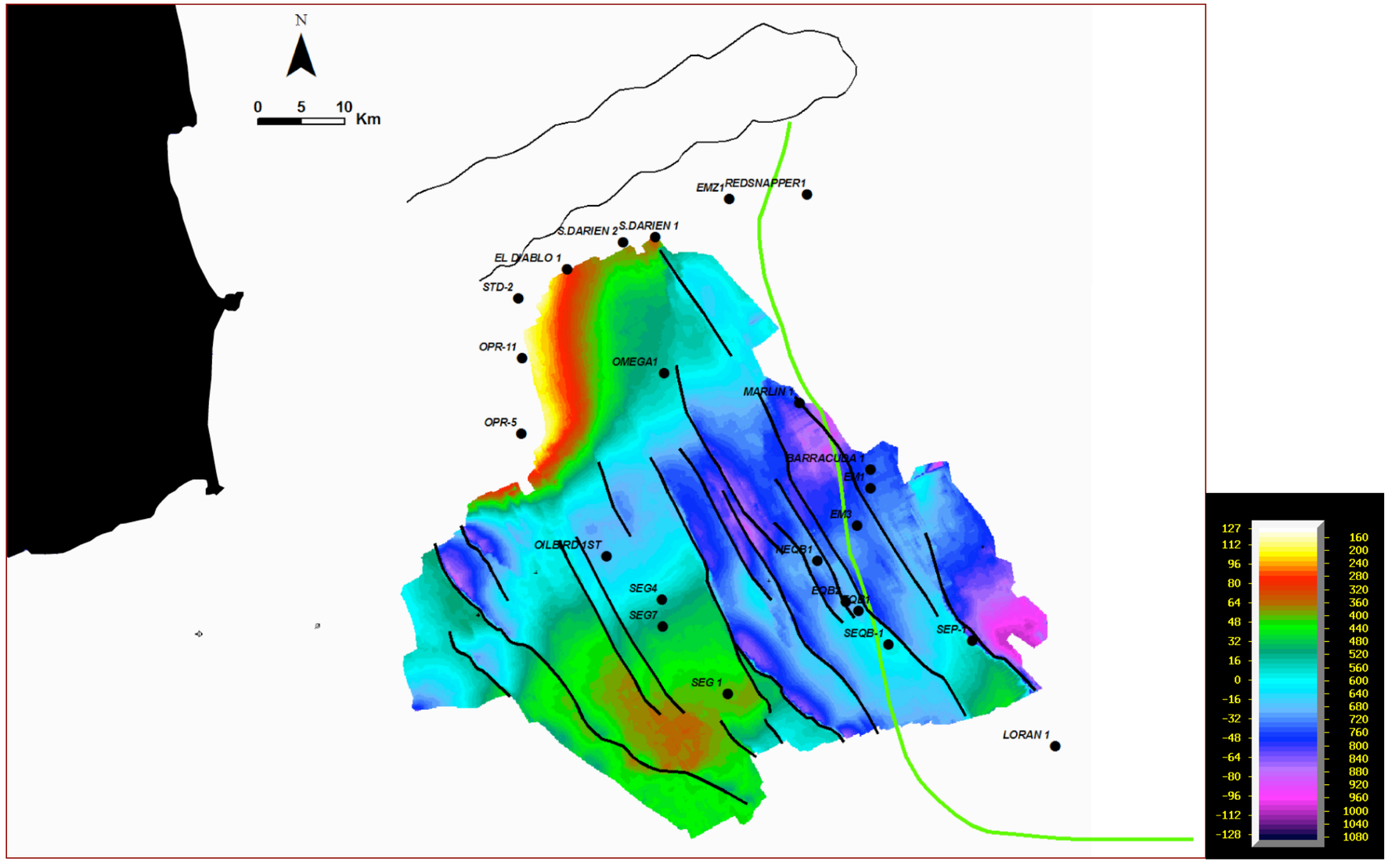

Figure B.3 Surface E map compiled from Alvarez (2008). Thick green line corresponds to the shelf- edge E

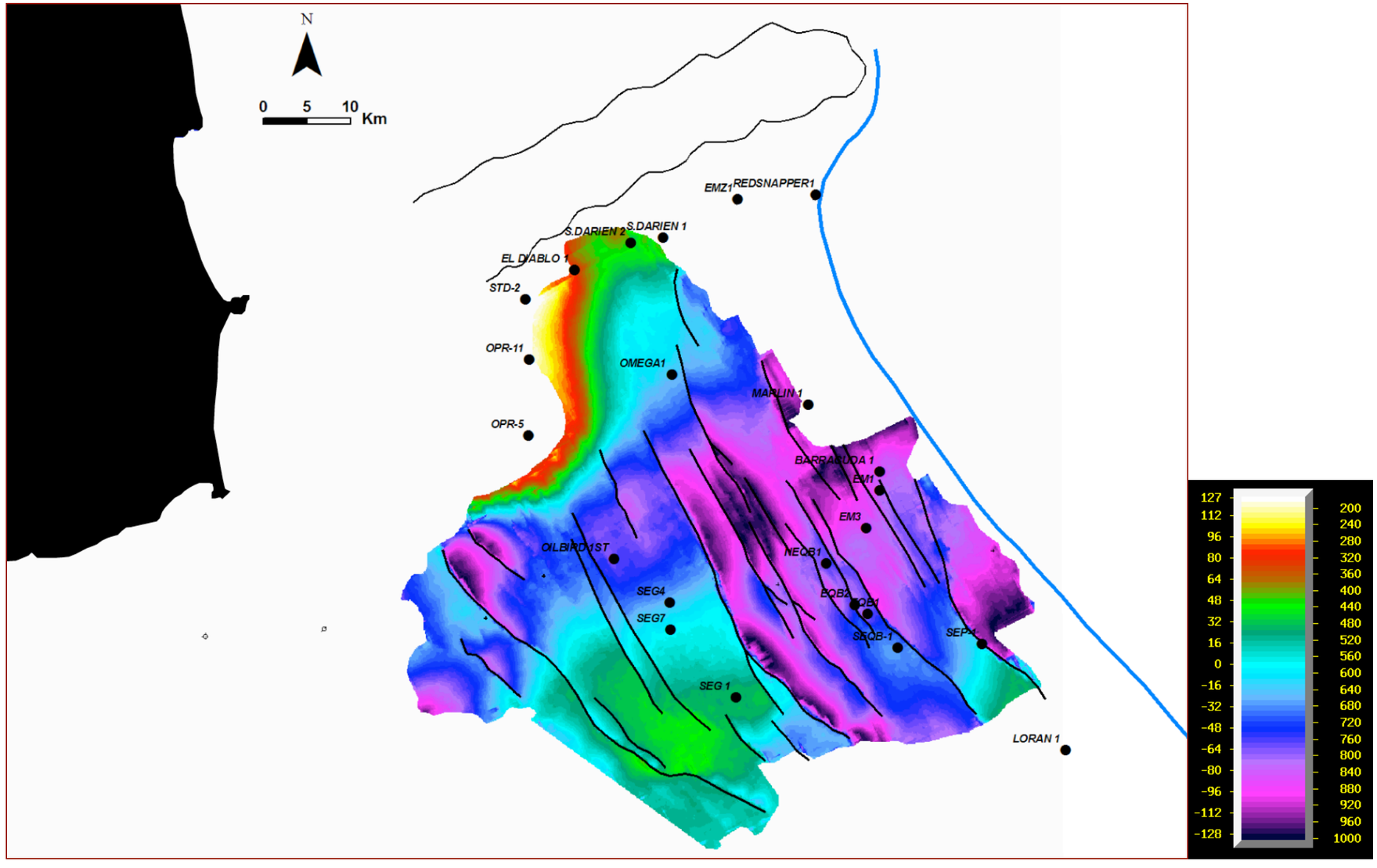

Figure B.4 Surface F map compiled from Alvarez (2008). Thick blue line corresponds to the shelf-

edge F

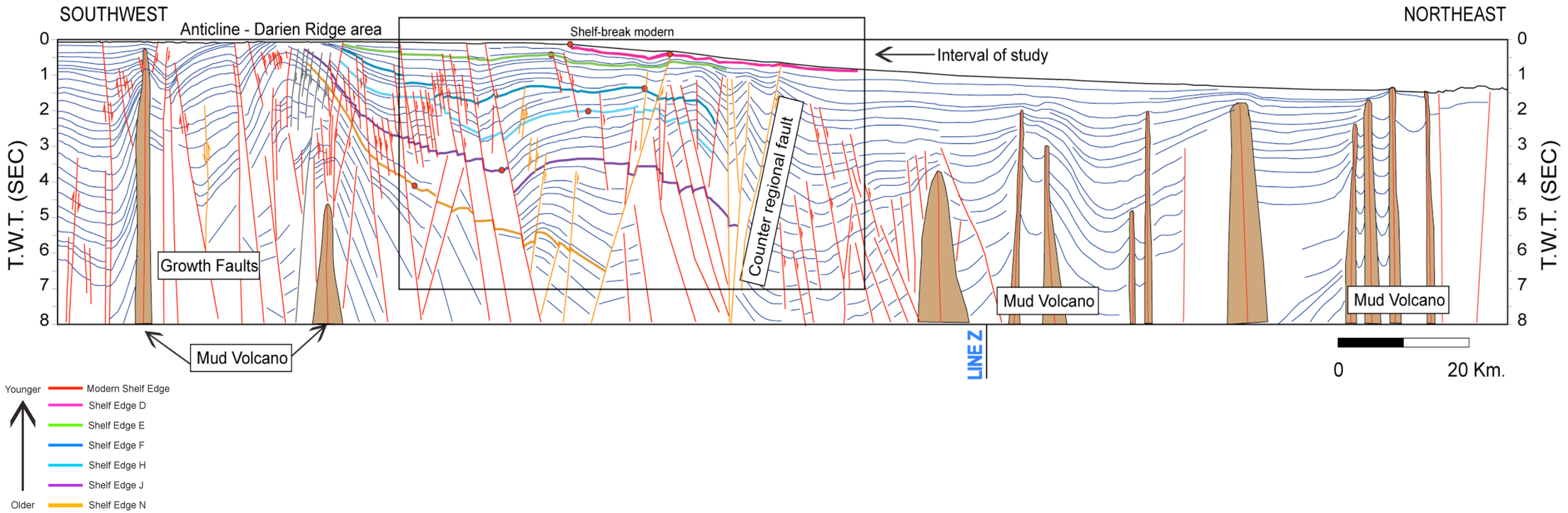

Figure B.5 Line X in the Northern Structural Domain. Red points represent shelf-break for each surface.

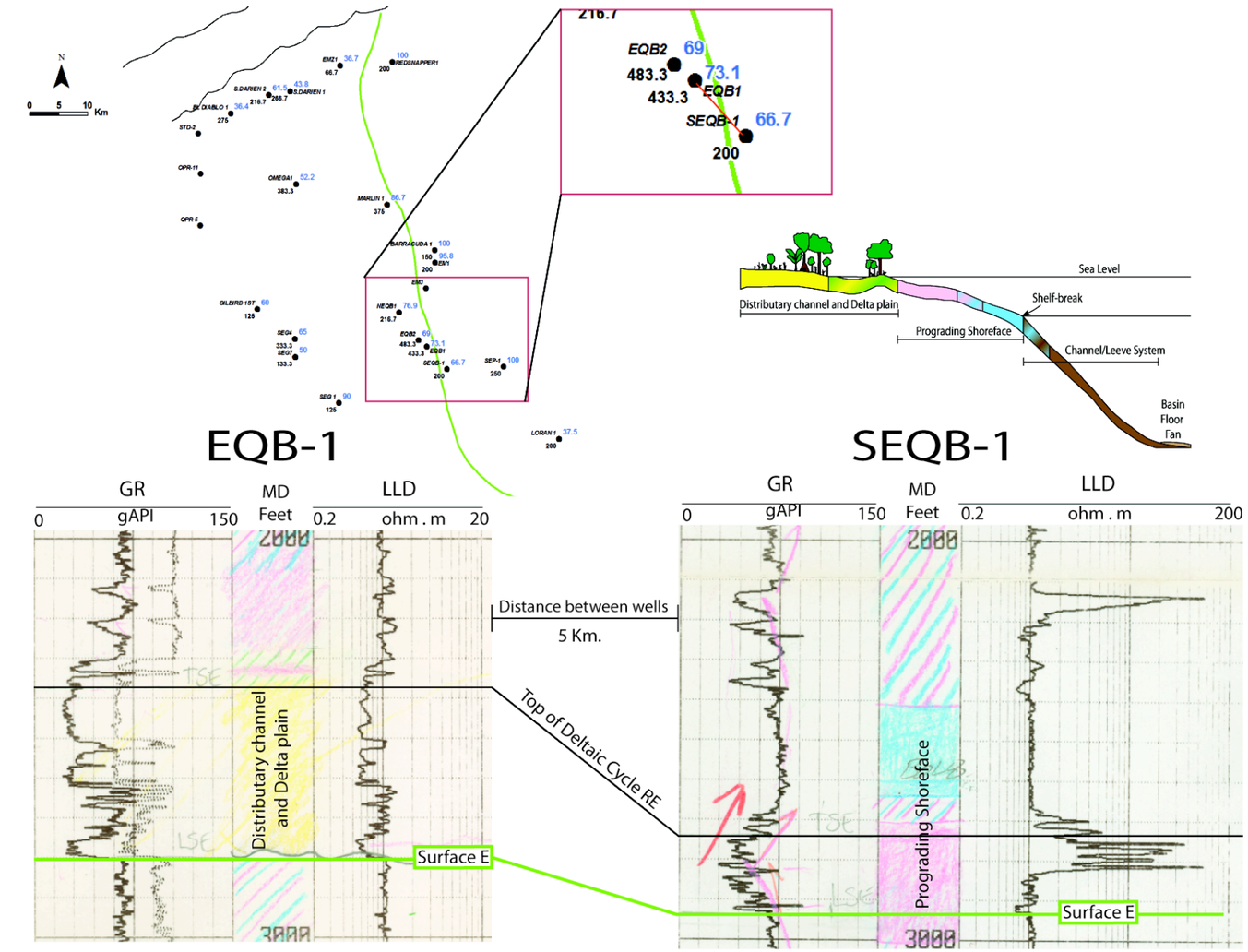

Figure B.6 Facies shift for shelf-edge E

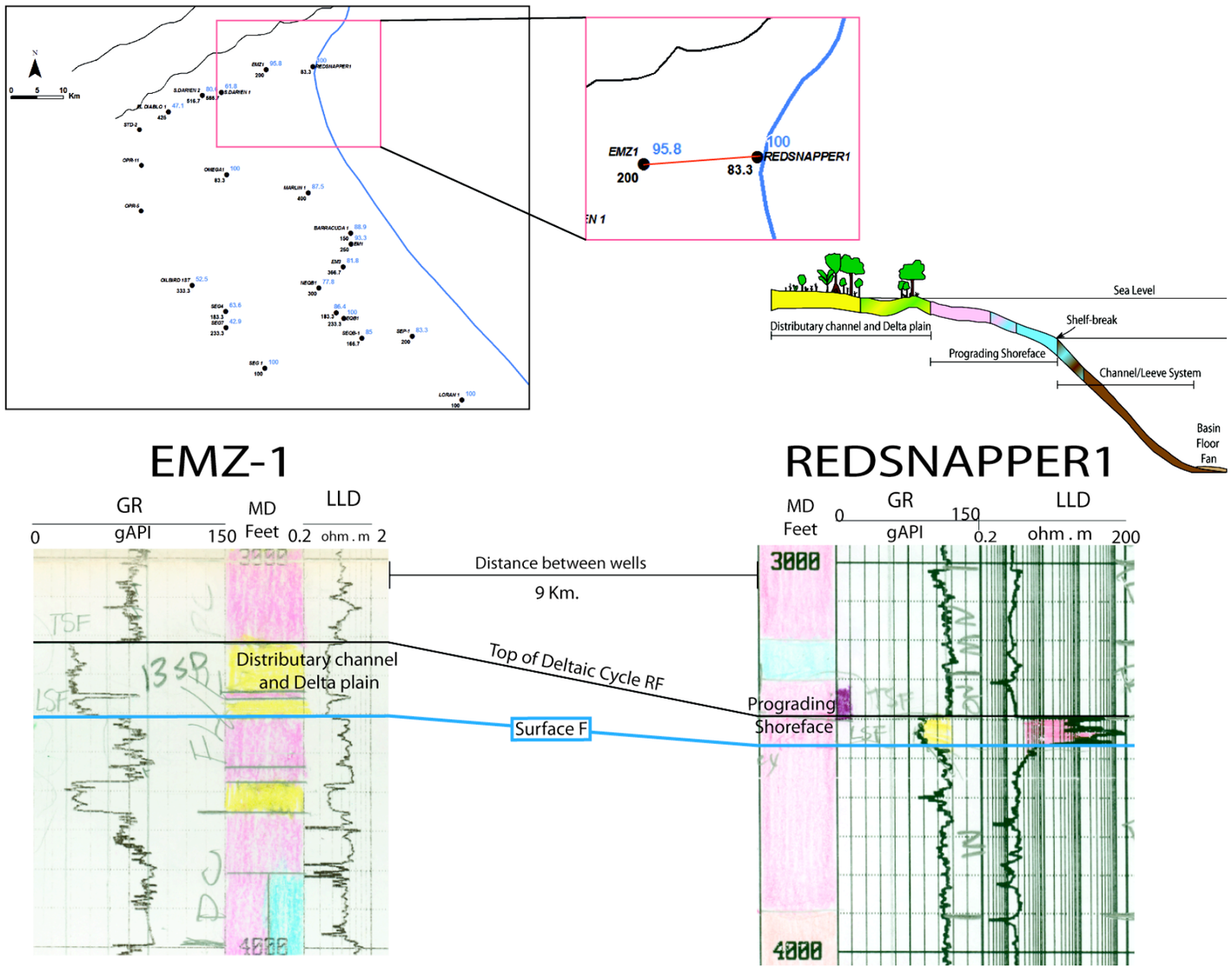

Figure B.7 Facies shift for shelf-edge F

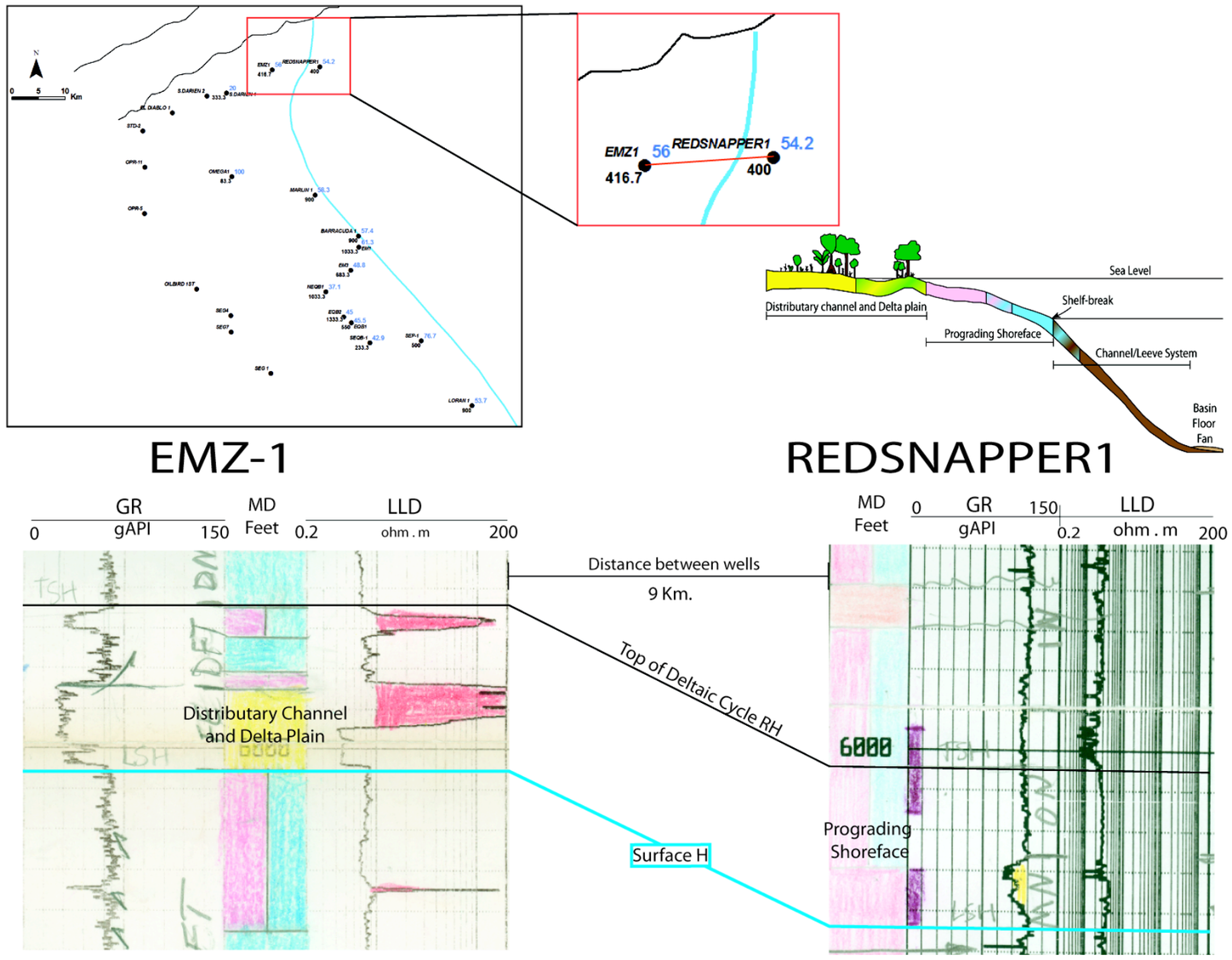

Figure B.8 Facies shift for shelf-edge H

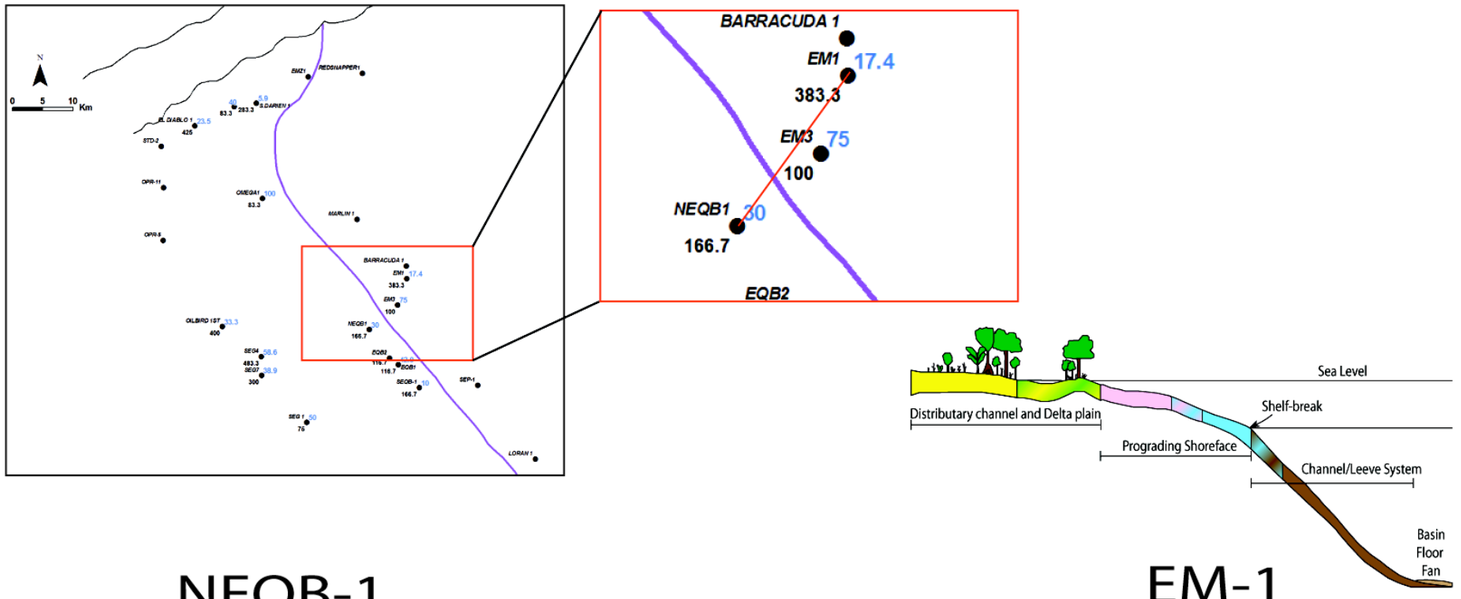

Figure B.9 Facies shift for shelf-edge J

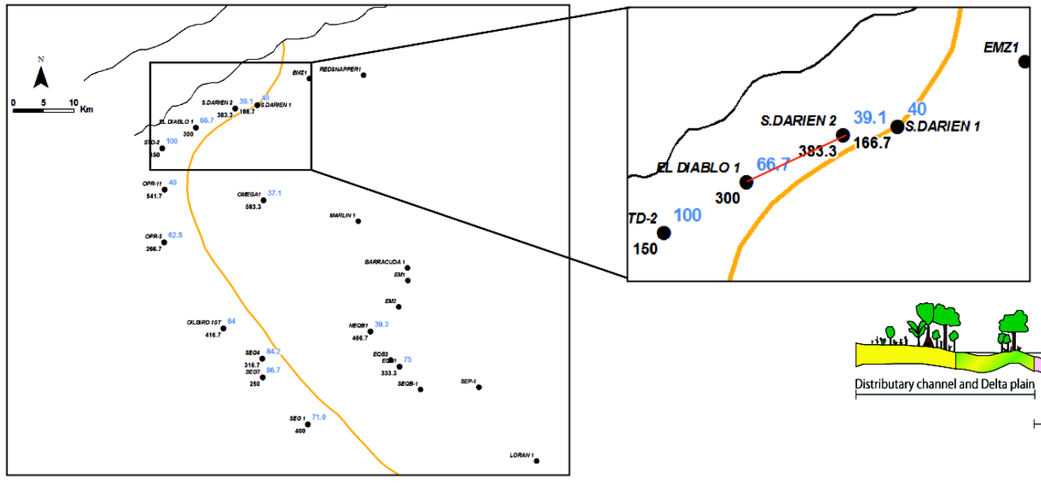

EL DIABLO 1

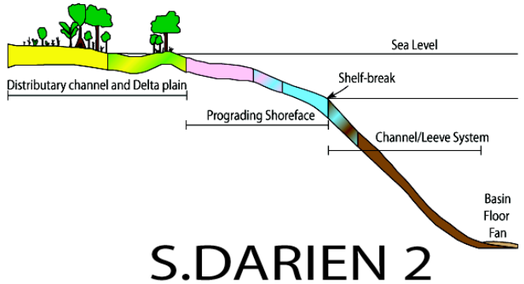

S.DARIEN 2

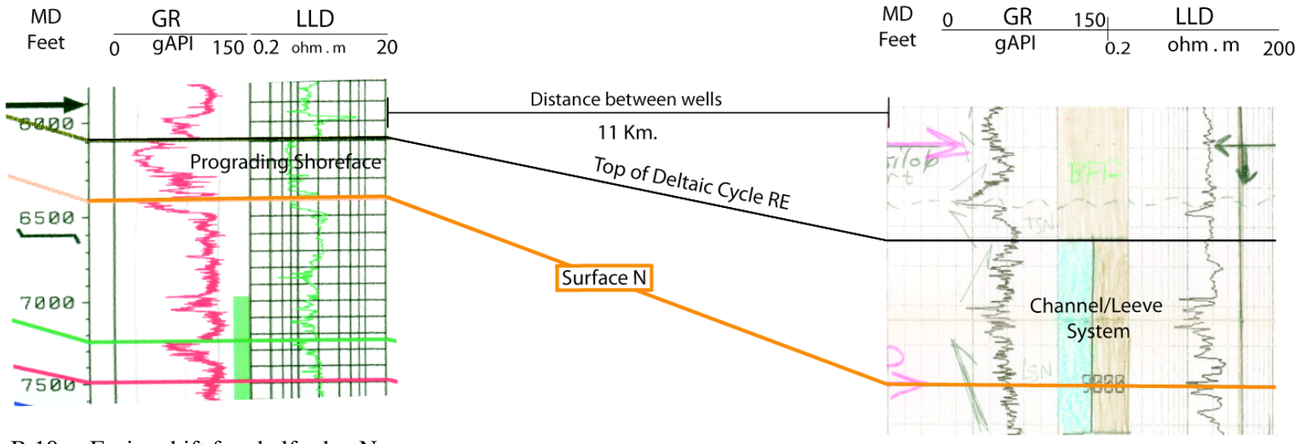

Figure B.10 Facies shift for shelf-edge N

References

Algar, S. T., and J. L. Pindell. 1993. Structure and deformation history of the northern range of Trinidad and adjacent areas. *Tectonics* 12, no. 4: 814.

Alvarez, Tricia. 2008. Tectonic Geomorphology of the Eastern Trinidad Shelf: Implications for Influence of Structure on Reservoir Distribution and Nature in Older Basin Fill. Unpublished M.Sc. The University of Texas at Austin.

Audemard, Franck, Michael Machette, Jonathan Cox, Richard Dart, and Kathleen Haller. 2000. Map and database of Quaternary faults in Venezuela and its offshore regions. U. S. Geological Survey.

Babb, Stephen, and Paul Mann. 1999. Chapter 18 Structural and sedimentary development of a neogene transpressional plate boundary between the Caribbean and South America plates in Trinidad and the Gulf of paria. In *Caribbean Basins*, ed. P. Mann, 4:495 - 557. Sedimentary Basins of the World. Elsevier.

Bowman, Andrew. 2003. Sequence Stratigraphy and Reservoir Characterisation in the Columbus Basin, Trinidad. PhD Dissertation, London, England: Imperial College of Science, Technology, and Medicine, University of London.

Carvajal, Cristian, Ron Steel, and Andrew Petter. 2009. Sediment supply: The main driver of shelf-margin growth. *Earth-Science Reviews* 96, no. 4: 221 - 248.

Diaz de Gamero, María L.. 1996. The changing course of the Orinoco River during the Neogene: a review. *Palaeogeography, Palaeoclimatology, Palaeoecology* 123, no. 1: 385 - 402.

Dyer, Brian L, and Cosgrove. 1992. Penal/Barrackpore Field; West Indies, South Trinidad Basin, Trinidad. *AAPG Treatise of Petroleum Geology, Atlas of Oil and Gas Fields* A-25: 139 - 157.

Eisma, D., S. J. Van Der Gaast, J. M. Martin, and A. J. Thomas. 1978. Suspended matter and bottom deposits of the Orinoco delta: Turbidity, mineralogy and elementary composition. *Netherlands Journal of Sea Research* 12, no. 2: 224 - 251.

Flinch, J.F., V. Rambaran, W. Ali, V. De Lisa, G. Hernández, K. Rodrigues, and R. Sams. 1999. Chapter 17 Structure of the Gulf of paria pull-apart basin (Eastern Venezuela-Trinidad). In *Caribbean Basins*, ed. P. Mann, 4:477 - 484, 487-494. Sedimentary Basins of the World.

Fugro Gulf. 1979. Geotechnical investigation Golfo de Paria, offshore Venezuela. Unpublished Report. Caracas, Venezuela: Instituto Tecnologico Venezolano del Petroleo (INTEVEP).

Garciacaro, Emilio, Paul Mann, and Alejandro Escalona. 2009. Regional structure and tectonic history of the obliquely colliding Columbus foreland basin, offshore Trinidad and Venezuela. *Marine and Petroleum Geology* In Press.

INTEVEP. 1981. Diseño Conceptual de Plataformas para el Norte de Paria y el Golfo de Paria. Unpublished Report. Caracas, Venezuela: PDVSA.

Leonard, Ray. 1983. Geology and Hydrocarbon Accumulations, Columbus Basin, Offshore Trinidad. *AAPG Bulletin 67*.

Levander, Alan, Hans Avé Lallemant, Zelt, James Pindell, Paul Mann, and Gail Christenson. 2003. Crust-Mantle Interactions During Continental Growth and High-Pressure Rock Exhumation at an Oblique Arc-Continent Collision Zone: The SE Caribbean margin. http://earthscience.rice.edu/centers/ccg/research-bolivar-collab-research.html.

Lugo, Jairo, and Paul Mann. 1995. Jurassic –Eocene tectonic evolution of Maracaibo Basin, Venezuela in A. Tankard, S. Suarez, and H. Welsink, eds, *Petroleum basins of South America*. *AAPG Memoir 62*.

Maher, Julie. 2007. Architecture and seismic geomorphology of shelf edge deltas along an active. Unpublished M.Sc. Thesis. The University of Texas at Austin.

Michelson, J. E. 1976. Miocene deltaic oil habitat, Trinidad. *AAPG Bulletin 60*, no. 9: 1502 - 1519.

Moscardelli, Lorena, Lesli Wood, and Paul Mann. 2006. Mass-transport complexes and associated processes in the offshore area of Trinidad and Venezuela. *AAPG Bulletin* 90, no. 7.

Moscardelli, Lorena, and Lesli Wood. 2008. New classification system for mass transport complexes in offshore Trinidad. *Basin Research* 20, no. 1 (March 1): 73-98.

Perez, Omar J, Bilham, Roger, and Bendick. 2001. Velocity field across the southern Caribbean plate boundary and estimates of Caribbean/South-American plate motion using GPS geodesy 1994-2000. *Geophysical Research Letters* 28, no. 15: 2987 - 2990.

Pindell, J, and Lorkan Kennan, L. 2001. Processes & Events in the Terrane Assembly of Trinidad and E. Venezuela. *GCSSEPM Foundation 21st Annual Research Conference Transactions, Petroleum Systems of Deep-Water Basins* (December): 159-192.

Pindell, J., and Lorkan Keenan. 2005. Plate-kinematics and crustal dynamics of Circum-Caribbean arc-continent interactions: tectonic controls on basin development in Proto-Caribbean margins. *In* H.G. Ave Lallemant and V.B. Sisson, eds., *Caribbean-South American Plate Interactions, Venezuela: GSA Special Paper*, no. 394: 7-52.

Pocknall, Wood, and Geen. 1995. Depositional facies in the Pliocene-Pleistocene section, offshore eastern Trinidad. *3rd Geological Conference of the Geological Society of Trinidad and Tobago - 1995*.

Pocknall, Wood, and Geen. 1995. 2001. Integrated Paleontological Studies of Pliocene toPleistocene Deposits of the Orinoco Delta, Eastern Venezuela and Trinidad. *Proceedings of the IX International Palynological Congress, Houston, Texas,U.s.A., 1996; American Association of Stratigraphic Palynologists Foundation*: 319-326.

Robertson, Paul, and Kevin Burke. 1989. Evolution of southern Caribbean Plate boundary, vicinity of Trinidad and Tobago. *AAPG Bulletin* Vol. 73. United States.

Russo, Raymond M, and R. Speed. 1992. Oblique collision and tectonic wedging of the South American continent and Caribbean terranes. *Geology [Boulder]* 20, no. 5: 447 - 450.

Saleh, J., K. Edwards, J. Barbaste, S. Balkaransingh, D. Grant, J. C Weber, and T. Leong. 2004. On some improvements in the geodetic framework of Trinidad and Tobago. *Survey Review* 37: 604-625(22).

Soto, David M., Paul Mann, Alejandro Escalona, and Lesli J. Wood. 2007. Late Holocene strike-slip offset of a subsurface channel interpreted from three-dimensional seismic data, eastern offshore Trinidad. *Geology* 35, no. 9: 859.

Speed, R. C. 1985. Cenozoic collision of the Lesser Antilles Arc and continental South America and the origin of the El Pilar Fault. *Tectonics* 4, no. 1: 41-69.

Sullivan, Sean. 2005. Geochemistry, Sedimentology, and morphology of mud volcanoes, eastern offshore Trinidad. Unpublished M.Sc. Thesis. The University of Texas at Austin.

Sydow, Johan; Joe Finneran, and Andrew Bowman. 2003. Stacked shelf-edge delta reservoirs of the Columbus Basin, Trinidad, West Indies. *23rd Annual GCSSEPM Foundation Bob F. Perkins Research Conference: Shelf Margin Deltas and linked down slope Petroleum Systems: Global Significance and future exploration potential*. Houston, TX. United States: Society for Sedimentary Geology, Gulf Coast Section

U.S. Energy Information Administration. 2010. U.S. Energy Information Administration - EIA - Independent Statistics and Analysis. http://www.eia.gov/.

Warne, Andrew G., Robert H. Meade, William A. White, Edgar H. Guevara, James Gibeaut, Rebecca C. Smyth, Andres Aslan, and Thomas Tremblay. 2002. Regional controls on geomorphology, hydrology, and ecosystem integrity in the Orinoco Delta, Venezuela. *Geomorphology* 44, no. 3: 273 - 307.

Weber, John C. 2001. GPS estimate of relative motion between the Caribbean and South American plates, and geologic implications for Trinidad and Venezuela. *Geology* 29, no. 1: 75 - 78.

Wood, Lesli J.;. 2000. Chronostratigraphy and tectonostratigraphy of the Columbus Basin, eastern offshore Trinidad. *AAPG Bulletin* 84, no. 12 (December 1): 1905-1928.

Wood, Lesli J., and Kristine L. Mize-Spansky. 2009. Quantitative seismic geomorphology of a Quaternary leveed-channel system, offshore eastern Trinidad and Tobago, northeastern South America. *AAPG Bulletin* 93, no. 1 (January 1): 101-125.]

Vita

Anmar Carolina Davila-Chacon was born to Mariemma and Antonio in Caracas, Venezuela. She attended Simon Bolivar University from 1995 to 2002 to pursue a B.E. in Geophysics. From 2001 to 2002 she attended Uppsala University as an Exchange Student, where she worked on her senior thesis. She came back to Venezuela and received her degree in Geophysical Engineering at Simon Bolivar University in Caracas, Venezuela in 2003.

Immediately after graduation, she started to work for a Venezuelan consulting company called Incostas, conducting marine geophysical surveys for geohazards assessments, where she worked as Geophysical Engineer from 2003 to 2005. She was promoted to Chief Geophysicist in 2005 and kept working until 2009.

In January 2009, she moved to Austin, Texas to pursue a Master of Sciences in Geological Sciences with focus on Sedimentology and Stratigraphy. She graduated on December 2010.

E-mail: anmar.davila at gmail.com

This thesis was typed by Anmar C. Davila-Chacon